Comparative Biochemical and Structural Analysis of the Alzheimer's Disease Related Proteins: Amyloid Precursor Protein and Notch1.

By

Catherine L. Deatherage

Dissertation
Submitted to the Faculty of the
Graduate School of Vanderbilt University
in partial fulfillment of the requirements
for the degree of

DOCTOR OF PHILOSOPHY
in

Biochemistry
May, 2016
Nashville, Tennessee

Approved:

Charles R. Sanders, Ph.D.

Walter Chazin, Ph.D.

Bruce Carter, Ph.D.

Borden Lacy, Ph.D.

Lauren Jackson, Ph.D.

To my parents Rebecca and Jim Deatherage

To my sisters Mary and Elizabeth

Thank you for always being there.

ACKNOWLEDGMENTS

I would like to take a moment to thank Dr. Charles Sanders for all of the time and energy that he spent helping me in my journey to becoming an independent researcher. He encouraged me to follow my research interests and pursue my own goals. I'd also like to thank the members of my committee for believing that I knew what I was doing and where I was going. Dr. Bruce Carter, Dr. Walter Chazin, Dr. Borden Lacy, and the late Dr. Richard Armstrong; I couldn't have done this without your support. I'd also like to thank Dr. Lauren Jackson for stepping up and being willing to join my committee in the final hour: you have always been helpful, no matter what questions I've asked. To the members of the Sanders Lab past and present: Thank you all. This work was made possible with the financial support of PO1 GM080513, R01GM106672 and funds provided by Aileen M. Lange and Annie Mary Lyle Chair in Cardiovascular Research.

On a personal level I need to thank my early research mentors, Dr. Mary Berry and Dr. Stanley May at the University of South Dakota and Dr. Andrew Byrd at the National Cancer Institute. I wouldn't be here without you. I would also like to thank my entire family for being so supportive. Thank you for not asking, "When are you going to finish?" I also need to thank my friends Reneé, Kate, and Joanna for not only listening as I babbled about my work over the years but also remembering enough to ask about how things are going.

To the lovely group of friends that I made here at Vanderbilt: Jim and Laura, Gus and Rachel, Whitney and Ben, Kallie and Ryan, Shaun and Noelle, Beth, Allison, Arina, and Drew. I enjoyed every conversation, outing, and girls' night out.

TABLE OF CONTENTS

LIST OF FIGURES

Figure

Page

LIST OF TABLES

Table

Page

LIST OF ABBREVIATIONS

HIV- Human Immunodeficiency Virus

AD- Alzheimer's disease

Aβ- amyloid beta

APP- Amyloid precursor protein

AICD- Amyloid precursor protein intracellular domain

sAPPβ- soluble amyloid precursor protein beta fragment

sAPPα- soluble amyloid precursor protein alpha fragment

ApoE- ApolipoproteinE

LOAD- Late onset Alzheimer's disease

ACAT- Acyl-CoA cholesterol acyltransferase

I-CLiP- intramembrane cleaving proteases

S2P- Site 2 Protease

APH-1- anterior pharynx defective-1

PEN2- presenilin enhancer-2

EM-electron microscopy

GSI- gamma-secretase inhibitor

GSM- gamma-secretase modulator

NSAID- non-steroidal anti-inflammatory drug

DAPT- N-[N-(3,5-Difluorophenacetyl)-L-alanyl]-S-phenylglycine t-butyl ester

NMR- nuclear magnetic resonance

SPR- surface plasmon resonance

SREBP- Sterol regulatory element-binding proteins

HMG-CoA- 3-hydroxy-3-methylglutaryl-CoA

ATP- adenosine triphosphate

BBB- blood brain barrier

IP- Immunoprecipitation

NEXT- Notch extracellular truncation

NICD- Notch intracellular domain

EGF- epidermal growth factor like repeat

NRR- negative regulatory region

LNR- Lin-12 Notch Repeat

RAM- RBPJ-associated molecule

PEST- protein sequence rich in proline (P), glutamic acid (E), serine (S) and threonine (T)

siRNA- small interfering RNA

CRAC- cholesterol recognition amino acid consensus

BCA- Brief communication arising

CD- circular dichroism

DM- n-decylmaltoside

DPC- n-dodecylphosphocholine

DTT- dithiothreitol

GSAP- gamma-secretase activating protein

IPTG- isopropyl β-D-1-thiogalactopyranoside

LMPG- lyso-myristoylphosphatidylglycerol

Ni-NTA- Ni(II) complex with nitrilotriacetic acid-derivatized agarose beads

NMR- nuclear magnetic resonance

PAGE- polyacrylamide gel electrophoresis

PCR- polymerase chain reaction

PION- pigeon homolog protein

SDS- sodium dodecylsulfate

ECD- extracellular domain

TM- transmembrane

JM- juxtamembrane

DMPC- dimyristoylphosphatidylcholine

DH_6PC- dihexanoylphosphatidylcholine

CPMG- Carr-Purcell-Meiboom-Gill

TROSY- Transverse relaxation optimized spectroscopy

Gd-DTPA- Gd(III)-diethylenetriaminepentaacetic acid

16-DSA- 16- DOXYL-steric acid

MSM- milk sphingomyelin

ESM- egg sphingomyelin

PRE- paramagnetic relaxation enhancement

MTSL- *S*-(1-oxyl-2,2,5,5-tetramethyl-2,5-dihydro-1H-pyrrol-3-yl)methyl methanesulfonothioate

CML- chronic myeloid leukemia

AMBER- Assisted Model Building with Energy Refinement

I. Introduction

Statement of Purpose

The purpose of this thesis is to elucidate biochemical and biophysical characteristics of various proteins thought to be involved in the etiology of Alzheimer's disease. One theory suggests the main cause of the disorder is the formation of toxic oligomers and aggregates following production of the amyloid-beta peptide by the enzyme gamma-secretase. The careful characterization of proteins that promote amyloid beta production, or confound anti-amyloid drug development will greatly contribute to the Alzheimer's field and aid in the future development of effective therapeutics.

The first chapter of this thesis introduces the essential features of Alzheimer's disease, the protein components and the confounding factors to drug development. The subsequent chapters describe the careful biochemical and biophysical characterization of the proteins thought to be related to the disorder. The final chapter discusses the conclusions from my experimental studies and future directions suggested by the work of this dissertation.

Introduction to Alzheimer's Disease

As modern medicine and therapeutics evolve, the percentage of people in the United States and around the world that die from serious illnesses like heart disease and cancers will continue to decrease. In fact, U.S. patients dying from diseases like heart disease, stroke and HIV have decreased significantly[1] with advances in drug

therapies. Patients that die from Alzheimer's disease (AD) however, are currently on the rise and the trend is expected to continue as people worldwide continue to live longer, healthier lives. According to reports by the Alzheimer's Association, it is thought that by 2050, the number of people over the age of 65 with AD will triple in the United States alone.[1] These numbers reflect only the United States, but European countries have similar trends and as 2nd and 3rd world countries improve healthcare, booms in AD are expected in these countries as well.

Alzheimer's disease is the most common form of dementia and is lethal. Symptoms of AD are generally characterized by a gradual progression towards dementia. In general, the symptoms are: confusion with time and place, difficulty completing familiar tasks, trouble understanding spatial relationships, memory loss that is disruptive to daily life, problems with planning or problem solving. As the disorder progresses symptoms can include new problems with words or speech, impaired judgment, social withdraw, and changes in mood and personality.[1] Patients typically live 4-8 years post-diagnosis, although patients can live as long as 20 years with the disease, the bulk of the time in the most advanced stage of the disorder.

Advanced stage patients require near round the clock caregiving to assist with mobility, hygiene, and general wellbeing. The total paid healthcare costs for patients with dementia in the US for 2015 was estimated to be greater than $ 225 billion. In addition, each year in the US unpaid caregivers provide additional billions of dollars worth of care to AD patients often to the detriment of the caregiver's own health and wellbeing. These caregivers report higher levels of stress, depression, and poorer physical health than caregivers of the elderly without AD. Nearly 50% of the caregivers

had to leave their employment to provide patient care.[1] As more people get AD this loss of employment could easily become a substantial burden on the world workforce.

Alzheimer's Disease Etiology

The exact etiology or mechanism of action of AD is unknown. This is one reason that despite first being described in 1907, we still do not have a cure for this devastating disorder. For many years the only way to concretely diagnose a patient with AD was a post-mortem autopsy and notation of severe brain vascularization and atrophy and the presence of aggregated protein deposits called "amyloid plaques" and tangles. The major component of the tangles was aggregated remains of hyper-phosphorylated tau, a microtubule stabilizing protein abundantly expressed in the central nervous system. [2] The plaque deposits of fibrilized proteins were the best signifier of the disorder. The major component of these plaques remained unknown until 1984 when researchers out of UCSD, Glenner and Wong, isolated a peptide from patient brains and named it amyloid-beta (Aβ). [3] Shortly after that another group determined that the Aβ peptide was a cleavage product of the larger protein that they named the amyloid precursor protein (APP).[4]

APP as a causative factor in AD was supported by the gene locus of the APP gene and the genetic disorder Down's syndrome or trisomy 21. Researchers found that the plaque deposits found in the brains of Down's syndrome patients and AD patients contained the same protein,[4] Aβ. The genetic locus of APP is on chromosome 21.[5] Given that Down's syndrome is a genetic disorder where there is a duplicate of chromosome 21, this means these patients have essentially a triple dose of the APP protein.[6] This overload likely explains the clinical feature that Down's syndrome patients

over the age of 30 have increased amyloid deposits and are likely to present clinical symptoms of AD early, in late 40s to early 50s.[7]

APP is proteolytically processed in two potentially competing pathways. When APP is cleaved by the enzyme α-secretase, it enters the "non-amyloidogenic pathway" where the end product is the APP intracellular domain (AICD) and a small soluble peptide called "p3." The second pathway, the "amyloidogenic pathway" ultimately yields the AICD and the Aβ peptide.[8] More details on these pathways can be seen in Figure 1.1. In the non-amyloidogenic pathway, APP is cleaved by α-secretase, a metalloprotease, to produce a transmembrane stub called C83. C83 is then cleaved in the membrane by γ-secretase to release the AICD and the soluble peptide p3. This p3 peptide may actually have neuroprotective characteristics.[9] The AICD may also have a role on cholesterol homeostasis, which will be addressed in a later section.

The amyloidogenic pathway is entered[8] when APP is processed by the enzyme β-secretase, BACE1. BACE1 would be an intriguing therapeutic target as inhibiting this reaction would likely favor the non-amyloidogenic pathway and thus limit the amount of Aβ.[10] After β-secretase cleavage, the transmembrane stub C99 is left in the membrane and a soluble fragment sAPPβ is released. There is research that indicates that the sAPPβ serves as a ligand and may help to stimulate caspase 6.[11] This would suggest that perhaps even this soluble domain contributes to apoptosis and thus the neuronal degradation seen in AD. The removal of the sAPPβ fragment also serves as a sheddase event required before γ-secretase can cleave the transmembrane stub C99.[12, 13] C99 is then cleaved in the membrane by γ-secretase to produce the AICD and the Aβ peptide.[8]

Due to the promiscuous nature of the γ-secretase complex,[13] there is not a single cleavage product of C99. Instead, the transmembrane segment of C99 is processively cleaved with little specificity.[14, 15] Processive cleavage results in Aβ peptide of differing lengths. The most abundant form of the Aβ peptide is the $A\beta_{40}$ with $A\beta_{42/38}$ being less prevalent. While not the major product $A\beta_{42}$, and the ratio of $A\beta_{40}$:$A\beta_{42}$ is thought to be a major pathological marker.[16-19] Genetic mutations and system changes that shift the ratio towards $A\beta_{42}$ are considered to be AD risk factors.[20-23]

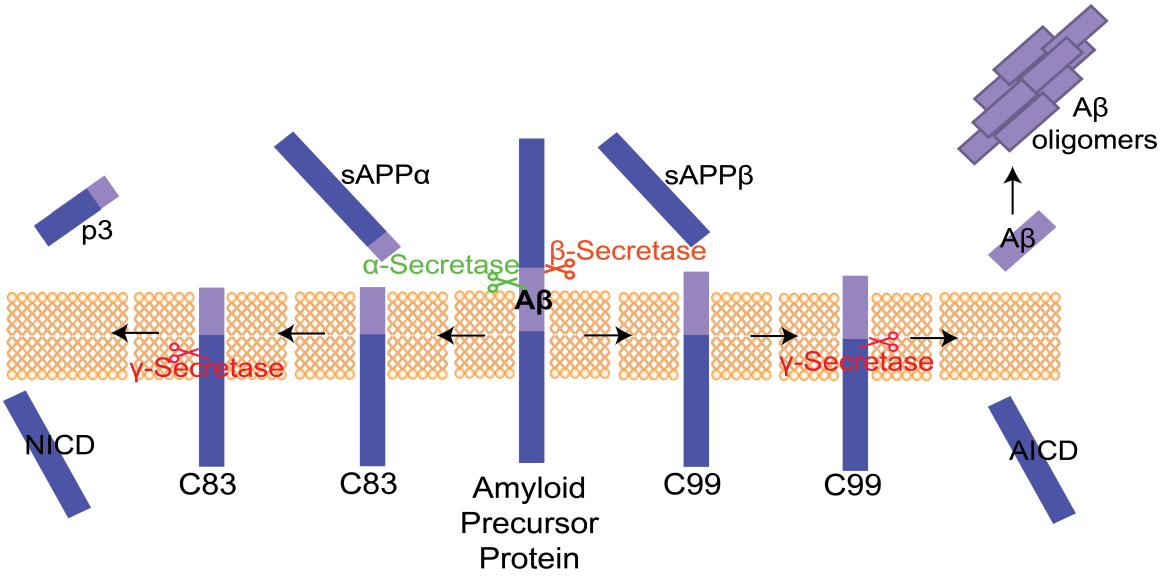

Figure 1.1- APP Processing. APP can be cleaved in two competing pathways. The "non-amyloidogenic" pathway is entered when APP is cleaved by α-secretase to produce the fragment soluble APPα (sAPPα) and the transmembrane stub C83. C83 is cleaved in the membrane by γ-secretase to produce two soluble peptides, p3 and the AICD. The "amyloidogenic pathway" begins when APP is cleaved by the β-secretase enzyme BACE1 to produce the transmembrane stub C99 and the fragment soluble APPβ (sAPPβ). C99 is then also cleaved by γ-secretase to produce two soluble peptides, Aβ and the AICD. The Aβ peptide continues on to form the Aβ oligomers implicated in AD etiology.

Given that the $A\beta_{42}$ form seems to be more prone to aggregation,[24] it is interesting that new research has indicated that the early stage of soluble Aβ oligomers/aggregates (Figure 1.1) may actually be responsible for the neurotoxicity seen during AD progression, not the large insoluble plaques.[25] This production of the Aβ peptide is thought to be the center of the Amyloid Cascade Hypothesis. [26] A brief visual representation of the amyloid cascade hypothesis can be seen in Figure 1.2.[27, 28] In this model, the production of the Aβ peptide is the central cause of the neuronal damage and eventual dementia seen in AD. There is a great deal of research that supports this claim and has been extensively reviewed.[26-33] That is not to say, however, that there are not detractors of the theory. Given that the amyloid cascade theory has been the major research focus for nearly a decade, and that there is still no cure some researchers are beginning to question the principle of having Aβ at the center of the theory and suggest researchers would be better suited to explore alternate etiological paradigms such as inflammation or oxidative damage as the major causative factor.[32, 34]

In spite of possible detractors, a great deal of work has been directed towards understanding the structural, biochemical, and biophysical characteristics of the protein C99 with the intention of using this *in vitro* information in the broad scheme of understanding APP processing and the etiology of AD. In the Sanders lab, extensive research has been conducted to determine how to express and purify the full-length C99 protein in a lipid mimetic, as well as to assess the backbone protein dynamics and the positioning of C99 relative to the membrane.[35] The structure of C99 in a detergent micelle and the novel fact that C99 will directly and specifically bind the molecule

cholesterol has also been determined.[36] Additional work to look at the competition between C99-cholesterol binding vs. dimerization[37] and how membrane bilayer thickness impacts C99 position relative to the membrane[38] has also been carried out. New work, geared towards new lipid mimetics that may better replicate cellular conditions is currently underway (unpublished). Overall, the Sanders group has carefully characterized the full-length C99 molecule and this characterization contributes to the scientific understanding of the field overall.

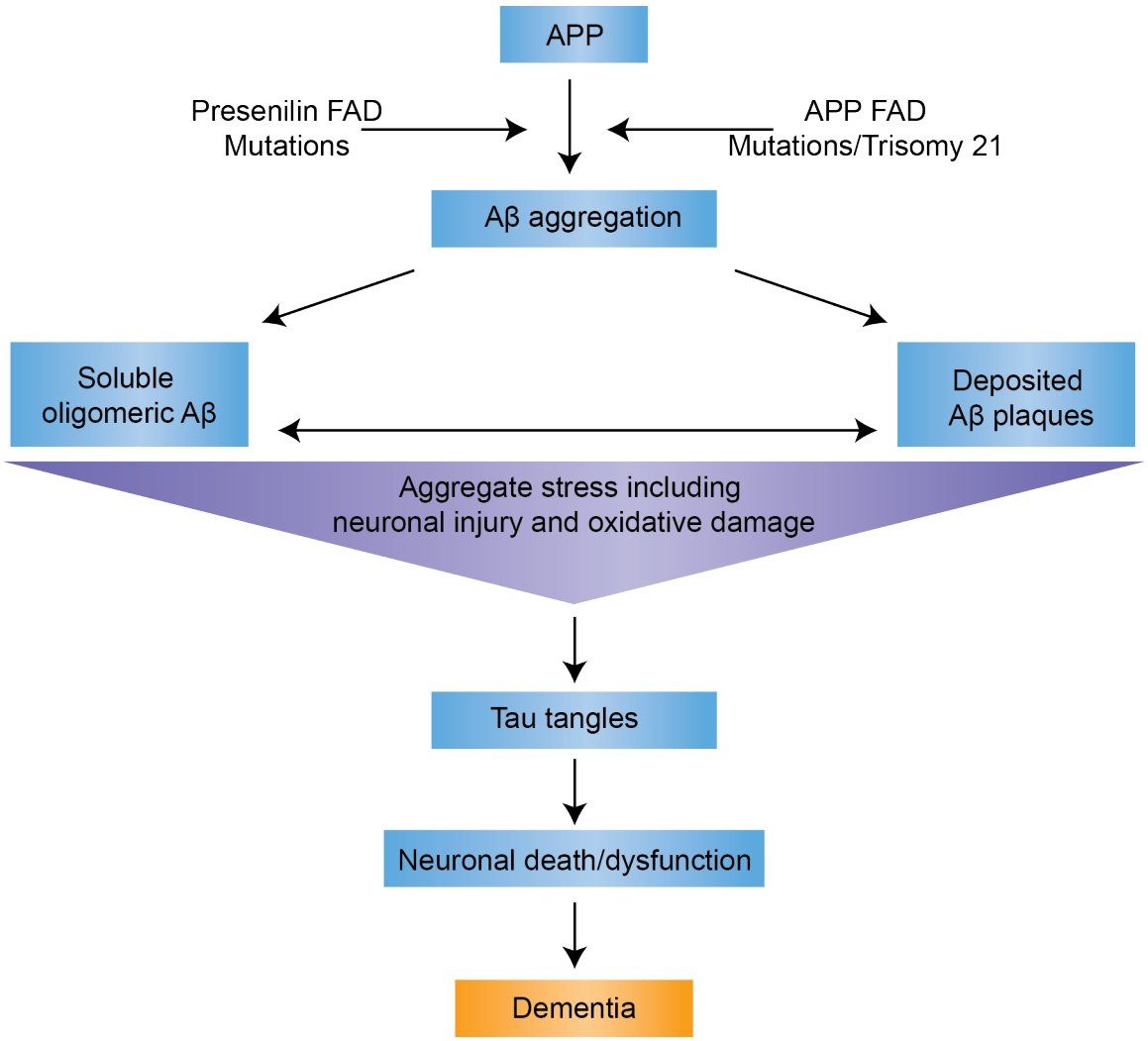

Figure 1.2- Amyloid Cascade Hypothesis. In this theory, AD etiology is based around the production of the Aβ peptide and the oxidative damage, stress, and neuronal damage that follows and how subsequent steps are the formation of tau tangles and neuronal dysfunction. This model is based on original figures in Broerson *et. al.* (2010)[27] and Karren *et. al.* (2011).[28]

APP and Cholesterol

The exact role that cholesterol plays in the etiology of Alzheimer's disease is still ambiguous. There is however, a stunning amount of research that has linked cholesterol and Alzheimer's disease. The initial evidence linking AD and cholesterol was published in 1994 when rabbits fed a high cholesterol diet ended up with plaques similar to those seen in AD patients brains[39] and humans with advanced coronary heart disease.[40] Since then, the effect of cholesterol has been studied largely in animal models and *in vitro* systems and has been extensively reviewed.[35, 41-49] This section will briefly touch on the relationship between AD and cholesterol and how different domains of APP can impact cholesterol homeostasis and biosynthesis. Cholesterol and lipid biosynthesis seem to be entangled with AD on multiple levels.

There are only two very strongly correlated risk factors of late onset AD (LOAD). The first is advanced age. The second is a genetic risk factor. ApolipoproteinE (ApoE) is a lipoprotein that transports cholesterol between neuronal cells. There are 4 genetic variations of this protein, and genetic screens and GWAS studies have indicated that the ApoE ε4 allele is one of the biggest risk factors for the development of LOAD beside old age,[50-52] although the ApoE ε4 allele alone is not sufficient to cause AD.[53]

Much of the relationship between cholesterol and AD may be due to APP and the proteolysis products of APP cleavage. Given that research suggests that the amyloidogenic pathway largely occurs in cholesterol and sphingholipid-rich lipid raft microdomains that include the enzymes β- and γ-secretase[42, 54, 55] the connection is strengthened. More information on lipid rafts and APP processing can be found in the next section. APP processing is closely regulated by cholesterol and APP fragments

regulate lipid homeostasis. Intracellular cholesterol regulates APP processing through the ACAT enzyme, an important acyltransferase involved in bile acid biosynthesis.[56] Expression of APP reduced HMG-CoA reductase regulated cholesterol biosynthesis, while the reduction of APP increased cholesterol biosynthesis. This change in cholesterol biosynthesis was likely mediated through an interaction between APP and the protein SREBP.[57] Therefore, APP regulates SREBP mediated cholesterol biosynthesis in cultured neurons, and the inhibition of cholesterol turnover/homeostasis inhibited neuron function.[57]

The products of APP proteolysis also play a role in cholesterol synthesis or homeostasis. Wang et. al. found in 2014, that the soluble sheddase product of APP processing in the lumen of the secretory pathway had a differential control of cholesterol synthesis through the interaction with SREBP.[58] The intracellular domain of APP, the AICD and the binding partners Fe65 and Tip60 work jointly to suppress expressing LRP1, an ApoE receptor that mediates cholesterol uptake and thus regulates cholesterol homeostasis.[59] Although, as with much of the research in the relationship between cholesterol and AD, this role has been questioned due to reported differences in the phosphorylation state of the AICD, as well as the role of the binding partners in signal transduction.[60]

The Aβ peptide is also strongly linked with cholesterol in results documented in the literature. Brain ischemia from atherosclerosis may promote APP expression which increases Aβ oligomers and senile plaque and neurofibrillary tangle depositions.[61, 62] Research indicates that lipids and cholesterol may control or enhance Aβ aggregation.[63-66] Aβ may also function as an inhibitor of HMG-CoA reductase, the rate

limiting enzyme in the cholesterol biosynthesis pathway.[67] A brief map of the putative roles of cholesterol in AD can be seen in Figure 1.3.

Given the interconnectedness of APP and cholesterol, it may be unsurprising that the cholesterol lowering drugs called statins have an interesting impact on AD. After a series of retrospective studies,[61] it was reported that statin reduced the risk of LOAD by approximately 50%.[68] The exact mechanism of this is unknown. One possible mechanism is: decreases in intracellular cholesterol from statins breaks down lipid rafts and thus favors the non-amyloidogenic pathway, and lowers the risk of AD.[42, 54, 69] Given the above information, it seems possible that APP functions in part as a cholesterol sensor.[35] This is again supported by the specific interaction between C99 and cholesterol.[36] These factors make statins and cholesterol analogs very attractive therapeutic possibilities that could be used to modulate the levels of Aβ production or even limit its aggregation.

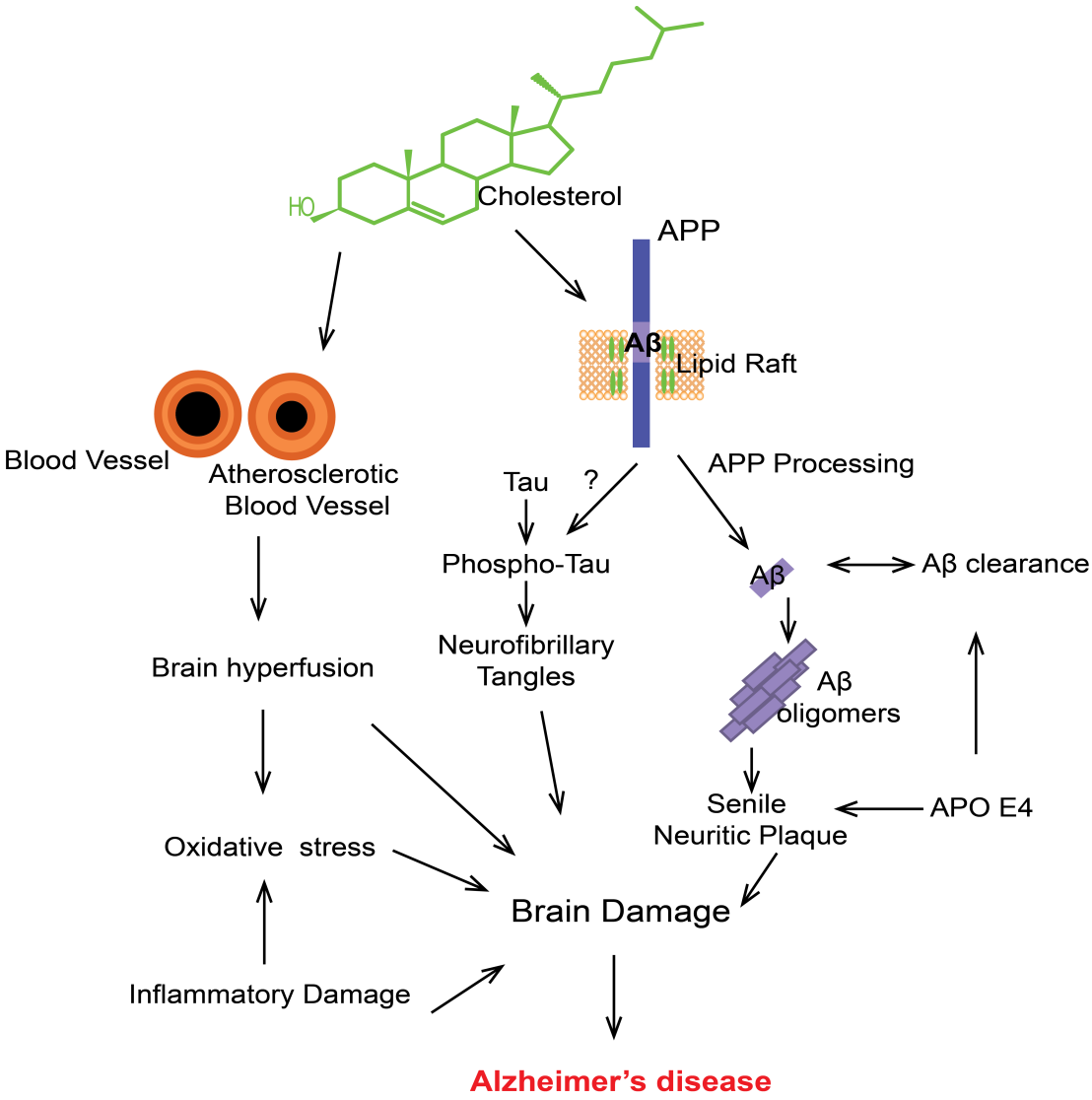

Figure 1.3- Map of how cholesterol can influence Alzheimer's disease. Cholesterol influences AD in multi-pronged way. It is the major component of lipid rafts that promotes the amyloidogenic pathway processing. Deposition of cholesterol in blood vessels can lead to atherosclerotic plaques and brain hyperfusion. The combination of these factors leads to brain damage and AD.

Gamma Secretase

The gamma-secretase enzyme (γ-secretase) plays a prominent role in the ongoing research on Alzheimer's disease. This enzyme complex is considered to be part of the intramembrane cleaving proteases or I-CLiPs family of enzymes.[70] This family of enzymes, including rhomboid and Site 2 Protease (S2P),[71] is capable of catalyzing a hydrolytic reaction within the hydrophobic domain of the lipid bilayer. The rhomboid catalytic site is a dyad of asparagine residues in the transmembrane region of the protein.[72] This is of particular interest because it is different from the typical catalytic modality. The catalytic component of γ-secretase, the protein presenilin, is a member of this I-CLiP family, the catalytic dyad a more traditional aspartyl dyad.[73]

γ-secretase was characterized to be part of AD pathogenesis in 2006.[74] γ-secretase is an unusual I-CLiP member because it is a four component complex. Presenilin is the catalytically active component, the other components are Nicastrin, anterior pharynx defective-1 (APH-1), and presenilin enhancer-2 (PEN2).[75] Nicastrin is thought to be involved in substrate recognition;[76] APH-1 largely serves as scaffolding and to stabilize the complex.[77] PEN-2 stimulates the required auto-catalysis of the presenilin protein and is an essential part of the complex.[78-80] Biochemical analysis has demonstrated that the stoichiometry of the complex is a 1:1:1:1 tetrameric complex.[81] The cleaved presenilin is stabilized by an interaction with the PEN2 component.[82] A cartoon of the γ-secretase complex can be seen in Figure 1.4.

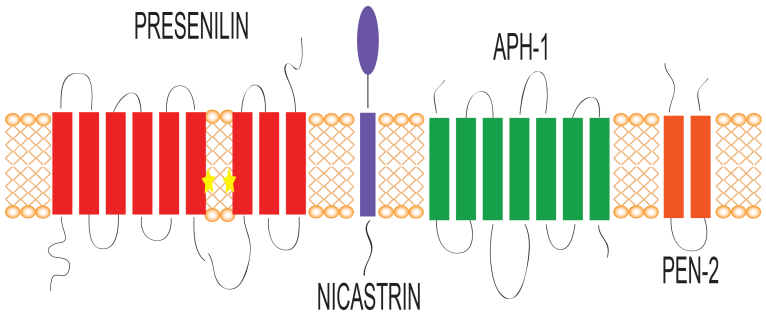

Figure 1.4- Gamma Secretase Components. The tetrameric gamma secretase complex has 4 components, all of which are transmembrane proteins. The catalytically active component presenilin (red, the active site residues are marked with stars), the scaffolding unit APH-1 (green), substrate selector, Nicastrin (purple) and PEN-2 (orange) responsible for stabilization and the autocatalysis of presenilin can be seen with the correct number of helices. Only nicastrin has a substantial extracellular domain.

One feature of this enzyme complex is the lack of substrate specificity. As of 2011 there were over 90 proteins thought to be substrates of γ-secretase. Table 1.1 contains known γ-secretase substrates.[83] What regulates the enzyme/substrate interaction is not known, although there are some intriguing theories. In 2013, the Urban lab proposed that intramembrane proteolysis is not a feature of substrate affinity, but instead is limited by the kinetics of the reaction itself.[84] The Urban study, done on the rhomboid protease, GlpG has significant ramifications for other members of the I-CLiP family. Their data would suggest that γ-secretase cleaves any membrane protein that fits within the active site and that there is no specific regulation. If this is the case, it leads to the question of why would there be multiple isoforms of both presenilin and APH-1, and further why would these different enzyme components have slightly different function.[85, 86] There are many other ways that γ-secretase may also be regulated. One possibility is that γ-secretase function is regulated by spatial segregation of enzyme and substrate.[87] Another plausible regulatory mechanism is that the lipid microenvironment itself helps to regulate γ-secretase function.

Research has shown that active γ-secretase is associated with "lipid rafts."[88-90] Lipid rafts can be defined as short-lived, ordered lipid microdomains enriched with cholesterol and sphingomyelin.[91] γ-secretase is sensitive to the membrane thickness as well as the chain length, saturation and lipid head group.[92-94] This suggests that γ-secretase is more sensitive to lipid environment, and that its activity can be regulated by the lipid composition. Thus the lipid microenvironment and the cellular compartment that γ-secretase is occupying at the time of enzyme substrate interaction may regulate

function. The different lipid composition present in the different cellular compartments[95] only serves to further support the idea that γ-secretase regulation may be a factor of both lipid microdomain identity and spatial sequestration. Lastly, given the wealth of information about the role of cholesterol in AD, it is not challenging to speculate about the role that cholesterol plays in regulating γ-secretase function and thus the development and progression of AD. It is important to note however, that none of these possible regulatory mechanisms invalidate the kinetic studies of the rhomboid protein; they instead suggest for γ-secretase there are additional levels of complexity that should be considered.

Table 1.1- List of known γ-secretase substrates as of 2011*

1	Alcadein α	**24**	EphrinB2	**47**	LRP2 (megalin)	**70**	Ptprz
2	Alcadein γ (calsyntenin)	**25**	ErbB4	**48**	LRP6	**71**	RAGE
3	APLP1	**26**	GHR	**49**	MUC1	**72**	RPTPκ
4	APLP2	**27**	HLA	**50**	N-cadherin	**73**	RPTPμ
5	ApoER2	**28**	HLA-A2	**51**	Nav-β1	**74**	ROBO1
6	AβPP	**29**	IFNaR2	**52**	Nav-β2	**75**	SorC3
7	Betacellulin (BTC)	**30**	IGF-1R	**53**	Nav-β3	**76**	SorCS1b
8	Betaglycan 9.	**31**	IL-1R1	**54**	Nav-β4	**77**	SorLA (LR11)
9	CD43	**32**	IL-1R2	**55**	Nectin-1α	**78**	Sortilin
10	CD44	**33**	IL6R	**56**	Neuregulin-1	**79**	Syndecan-1
11	CSF1R	**34**	IR	**57**	Neuregulin-2	**80**	Syndecan-2
12	CXCL16	**35**	Ire1α	**58**	Notch 1	**81**	Syndecan-3
13	CX3CL1 (fractalkine)	**36**	Ire1 β	**59**	Notch-2	**82**	Tie1
14	DCC	**37**	Jagged2	**60**	Notch-3	**83**	Tyrosinase
15	Delta1	**38**	KCNE1	**61**	Notch-4	**84**	TYRP1
16	Desmoglein-2	**39**	KCNE2	**62**	NPR-C	**85**	TYRP2
17	DNER	**40**	KCNE3	**63**	NRADD	**86**	Vasorin
18	Dystroglycan	**41**	KCNE4	**64**	p75NTR	**87**	VE-cadherin
19	E-cadherin	**42**	Klotho	**65**	PAM	**88**	VEGF-R1
20	EpCAM	**43**	L1	**66**	PLXDC2	**89**	VLDLR
21	EphA4	**44**	LAR	**67**	Polyductin (PKHD1)	**90**	GluR3
22	EphB2	**45**	LRP1(LDLR)	**68**	Protocadherin-α4 (Pcdh-α4)	**91**	GnT-V
23	EphrinB1	**46**	LRP1 b	**69**	Protocadherin-γ-C3 (Pcdh-γC3)		

*Based on data complied by Annakaisa Haapasalo and Dora M. Kovacs in the 2011 review "The many substrates of presenilin/γ-secretase."[83]

Until 2014, there was no high-resolution structure of γ-secretase. This was, in part, due to the inability to produce sufficient quantities of functional enzyme complex for structure determination. The next challenge was a technical one; γ-secretase was too large for NMR, too flexible for x-ray crystallography and too small for cryo-EM (cryo-electron microscopy). In 2015, with the use of a direct electron detector and the collection of nearly 1 million particles, the Shi research group was able to reconstruct a cryo-EM structure of the full and active γ-secretase complex. This structure resolved at ~3.4Å, and the helices are assigned. This assignment allows the active site of the enzyme complex to be seen in depth for the first time.[96] A second work, elaborating on the structure shows the different conformations that the γ-secretase catalytic subunit can have.[97] Figure 1.5 is the 3.4Å structure of γ-secretase. As in Figure 1.4, presenilin is colored red, Nicastrin is colored purple, PEN2 is orange and APH-1 is green. The active site aspartate residues are colored cyan. These new structures will allow for a careful examination of the active site in order to better understand the γ-secretase mechanism of action. It will also allow for docking studies of γ-secretase and the varied substrates to get a better understanding of how γ-secretase functions.

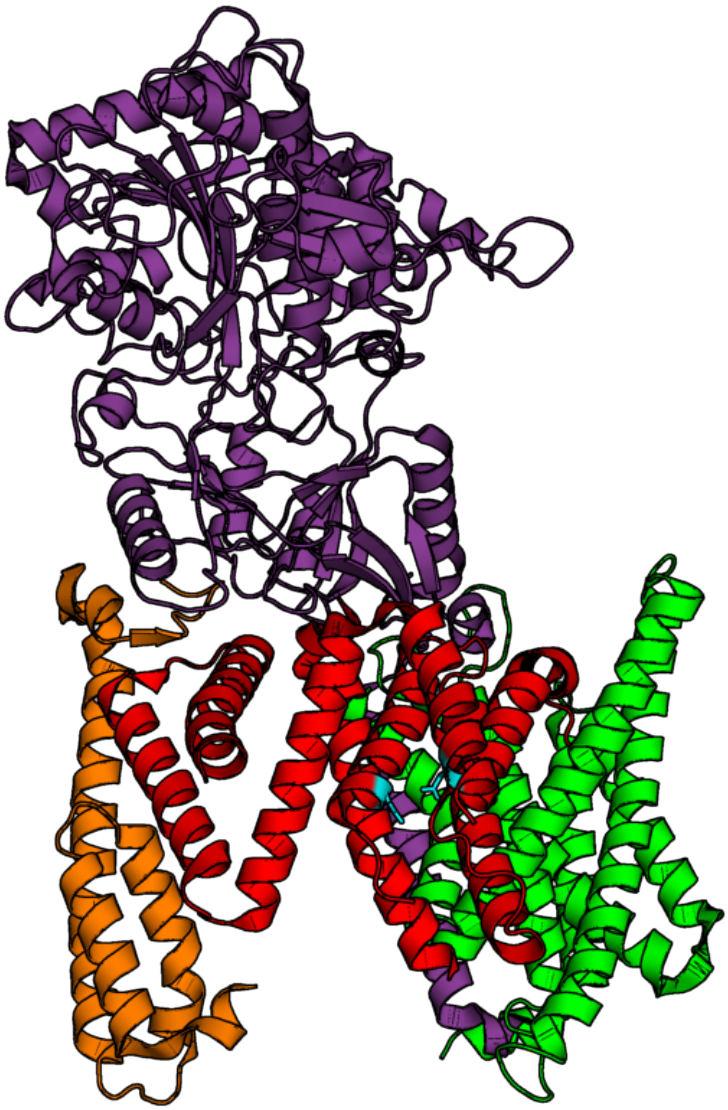

Figure 1.5- Cryo-EM structure of γ-Secretase. Adapted from PDB: 5A63. Presenilin is colored red. The active site aspartate residues are colored cyan. Nicastrin is purple, APH-1 is green and PEN2 is orange. This depiction of the structure is modified from the original publication (Cryo-EM structure of the human gamma-secretase complex at 3.4 angstrom resolution) by coloring and the display of the active site.

Preventing APP Processing

Curing Alzheimer's disease by either preventing or clearing the Aβ oligomers/deposits has long been a dream in the Alzheimer's field. Unfortunately, it is far more challenging a feat than originally thought. Since the amyloid cascade hypothesis first took center stage,[26] there have been 3 major approaches to "curing AD." The first approach, which has resulted in 2 failed clinical trials, was to use anti-Aβ antibodies that were supposed to induce phagocytic clearance of the amyloid plaques and thus prevent the cognitive problems of AD.[98-101] Both of these clinical trials ended with no significant cognitive improvement seen in trial participants. The failure of these expensive clinical trials has many researchers questioning if the antibody approach is the correct avenue.[102] The other two approaches are designed to prevent or mitigate the production of Aβ. The first, gamma-secretase inhibitors (GSI) are defined as small molecules that inhibit the function of γ-secretase completely. The second, gamma secretase modulators (GSM) moderate the processive cleavage of the enzyme, thus changing the length of the Aβ product.[103]

The first generation of the GSI molecules were exceptionally useful in the analysis of how γ-secretase functions, but were not part of an actual AD clinical trial. In 1999 the Selkoe lab developed a series of inhibitors based on the $A\beta_{42}$ cut site. These inhibitors were designed to resemble the transition state of the C99 cut site.[104] It was this inhibitor binding that helped to confirm that presenilin was the catalytic part of γ-secretase.[105, 106] The inhibitor L-685.458 was synthesized around the same time, and is a potent inhibitor of γ-secretase cleavage.[107] This is one of the γ-secretase inhibitors still

used in γ-secretase research. The excellent 2009 review by Anthony Kreft has more information about the chemistry and the development of these early γ-secretase inhibitors.[108]

A second cohort of allosteric GSIs bind to presenilin.[108] This family includes the molecule DAPT, another potent γ-secretase inhibitor used in research.[109] These inhibitors broadly inhibit γ-secretase function and are not substrate specific.[110] Semagacestat, an allosteric inhibitor, made it to Phase 3 clinical trials before they had to be cancelled.[111] Trial participants experienced skin problems and a wealth of physical issues, but perhaps the most troubling was a decline in cognitive capabilities. It was determined that the inhibition of Notch signaling was the likely culprit. A third cohort of inhibitors was produced that were thought to be "Notch sparing." These inhibitors supposedly only inhibited APP cleavage and the Notch processing was modulated not stopped. Despite this, clinical trials had to be halted due to Notch induced toxicity.[112] It is possible that the "Notch sparing" effects were overestimated and were never promising candidates.[110]

Drugs that mitigate γ-secretase function instead of inhibiting it are called gamma-secretase modulators: GSMs. Many of this drug class can change the length ratio of the generated Aβ peptides. One subset of these GSMs are based on NSAID drugs including ibuprofen and naproxen.[110] Another class are heterocyclic GSM not derived from NSAIDs. Interestingly, these different classes of drugs seem to have a similar effect on γ-secretase function. The heterocyclic GSM lowers $A\beta_{40/42}$ and increases the amount of $A\beta_{37/38}$.[113] The NSAID-GSM also lowers $A\beta_{42}$ and increases $A\beta_{38}$ while not impacting the cleavage of the Notch substrate making the drug specific to C99.[110, 114] It

is possible that some of these NSAID-GSM drugs order lipid bilayers like cholesterol do, and this may factor into their mechanism of action.[115]

In 2008, a paper published by the Golde lab reported that a specific subset of NSAID-based GSM compounds has a direct and specific interaction with C99, which defines the C99 specificity.[116] The Sanders lab used NMR and purified C99 to demonstrate that any interaction between these drugs and C99 was weak and non-specific and that there may have been confounding aggregation in the original paper.[117] This report incited controversy, and in 2010 and 2011 the Multhaup group published two papers that reinforced their interpretation that the NSAID-GSM drugs directly interacted with the Aβ portion of C99. They used NMR, SPR and a bacterial reporter gene dimerization assay.[118, 119] These contrasting results encouraged the Sanders group to return to the NSAID-GSMs. They used the drug sulindac sulfide and the Aβ and ultimately saw no specific interaction between the drug and the peptide. The results of their study ultimately led them to conclude there was no interaction between the GSMs and Aβ, and thus, that complex formation could not be the underpinning of GSM mechanism of action and specificity.[120]

To date, none of these NSAID-based GSMs have made it to clinical trial and, given the conflicting reports on the mechanism of action for the Notch sparing behavior, researchers are still actively looking for a target that may be the key for APP-specific druggability.

Gamma Secretase Activating Protein

The sole focus on APP processing has not yielded a viable drug or drug target to date. Now researchers are attempting to find drugs or proteins that will impact

accessory proteins or currently unknown protein cofactors. In 1999, the Greengard group developed a cell free assay to study Aβ generation and trafficking that had a pronounced ATP energy requirement.[121] As a follow up study, in 2003 the same group thought to use small molecules with ATP activity as a method for inhibiting Aβ.[122] They selected the tyrosine-kinase inhibitor imatinib mesylate, or Gleevac, a well-known cancer drug. It binds to the ATP binding site of the kinase and inhibits activity. The results from this study suggested that not only does γ-secretase cleavage have an ATP requirement, but the addition of imatinib mesylate was able to prevent the production of the Aβ peptide.[122] Imatinib mesylate inhibition of APP processing also had no effect on the processing of Notch.[122] The mechanism of action of the selective inhibition was unknown but a promising avenue of research despite the fact that imatinib mesylate will not cross the blood brain barrier (BBB).

In 2010, the Greengard group published a new study in *Nature* that suggested they had determined the imatinib mechanism and discovered a novel therapeutic target.[123] The Greengard group created an immobilized imatinib pull-down assay, to try and identify any proteins that would bind to this drug. In this assay, the components of γ-secretase were isolated along with a new protein that ran at approximately 16kDa on an SDS-PAGE gel. This gel band was identified using mass spectrometry as the previously uncharacterized pigeon homologue protein (PION). The protein was then characterized as the gamma secretase activating protein (GSAP).[123] The imatinib/γ-secretase interaction is dependent on GSAP, when GSAP is knocked down, the interaction between the drug and the complex is reduced. Further, when GSAP was knocked down with siRNA, the levels of Aβ were significantly reduced, while imatinib alone didn't

change anything. This suggests that GSAP modulates the inhibitory function of imatinib. In mouse models, GSAP knockdown reduces the plaque load in mouse brains. When recombinant GSAP was added to cell culture, the concentration of Aβ increased while AICD levels were reduced. This would suggest GSAP differentially affects the processivity of γ-secretase.[123] Finally, in cells expressing the Notch extracellular truncation (NEXT), the γ-secretase substrate, the levels of the Notch intracellular domain (NICD), a γ-secretase cleavage product, was not altered by either the presence of recombinant GSAP or by GSAP knock-down.[123]

This APP specificity was essential to the use of GSAP as a therapeutic target. The authors then sought to hypothesize on the specificity of GSAP modulation. Immunoprecipitation (IP) experiments suggested that GSAP exists in a complex with γ-secretase, acting as a co-factor. Further IP experiments and preliminary domain mapping suggest that GSAP functions by directly interacting with the cytosolic juxtamembrane segment of C99.[123] The C99:GSAP complex became a very interesting structural target in the Sanders group in light of the structure of C99 that our lab had been working on at the time. Work done to replicate the interaction between C99 and GSAP as well as to structurally characterize this interaction will be detailed in depth in Chapter 2, and future thoughts about the protein and eventual controversy regarding the overall reproducibility of the GSAP narrative will be discussed in Chapter 5.

Notch

As detailed in previous sections, the sheer number of γ-secretase substrates and the challenge of finding an APP-specific drug preventing γ-secretase cleavage as a therapeutic strategy of AD has caused a significant bottleneck. Arguably, the γ-

secretase substrate that has caused the most significant problems in AD drug development[98, 100, 101, 111, 112] is the Notch family of proteins.

Notch was first discovered and studied in the context of *Drosophila* genetics and in embryogenesis. The Notch gene was named for the "notch" winged fly phenotype found by Morgan.[124, 125] The role Notch plays in development and embryogenesis was determined when it was found that loss of the Notch gene function was responsible for an embryonic lethal alteration to the nervous system.[126] The Notch gene and notch signaling occur in all vertebrate organisms.[127-130] Notch is the critical mediator of binary cell fate decisions as well as developmental lateral inhibition. In vertebrates, Notch signaling has been implicated in a diverse array of patterning choices. Some of these include inner ear hair cell formation, pancreatic cell production, intestinal cell differentiation, and immune cell selection.[131-134] Notch signaling also controls neurogenesis, axon and dendrite growth, and synapse plasticity, as well as neuronal death.[135-143]

There is one Notch gene in *Drosophila melanogaster*, and as organism complexity increases so do the number of homologs. *Caenorhabditis Elegans* has 2 homologs, and humans have 4.[144-148] One significant difference between the homologs beyond tissue expression variation and function is differences in the domains of the protein. Notch is a type 1 membrane receptor with a series of modular domains with distinct function. Notch organization can be seen in Figure 1.6. There are eight discreet domains, extracellularly; there are the EGF repeats, three LNR repeats, and the heterodimerization domain. The LNR repeats and the heterodimerization domain make up the negative regulatory region (NRR). Then there is the transmembrane segment.

On the intracellular side, there is the RAM domain, a series of ankyrin repeats, a transcriptional activation domain (TAD) and a PEST domain. The first domain, EGF repeats, is the ligand-binding domain. Mammalian Notch proteins have between 29 and 36 repeats, and ligand binding generally occurs through an interaction with repeats 11-13. Many of the EGF repeats bind calcium, and this binding regulates signaling activity.[149, 150] The EGF repeats are also heavily glycosylated, and this glycosylation can moderate the signaling.[151] A family of glycosyltransferase proteins change the fucosylation pattern at specific EGF repeats and are able to tune how sensitive the receptor is to the ligand.[152] Canonical Notch ligands bind the receptor through EGF-like domains on both Notch and ligand.[153, 154] Non-canonical ligands are not going to be discussed but were reviewed by Michael Wang in 2011.[155]

The NRR region is a very important segment of the protein. This segment contains both the heterodimerization domain and three LNR repeats. It is called the NRR because the fold of this segment mask the S2 cut site that is the committed step of the Notch signaling pathway and regulates the signaling.[140, 156] The heterodimerization domain is the site of the initial S1 cleavage step, where the intact Notch protein is cleaved in the Golgi extracellularly by a furin-like convertase.[143] This cleavage event leaves the protein as a heterodimer with the extracellular domain (ECD) linked to the combined TM and intracellular domains in a non-covalent manner.[157, 158] Questions regarding how the NRR functioned were answered by a structure of the complete NRR domain.[156, 159] In this structure, the 3 LNR repeats wrap around the heterodimerization domain and the S2 cut-site and prevent functional exposure, (see middle panel in Figure 1.6).[159]

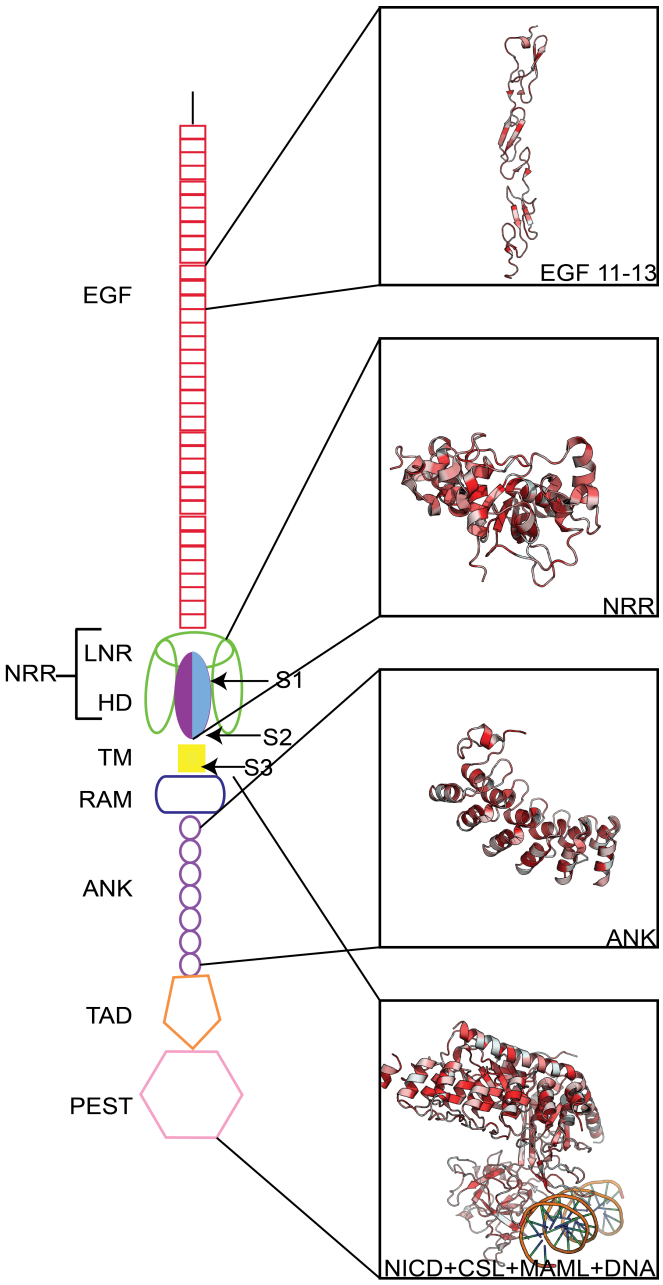

Figure 1.6- Domains of Notch1. Notch 1 has 8 distinct domains. Major soluble domains structures have been determined. Known structures of complete domains are aligned with model representation. Structures colored by hydrophobicity in Pymol. PDB accession codes: 4D0E, 3IO8, 2F8Y, and 3V79 (top down).

The transmembrane segment (TM) links the extracellular domain to the intracellular. Despite the fact that TM cleavage is as an essential part of the signal activation; the TM segment has not been extensively studied until recently (see Chapter 3 and 4). It is known that the TM segment is cleaved in the membrane by γ-secretase,[160] releasing a small extracellular peptide (Nβ)[161] and the large Notch intracellular domain (NICD).[92, 162-164]

The first segment of the NICD is the RAM domain. This stands for RBPJ-associated molecule, and this is where the NICD binds with the transcription partner RBP-Jκ (also known as CSL).[165, 166] It is thought that until binding of the complex occurs, the RAM domain is unstructured.[167] Following the RAM domain is a series of 7 ankyrin repeats that are required for signal transduction.[168] This segment has contacts with the RBP-Jκ partner and is essential for the recruitment of the third transcription factor partner Maml (Mastermind in Drosophila).[167, 169, 170] The penultimate segment of the NICD is the transcriptional activation domain. This portion of the molecule is where the transcriptional activity occurs and can happen in an autonomous manner.[171-174] The final segment is the PEST domain. The PEST stands for a protein sequence rich in proline (P), glutamic acid (E), serine (S) and threonine (T). These sequences are generally associated with proteins that are rapidly degraded.[175] This domain is phosphorylated by CDK8 and targeted for polyubiquitination and proteosomal degradation after signaling. Rapid degradation of the NICD transcription factor serves to regulate gene transcription and to rapidly respond to the cellular input during development. This allows for careful control of the duration of Notch signaling.[171, 176, 177]

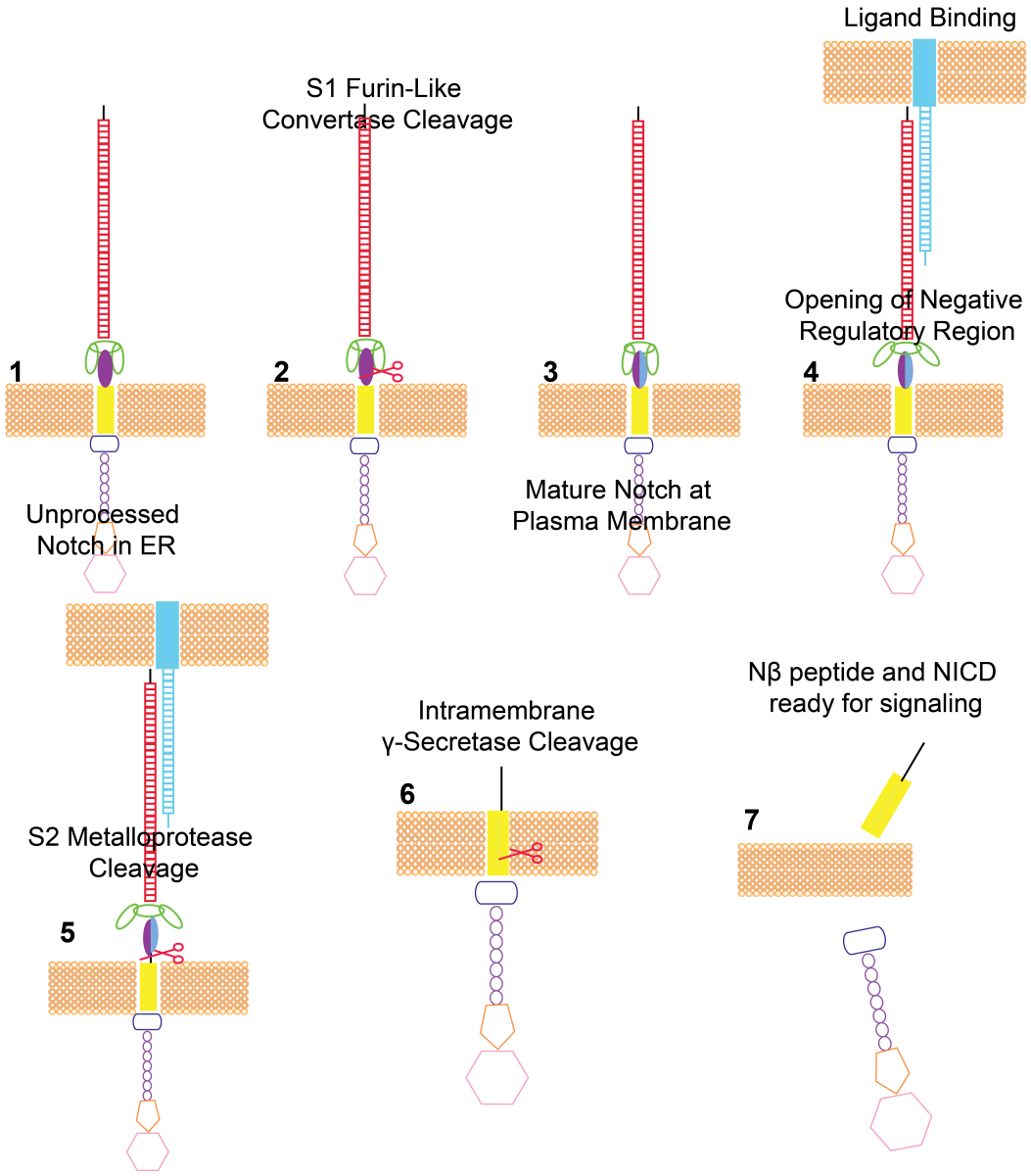

Figure 1.7- Notch Processing. Notch is cleaved at site S1 to form a heterodimer. The heterodimer is transported to the plasma membrane. A trans binding with a ligand induces the opening of the negative regulatory region. Opening of the negative regulatory region exposes the S2 cut site to a metalloprotease and is cleaved allowing the extracellular domain to be endocytosed by the ligand. The NEXT is cleaved in the membrane to release the NICD and a soluble peptide Nβ.

The life cycle of Notch signaling/ processing is mapped out in Figure 1.7. Notch begins in the ER as a holoprotein (**1**). In the Golgi the protein is extensively glycosylated, and cleaved by a furin-like convertase, resulting in a dimer of two non-covalently linked portions (**2**). The heterodimer is trafficked to the plasma membrane where signaling can begin (**3**). In general, the signaling pathway is initiated when mature Notch at the plasma membrane has a *trans* binding interaction with a membrane bound protein ligand from a neighboring cell to the extracellular EGF domain of the Notch protein (**4**).[150] There are also data that suggest that a cis interaction is actually inhibitory.[178] This binding event triggers trans-endocytosis of the Notch-bound ligand.[179]

The role of endocytosis in the signaling pathway is very important. In canonical Notch signaling the ligand is also a type 1 membrane protein on a neighboring cell. After ligand binding, productive signaling generally requires the endocytosis of the ligand back into the cell.[180, 181] Endocytosis induces a force on the Notch extracellular domain that mechanically extends the negative regulatory region of the protein including residues 1449-1731.[156] This force exposes the previously buried S2 cut site (**4**) to the ADAM 10/17 metalloprotease,[182-184] which cleaves the protein to release the extracellular domain (**5**) in the committed step of the signaling pathway. Research has indicated that after the Notch extracellular domain has been cleaved at S2, the ectodomain is endocytosed into the signal-donor cell.[179, 181]

While the exact order of the subsequent processing, trafficking, and cleavage steps are still being investigated, Notch is endocytosed and cleaved in its TMD by γ-secretase (**6**),[160] releasing a small extracellular peptide (Nβ)[161] and the large Notch

intracellular domain (NICD) (**7**).[92, 162-164] After translocation to the nucleus, the NICD forms a transcriptional activator complex with CSL[168] and MAML[185] that targets a number of different genes.[186, 187] Further exploration behind the mechanism of Notch processing is important both to understanding Notch biology and to a better understanding of the mechanism of action of γ-secretase and thus AD.

Summary

The work in this dissertation is an exploration of the proteins related to AD and how increasing the biochemical and biophysical knowledge can enhance the field's understanding of AD etiology. This work includes careful protein expression and biochemistry, NMR, circular dichroism, and computational analysis of protein structure. Chapter 2 describes the characterization of GSAP, leading to results that challenge what had been originally published. Chapter 3 describes the work to purify the transmembrane segment of Notch, assign the backbone, and analyze the protein topology and backbone dynamics. Chapter 4 provides a careful comparison of the structure, membrane tolerance, and cholesterol binding of the Notch TM segment with the protein C99. This comparison will help to differentiate these two proteins in a way that may lead to a Notch sparing γ-secretase inhibitor.

II. Purification and Characterization of the Human γ-Secretase Activating Protein[1]

Introduction

Alzheimer's Disease (AD) is a devastating neurodegenerative disease that impacts millions of people worldwide at enormous personal and economic cost.[188] Unfortunately, there is currently no cure or effective treatment, but researchers have made significant progress in characterizing the pathophysiology of AD.[189] The most widely-accepted hypothesis for disease etiology revolves around the amyloid precursor protein (APP).[29] APP is cleaved by β-secretase to generate its 99 residue transmembrane C-terminus (C99), which is then cleaved by γ-secretase to produce amyloid beta (Aβ) peptides of different lengths. These peptides form neurotoxic oligomers that go on to deposit as neuritic plaques, the pathological markers of the disease.

Inhibition of the heterotetrameric γ-secretase to block cleavage of C99 would reduce Aβ production.[75, 190, 191] Unfortunately, γ-secretase has numerous substrates and has not, so far, been an effective therapeutic target because of the important role that its cleavage of other substrates, particularly Notch, plays in cellular differentiation.[192] As such, there is great interest in exploring how to prevent or modulate C99 cleavage

[1] This work is adapted from Deatherage CL, Hadziselimovic A, Sanders CR Purification and characterization of the human γ-secretase activating protein. Biochemistry. 2012 Jun 26;51(25):5153-9. doi: 10.1021/bi300605u

without inhibiting cleavage of other γ-secretase substrates. This imperative resulted in the discovery of the γ-secretase activating protein (GSAP).

GSAP was first described by He et al. 2010.[123] A previous study had shown that the Abl kinase inhibitor imatinib decreases Aβ production, likely by inhibiting γ-secretase activity.[122] The search for the imatinib target led to photo-labeling of the C-terminal domain of the uncharacterized Pigeon Homolog Protein (PION). The domain is proteolytically released from PION under cellular conditions, the resulting protein being referred to as GSAP. GSAP appears to form a ternary complex with γ-secretase and C99, as determined through immunoprecipitation reactions and pull-down assays. Knockdown of GSAP through siRNA in N2a cells selectively lowered Aβ levels, and did not reduce the cleavage of other γ-secretase substrates. GSAP knockdown also reduced Aβ plaque burden in a mouse model of AD.[123] These data suggest that GSAP may selectively promote Aβ production by promoting γ-secretase cleavage of C99, making GSAP a potential AD drug target. Since the initial discovery of GSAP, one additional research paper has been published, which characterized the immunohistochemical distribution of GSAP in the brains of AD patients.[193] GSAP immunoreactivity was observed in four distinct morphological structures present in different regions of the brain in AD patients, one of these structures was largely unique to AD brains as compared to age-matched control brains. GSAP immunoreactivity was also detected in close proximity to presenilin (PS1, a component of γ-secretase) as well as in close association with Aβ-containing senile plaques. While recombinant expression and purification of GSAP was briefly mentioned in these reports, methods

were not provided. This paper details the expression, purification, and characterization of GSAP.

Materials and Methods

Materials. BL21 (DE3) and Rosetta (DE3) competent cell lines and the pET32a vector were purchased from EMD Millipore (Darmstadt, Germany). The restriction enzymes NdeI, XhoI, BamI and NcoI were purchased from New England Biolabs (Ipswich, MA). The $^{15}NH_4Cl$ used to isotopically label GSAP was purchased from Cambridge Isotope Laboratories (Andover, MA). Ampicillin and MEM vitamin solution were purchased from Cellgro (Manassas, VA). Imatinib mesylate was purchased from Selleck Chemical Company (Houston, TX). Ni-NTA chromatography resin was purchased from Qiagen (Valencia, CA). The protease inhibitor P8849, Empigen BB detergent (n-dodecyl-N,N-dimethylglycine) and imidazole (≥99% titration grade) were purchased from Sigma-Aldrich (Saint Louis, MO). n-Dodecylphosphocholine (DPC), lyso-myristoylphosphatidylglycerol (LMPG) and isopropyl β-D-1-thiogalactopyranoside (IPTG) were purchased from Affymetrix/Anatrace (Maumee, OH).

Cloning and Construction of the vectors encoding His-tagged forms of GSAP. GSAP corresponds to the 121 residue (amino acids 733-854) C-terminus of the human pigeon homolog protein (PION). The GSAP gene (NM_017439.3) was purchased from GeneCopoeia (Rockville, MD). Two constructs were prepared, with either N- or C-terminal His purification tags (His_6 and His_{10}, respectively). To construct the C-terminally His_{10}-tagged construct, the GSAP DNA was digested with *Nde*I and *Xho*I after PCR amplification, and was then was inserted into the pET-21b vector. The N-terminal His_6-

tagged construct was similarly engineered using *Nco*I and *Xho*I restriction enzymes and a pET-16a vector. Constructs were confirmed by DNA sequencing.

A second set of constructs was prepared to replicate as closely as possible the constructs used in He et al. 2010.[123] The first was a pET-32a vector encoding a fusion protein in which thioredoxin is linked to the N-terminus GSAP through an intervening His_6 tag. As with the His_6-tagged constructs expressing only GSAP, the thioredoxin fusion protein was constructed from the DNA digested with *Bam*I and *Xho*I after PCR amplification of the GSAP gene and was then inserted into the pET-32a vector. A second construct, expressing only thioredoxin, was prepared as a control by inserting a stop codon just before the start of the GSAP coding region in a pET-32a vector. This was accomplished using standard site-directed mutagenesis methods (QuickChange, Agilent Technologies, Santa Clara, CA).

Expression of GSAP in E. coli. Vectors were transformed into *E. coli* BL21(DE3) cells, which were plated onto ampicillin LB-agar plates and then incubated overnight at 37°C. A single colony was used to inoculate a 5ml culture of LB media containing 100μg/ml of ampicillin. The starter culture was grown for eight hours at 37°C. A 1 L culture of M9 minimal media was prepared using $^{15}NH_4Cl$ for isotopic labeling. The medium for large-scale growth also included ampicillin, glucose, MEM vitamins, 0.1 mM $CaCl_2$, and 1 mM $MgSO_4$. Starter culture (1.2 ml) was added directly to the 1 L culture and the cells were grown at room temperature until the OD_{600} reached 0.8. Protein expression was induced using 1 mM IPTG, and the cells were harvested by centrifugation 24 hours after induction. Expression of the recombinant GSAP was confirmed by Western blotting

using a monoclonal anti-5X His mouse antibody (Cell Signaling Technology, Danvers, MA).

Purification of N- and C-Terminally His_6-Tagged GSAP. The harvested cells were weighed and lysed in 20 ml of lysis buffer (75 mM Tris, 300 mM NaCl, 0.2 mM EDTA, pH 7.8) per gram of cells. Also added to the following concentrations were 5 mM MgAcetate, 2 mg/ml of lysozyme, 0.2 mg/ml DNase and RNase, and 50 μl of protease inhibitor per gram of cells. The suspension was tumbled for 90 minutes at room temperature. Following tumbling, cells were further disrupted by five-minute probe sonication with a 50% duty cycle at approximately 57 watts using a Misonix (Farmingdale, NY) sonicator. The lysate was centrifuged at 20,000 rpm in a Beckman-Coulter (Indianapolis, IN) JA 25.5 rotor (approximately 48,000xg) and the pellet, which includes inclusion bodies, was retained. The inclusion bodies containing GSAP were solubilized in 20 ml of lysis buffer per original gram of cells using 3% Empigen (%v/v), a harsh detergent. This solution was tumbled at room temperature until a clear mixture was observed (approximately 4.5 hours). The sample was then centrifuged to remove any remaining insoluble particulates. Ni-NTA resin (1.2 ml per gram of cells) was equilibrated with buffer A (40 mM HEPES, 300 mM NaCl pH 7.8). The supernatant was tumbled with the resin for one hour at room temperature. The resin was loaded into a column and sequentially washed with buffer A containing 3% Empigen (%v/v), and buffer A containing 30 mM imidazole and 1.5% Empigen (%v/v), respectively, to elute all non-His_{10}-tagged proteins from the resin. Empigen was then exchanged for the detergent n-dodecylphosphocholine (DPC) by re-equilibrating the column with 12 column volumes of 20 mM phosphate, pH 7.2, containing 0.5% DPC (%w/v). GSAP was

eluted from the column with 250 mM imidazole containing 0.5% DPC (%w/v), pH 7.8. Purification was monitored by A_{280}. After purification, 2 mM DTT was added to the sample to reduce disulfide bonds.

The purification process was monitored by SDS-PAGE gel electrophoresis. Electrophoresis experiments were carried out using an Invitrogen (Grand Island, NY) Novex-Mini Gel system and NuPAGE 4-12% Bis-Tris polyacrylamide gels and MES running buffer.

Purification of Thioredoxin-His_6-GSAP Fusion Protein. The purification of Trx-His_6-GSAP was alluded to but not described in the original paper,[123] but is similar to the His_{10}-GSAP purification strategy described above (personal communication). Trx-His_6-GSAP expressing cells were grown, harvested, and lysed as above. After lysis, the supernatant was collected and bound to Ni-NTA resin equilibrated in 50 mM phosphate, 500 mM NaCl pH 7.8. The slurry tumbled for one hour at room temperature. The resin was rinsed with 50 mM phosphate, 500 mM NaCl pH 7.8 and then washed with 50 mM phosphate, 500 mM NaCl, 40 mM imidazole pH 7.8 to remove any remaining non-specifically bound protein. Trx-His_6-GSAP was eluted from the column with 50 mM phosphate, 500 mM NaCl, 300 mM imidazole pH 7.8. The eluate was concentrated to a volume below 5 ml and filtered with a 0.2 μm filter. The sample was then subjected to size exclusion chromatography using a HiPrep™ Sephacryl™ S300 16/60 gel filtration column on an AKTAprime™-plus FPLC eluted with 20 mM HEPES, 200 mM NaCl, 1 mM EDTA pH 8.0.

Circular Dichroism (CD) Spectroscopy. Protein samples were purified as described above and were exchanged into a 25 mM sodium phosphate buffer, pH 7.5, containing

0.5% DPC using a PD-10 desalting column (Bio-Rad). The sample and buffers were passed through a 0.2 μm filter before CD data collection. Far-UV CD data was collected from 190 to 260 nm on a Jasco (Easton, MD) J-810 CD spectropolarimeter. Data from five scans were averaged together and blank-corrected.

Solution NMR Spectroscopy. For NMR spectroscopy, the pH of GSAP was adjusted to 7.5 and D_2O to 10% was added, followed by concentration through ultrafiltration using an Amicon Centrifugal Filter unit molecular weight cut-off 10,000 Da (Millipore, Billerica, MA). An HSQC spectrum was collected on a 600 MHz Bruker AVANCE III spectrometer at 298 K using TopSpin3 and a standard Bruker pulse sequence.

Titration of C99 by GSAP. Uniformly ^{15}N-labeled C99 with a His_6-containing purification tag at its C-terminus was expressed and purified as described in Beel et al. 2008,[35] with a few minor variations. Cultures of *E. coli* with an expression vector encoding C-terminally His_6-tagged human C99 were grown at 37°C in minimal media with Cellgro MEM vitamins and induced at OD_{600}= 0.8 using IPTG, at 18°C overnight. Cells were lysed and inclusion bodies were isolated and washed three times with lysis buffer followed by sonication and recentrifugation. Tagged C99 was then purified using Ni-NTA affinity chromatography into 0.05% LMPG micelles with 250 mM imidazole pH 7.8. After purification, U-^{15}N-C99 was buffer-exchanged and centrifugally concentrated in Amicon concentrators to a final condition of 0.6 mM, with 2.5% LMPG and 100 mM imidazole. The pH was adjusted to 7.5 using glacial acetic acid and ammonium hydroxide. Unlabeled GSAP was prepared as described above using 0.05% LMPG as the detergent for the final purification steps. The purified protein was buffer-exchanged

to reduce the imidazole concentration to 100 mM and concentrated to 0.45 mM. The pH was adjusted to 7.5 and LMPG was added to a final concentration of 2.5%.

For titrations, NMR samples were prepared with 0.1 mM C99 in each sample and increasing molar ratios GSAP up to 4:1 GSAP:C99, in 100 mM imidazole, 2.5% or 10% LMPG. $^{1}H,^{15}N$-TROSY spectra were collected at 298 K for each sample to determine the effect of GSAP on the chemical shifts of the peaks in the C99 spectrum.

Titration of Imatinib by GSAP. GSAP was prepared as described, except that the final buffers were made using D_2O. The sample was concentrated and passed over a PD-10 desalting column to remove all traces of imidazole. This sample contained 0.325 mM GSAP in 25 mM sodium phosphate in D_2O, 1% DPC, pH 7.5 and served as a stock solution for the titration. Starting with a solution of 339 mM imatinib mesylate in DMSO, a 1 mM stock solution of the drug in 1% DPC (%w/v) in D_2O was prepared. The NMR samples were prepared with 50 μM imatinib, 25 mM imidazole and increasing amounts of GSAP up to a four-fold molar excess. The imatinib 1-D ^{1}H NMR peaks not obscured by detergent and protein were monitored for changes with increasing amounts of GSAP using a 600 MHz magnet at 298 K.

Results

Expression and Purification of GSAP. The GSAP domain of the PION [123] was cloned into pET vectors. Two constructs, one with an N-terminal (pET16) His_6- and one with a C-terminal (pET21) His_{10}- purification tag were cloned. Both constructs overexpressed well in different strains of *E. coli* (BL21(DE3) and Rosetta(DE3)). It was found that the N-terminally tagged construct was highly expressed, but was highly unstable and prone

to aggregation. For this reason, the experiments here were conducted using the C-terminally tagged construct, which behaved more favorably.

Following expression, cell lysis, and centrifugation, GSAP was located primarily in inclusion bodies (IB), despite culturing the cells in minimal medium at room temperature, conditions sometimes found to promote folding of unstable or misfolding-prone recombinant proteins. Consequently, IB solubilization and protein refolding was necessary. Solubilization methods tested included dissolution of IB in 8M urea and 0.2% sodium dodecyl sulfate (SDS), both together and separately, followed by removal of the denaturant under different buffer and pH conditions, ranging from pH 5.5 to 7.8. Unfortunately, despite much effort all refolding attempts resulted in precipitation of GSAP. For further details on refolding attempts and outcomes, see Table 2.1.

Table 2.1- Summary of Attempts to refold Non-immobilized GSAP

Experiment	Method	Outcome
Dialysis-Based Refolding	After solubilization of IB by SDS and 8M urea, sample was dialyzed against decreasing amounts of denaturant at pH 7.8.	GSAP precipitated out of solution during dialysis in 0M urea.
Dialysis-based refolding after purification in denaturant	IB were solubilized in 8M urea overnight, followed by metal ion affinity chromatography-based purification of GSAP in the presence of 8M urea. After purification, the denatured protein was dialyzed against successively decreasing amounts of urea. This was preformed in different buffer conditions at pH 5.5, 6.5 and 7.8.	Purified GSAP eluted cleanly from the nickel column and was soluble indefinitely in 8M urea. Protein began to precipitate during the 4M urea dialysis step, ending with a total loss of GSAP due to precipitation by the final 0M urea stage.
Rapid dilution refolding after purification	IB was solubilized overnight in 8M urea, and then purified as usual in 8M urea. After purification, the urea-denatured protein was slowly added drop-wise into a large volume of rapidly stirring buffer containing 50 mM HEPES, 300 mM NaCl, and 400 mM L-Arginine	Protocol initially seemed to be effective; there was no visible precipitation in the large rapidly stirring volume. However, when sample concentration was initiated through both centrifugal and stirred cell concentration the protein catastrophically precipitated from solution.
Refolding after purification in detergent	After solubilization of IB by SDS and 8M urea, sample was bound to column and purified in 0.2% SDS. SDS was then dialyzed out of solution at pH 7.8	The protein precipitated out of solution as SDS was fully dialyzed out of the sample.

Additional experiments were carried out in an effort to refold the protein, this time with GSAP immobilized by binding to Ni-NTA resin through its His_{10} tag. Inclusion bodies were solubilized with 8M urea and 0.2% SDS and incubated with Ni-NTA resin. The first on-column refolding test involved the stepwise removal of SDS and urea from the solution bathing the resin. Subsequent on-column refolding attempts and the outcome are listed in Table 2.2.

Table 2.2- On-column refolding attempts

Experiment	Method	Outcome
Refolding on the column by urea removal	After solubilization of IB by SDS and 8M urea, sample was bound to column and refolded with 15% glycerol and decreasing amounts denaturant on the column.	GSAP could not be eluted from the resin after all of the denaturant had been rinsed away.
Purification with DM	IB solubilized with Empigen, bound to the metal ion affinity resin, followed by equilibration and attempted elution with a solution containing the mild non-ionic detergent, β-decylmaltoside.	GSAP failed to elute from column with 250 mM imidazole and 0.5% DM at pH 7.8.
Purification without detergent	IB were solubilized with Empigen, followed by binding of GSAP to metal ion affinity resin and successive re-equilibration with DPC and DM solutions, with a detergent free solution, followed by attempted elution of the protein using a detergent-free buffer.	GSAP failed to elute from column upon attempted elution using 250 mM imidazole, pH 7.8.

After complete removal of denaturant, an attempt was made to elute the protein from the column with 250 mM imidazole, pH 7.8. However, GSAP did not elute, indicating insolubility in a denaturant-free and detergent-free elution buffer. Based on the knowledge that GSAP can be solubilized using a harsh detergent (SDS), additional attempts were made to refold GSAP in the presence of a milder detergent.

Inclusion bodies were solubilized using the harsh zwitterionic detergent Empigen and GSAP was then associated with the nickel resin. The detergent present in the solution that bathes the Ni-NTA-bound GSAP was then switched from Empigen to one of several detergents: DPC, lyso-myristoylphosphatidylglycerol (LMPG) or decylmaltoside (DM), followed by attempted elution using 250 mM imidazole in that same detergent solution. It was found that GSAP could not be eluted in DM detergent micelle solutions, but did elute when either DPC or LMPG solutions were used. Both of these detergents have previously been widely used as membrane mimetics in studies of membrane proteins.[194] Figure 2.1 shows an SDS-PAGE gel that documents protein purification. The elution fraction has only two bands, which have been confirmed by mass spectrometry to be the monomer and dimer forms of GSAP. The dimer band is likely due to the presence of the single cysteine at amino acid position 32, as this band is absent in the presence of a reducing agent. The total yield of purified protein was approximately 15 mg per liter of culture.

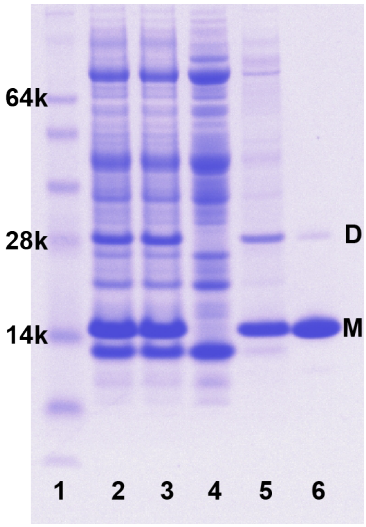

Figure 2.1- GSAP Purification. A 4-12% polyacrylamide gel was stained with Coomassie R-250 brilliant blue, with lanes: 1) SeeBlue Plus 2 protein molecular weight markers. 2) Whole cell lysate solubilized with 4M urea and SDS. 3) Sonicated cell lysate further solubilized with 4M urea and SDS. 4) Cellular supernatant after centrifugation. 5) Insoluble inclusion bodies solubilized with SDS. 6) Purified protein fraction after elution with 250mM imidazole elution plus 0.5% DPC. All samples were first mixed with an SDS loading buffer prior to loading on the gel. (M) monomeric GSAP and (D) dimeric GSAP, as confirmed by mass spectrometry.

These results indicate that GSAP is highly prone to form insoluble aggregates. Despite extensive testing of refolding conditions we found the protein could be solubilized only in the presence of detergents or denaturing agents.

We next tested a fusion protein form of GSAP. In previous work,[123] recombinant GSAP was expressed as a fusion protein with thioredoxin, a widely used fusion partner for enhancing the solubility and stability of partner proteins.[195, 196] We therefore constructed and tested a thioredoxin-His_6-GSAP-thioredoxin fusion protein. We found that the fusion protein also expressed primarily into inclusion bodies. A small fraction that expressed in soluble form in the supernatant was associated with Ni-NTA resin, but could not then be eluted from the column in the absence of a harsh detergent, such as SDS. The amount of protein that was purified without detergent was negligible.

We also attempted to generate soluble GSAP without a fusion partner in the commercial competent cell line SoluBL21™ (AMS Biotechnology, El Toro, CA). This cell line has been modified to enhance the solubility of difficult proteins and to allow for soluble expression where no soluble expression is seen in standard competent cell lines. When expressed in SoluBL21 cells, GSAP was initially soluble based on detection of a GSAP band on an SDS-PAGE gel in the supernatant of the cell lysate after centrifugation. However, after binding to the nickel resin followed by elution of all impurities in a low concentration imidazole buffer, GSAP failed to elute from the nickel resin in the presence of 250 mM imidazole. Application of SDS to the resin released the protein (data not shown). This suggests that while expression conditions can be found that initially produce a soluble form of GSAP, the protein is highly susceptible to

aggregation. This result implies that a propensity of GSAP to aggregate is an intrinsic property of this protein.

Characterization of Solubilized GSAP. The properties of GSAP were examined in detergent-containing solutions in which the protein was soluble. Secondary structure predictions indicate that GSAP is largely α-helical with stretches of random coil or unstructured loops between helices. Near-UV CD spectroscopy in the 250-310 nm range (25 mM $NaPO_4$ pH 7.5) revealed a flat spectrum, providing no evidence for stable tertiary structure (data not shown). The far-UV CD spectrum collected under the same sample conditions shows a pattern consistent with mostly helical secondary structure (Figure 2.2). Analysis of this spectrum using the secondary structure prediction server K2D3 suggests that GSAP is 92% helical.[197]

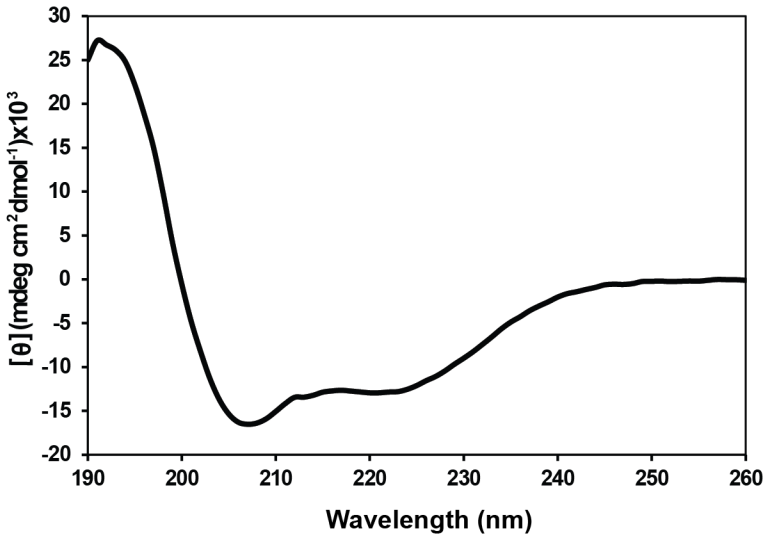

Figure 2.2- Estimation of secondary structure from CD data. This spectrum indicates that GSAP is largely α-helical with approximately 92% helicity based on analysis using the K2D3 secondary structure prediction server. The data represents an average of 5 scans.

Two-dimensional $^{1}H,^{15}N$-HSQC NMR spectra are routinely used to provide general insight into protein structure. All NMR spectra of GSAP-containing samples were collected at pH 7.5 because the protein precipitated when reduced to a neutral or acidic pH. The HSQC spectrum of ^{15}N-GSAP in DPC micelles is shown in Figure 2.3 and is poorly dispersed, showing only a fraction of the expected 126 backbone amide peaks. This spectrum is consistent with GSAP being largely α-helical but lacking well-defined tertiary structure, suggestive of a molten globular protein.

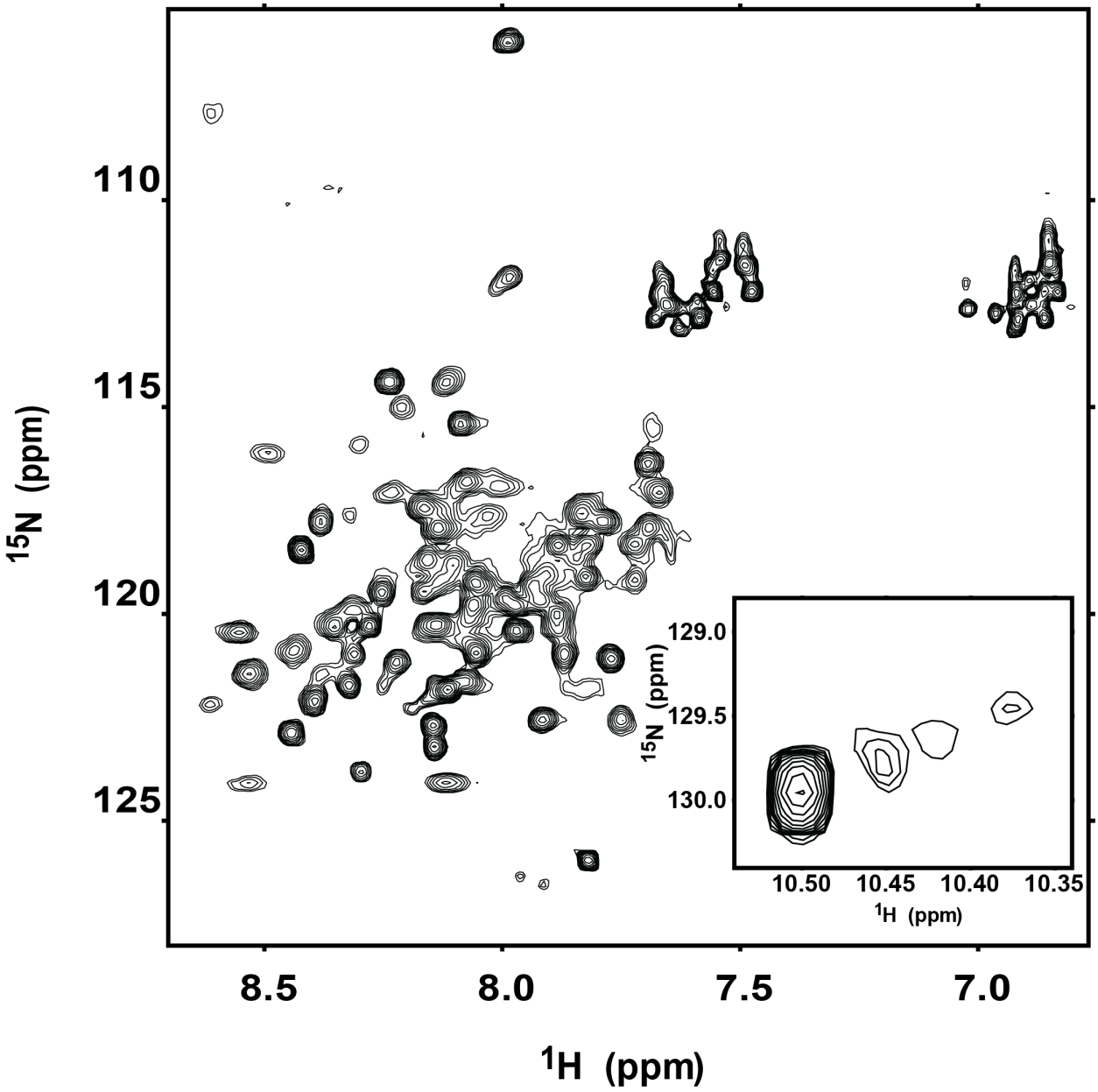

Figure 2.3- 600MHz spectrum of GSAP. The sample contains ca. 300 μM uniformly ^{15}N-labeled GSAP in 0.5% DPC, pH 7.5, 2 mM DTT and 10% D_2O at 298 K. The protein precipitated when the pH was reduced to neutral or acidic values.

GSAP has previously been shown to bind both the small molecule kinase inhibitor imatinib and the 99 residue transmembrane C-terminal domain of the amyloid precursor protein (C99), which serves as the substrate for γ-secretase cleavage to produce the amyloid-β polypeptides.[123] However, in neither case is it clear whether binary GSAP-imatinib or GASP-C99 complexes are formed, or whether they form complexes only in the presence of a tertiary partner such as γ-secretase. We therefore tested whether recombinant GSAP can form binary complexes with either imatinib or GSAP.

$^{1}H,^{15}N$-HSQC NMR spectra of 150 μM isotopically-labeled GSAP were collected in the absence and presence of a 1:1 molar ratio of imatinib. No shifts in GSAP resonances were seen upon addition of imatinib, as shown in Figure 2.4. In the reverse experiment, 1D NMR spectra were taken of 50 μM imatinib upon titration with increasing amounts of GSAP. Addition of GSAP to a 4X molar excess relative to the drug did not significantly affect the imatinib peaks (Figure 2.5). The results suggest that affinity between GSAP and imatinib under the tested conditions is weak or non-existent.

To test for complex formation between C99 and GSAP, $^{1}H,^{15}N$-HSQC NMR was used to monitor titration of uniformly ^{15}N-labeled C99 by increasing molar ratios of unlabeled GSAP. These experiments were initially carried out in 2.5% (w/v) LMPG micelles. Under these conditions only modest and non-saturable changes were seen in backbone amide $^{1}H,^{15}N$ peak positions (Figure 2.6), consistent with non-specific or weak interactions between these two proteins under the conditions of this experiment.

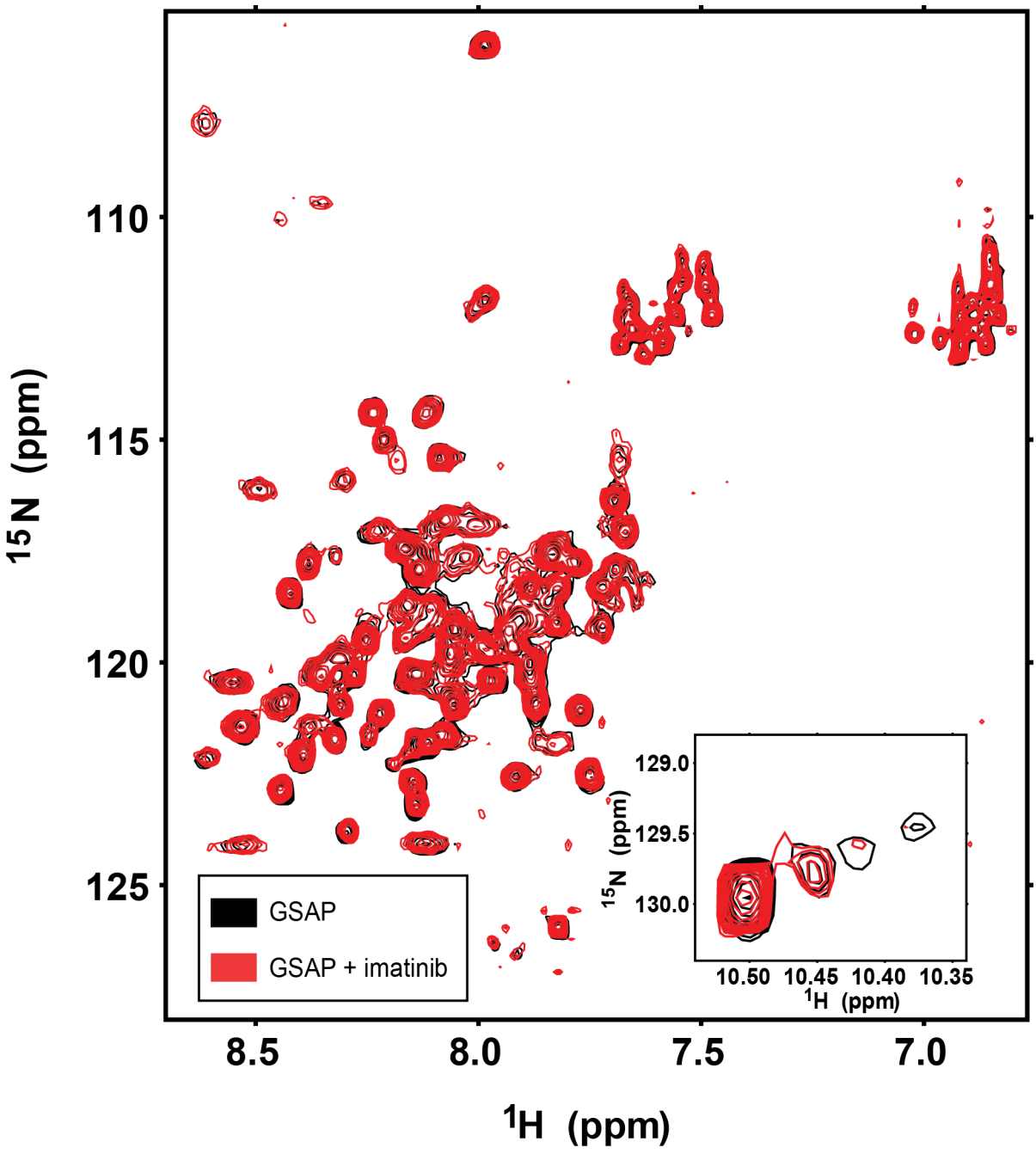

Figure 2.4. GSAP interaction with imatinib. An overlay is shown of 600 MHz HSQC NMR spectra of U-^{15}N-GSAP and no imatinib (black) and of GSAP in the presence of 1:1 molar ratio of imatinib (red). These samples contained 0.15 mM GSAP in 0.5% DPC, pH 7.5, 2 mM DTT, and 10%D_2O at 298 K.

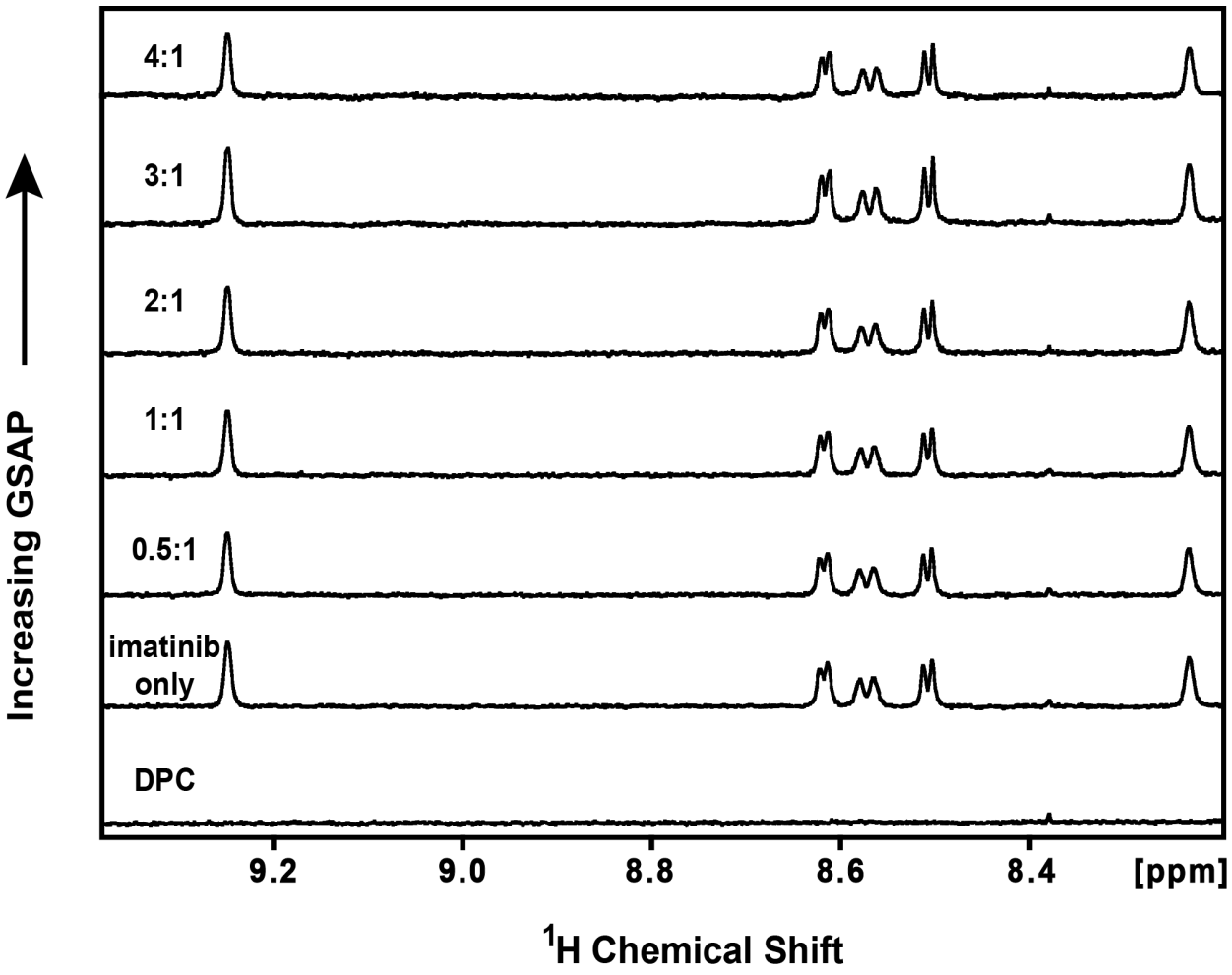

Figure 2.5. Imatinib titration by GSAP. The aromatic regions of the 1D ^{1}H NMR spectra of 50 μM imatinib are shown as a function of increasing GSAP concentrations: 0 μM, 25 μM, 50 μM, 100 μM, 200 μM. Spectra were acquired in the presence of 1% DPC and 100% D_2O at pH 7.5 and 298 K and normalized to an internal standard. The listed ratios are the GSAP:imatinib mole to mole ratios.

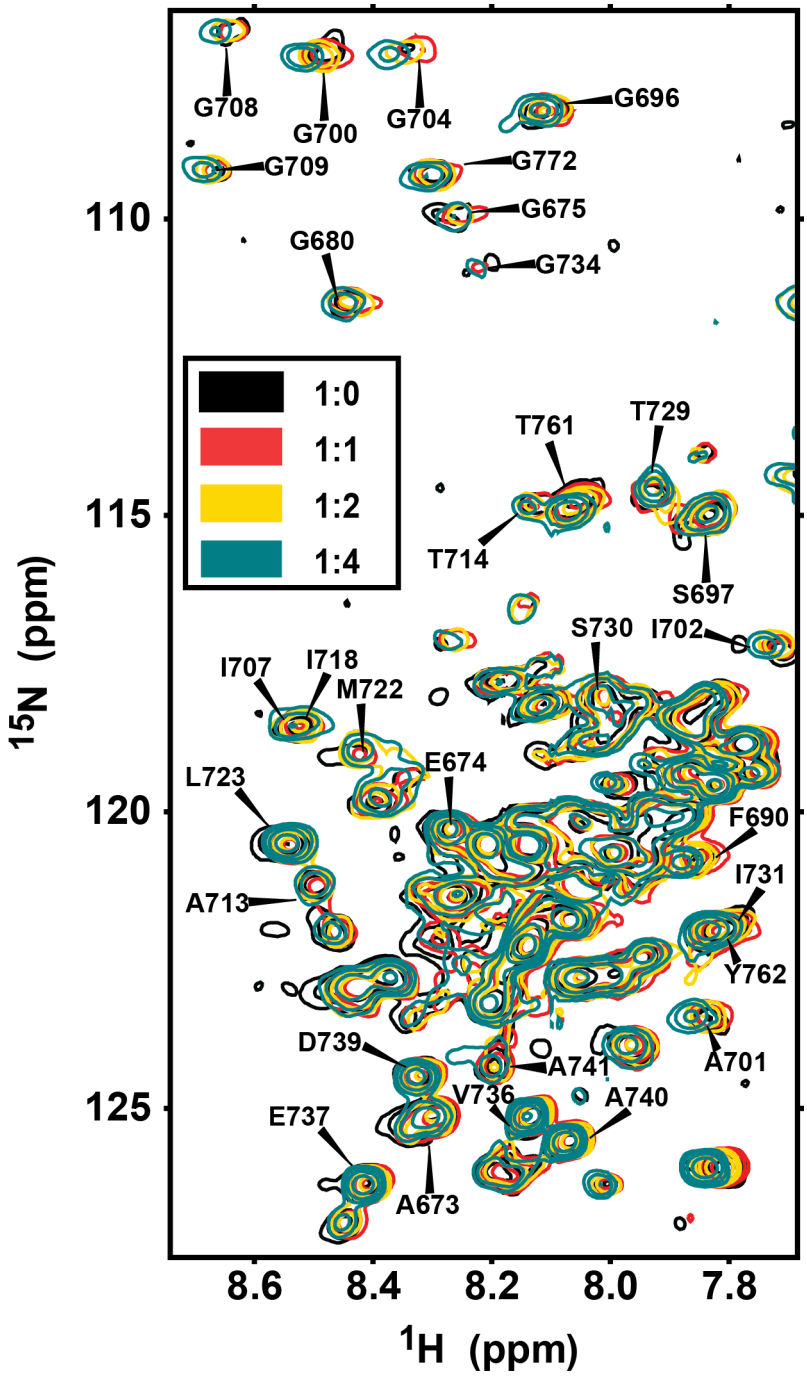

Figure 2.6. Titration of U-^{15}N-C99 by GSAP. The lower portion represents backbone amide peaks from most residues except for glycines, while the upper portion shows the region of the spectrum dominated by glycine resonances. The samples contained 2.5% LMPG, pH 7.5, at 298 K. The listed ratios in the upper panel are the C99:GSAP mole to mole ratios.

Indeed, while the GSAP interaction domain on C99 was proposed to be localized to residues 725-735 in the juxtamembrane cytosolic domain [123], peaks from this domain were no more likely to undergo large shifts in response to GSAP than peaks found in the transmembrane domain (residues 700-723) for from the extracellular domain of C99 (residues 672-699), the latter of which is located on the other side of the membrane from GSAP under physiological conditions. An additional titration was completed in which the same protein concentrations were used but the detergent concentration was increased to 10% LMPG. Under these conditions little to no chemical shift changes were seen for C99 peaks upon titration by GSAP. The fact that the GSAP-induced changes in the spectrum seen at 2.5% LMPG in Figure 2.6 can be eliminated by increasing the micelle concentration (at fixed protein concentration) suggests that GSAP has some affinity for the micelle surface that leads to non-specific interaction between GSAP and C99 when both are confined to the same micelle, an interaction that can be minimized by simply adding excess (C99-free) micelles, to which GSAP will redistribute. These results indicate that any binding of GSAP to C99 in LMPG micelles is either non-specific or very weak. These results do not, of course, rule out the possibility that GSAP and C99 do specifically and avidly interact, but only when both are bound to γ-secretase.

Discussion

The notion that GSAP represents a protein that can be targeted by an already-approved drug to reduce production of the amyloid-β polypeptides is extremely appealing. Accordingly, there is a compelling impetus to conduct biochemical and biophysical studies of the structure and interactions of this protein. Unfortunately, based

on the work presented here, working with GSAP is likely to be challenging. It appears to be insoluble in many conditions and was seen to be molten globular under detergent micellar conditions in which it is soluble. These observations hold regardless of the nature of the protein construct, regardless of the *E. coli* expression strain, and regardless of the refolding methods and final solution composition. While we cannot rule out the possibility that a refolding method and/or solution conditions may ultimately be found in which GSAP is both soluble and well folded, we were not able to identify any such conditions despite considerable effort.

Under conditions in which GSAP is solubilized by the presence of DPC micelles it was seen to be a mostly α-helical protein, but did not form well-ordered tertiary structure. It was also observed that under micellar conditions GSAP does not undergo specific association with either imatinib or the C99 domain of the amyloid precursor protein. It does not appear that the molten globular form of GSAP can be induced to adopt stable tertiary structure by interaction with either of these potential binding partners.

Despite the failure in this work to observe formation of well-ordered tertiary structure by GSAP or complex formation with either imatinib or C99 titrations, our results are not definitively negative. We cannot rule out the possibility that an unidentified refolding pathway and/or folding-favorable final solution conditions exist that we have not discovered. We also cannot rule out the possibility that GSAP is subject to an unidentified post-translational modification under native cellular conditions that is required for folding or solubility in detergent-free solutions. While GSAP was not seen to form binary complexes with either imatinib or C99, it may do so under cellular

conditions, perhaps as a result of ternary complex formation with an additional binding partner such as γ-secretase.

Our results should not be taken to imply a challenge of the data or interpretations regarding the GSAP protein as presented in previous work.[122, 123] The previous studies were carried out primarily using cell-based methods involving model mammalian cell lines. However, for those considering the pursuit of biophysical studies on this protein, our results suggest that work with recombinant GSAP may prove difficult. We were unable to find conditions in which this protein is water soluble to an appreciable degree unless detergent micelles were used to facilitate solubilization, presumably by stabilizing a hydrophobic surface on GSAP that otherwise drives aggregation. When solubilized, GSAP was found to be mostly helical, though it did not adopt a stable tertiary structure. Nevertheless, we cannot rule out the possibility that further exploration of expression, purification, and protein refolding methods may eventually lead to a form of GSAP that is soluble, folded, and competent to bind imatinib and/or C99.

Acknowledgment

This work was supported by US NIH grant PO1 GM080513. We thank Dr. Paul Greengard and Arvys Proteins for providing us with additional details regarding the GSAP-containing fusion protein expression vector previously used to prepare the protein.[123]

III. Notch Transmembrane Domain: Secondary Structure and Topology[2]

Introduction

The Notch signaling pathway is essential to development, neuronal maintenance, and hematopoiesis. Notch signaling also controls neurogenesis, synaptic plasticity, axonal and dendritic growth, and neuronal death.[135-143] In this pathway the Notch receptor (Figure 3.2A) is cleaved in its luminal domain by a furin-like convertase in the Golgi.[143] This cleavage event leaves the protein as a heterodimer with the extracellular domain (ECD) linked to the combined TM and intracellular domains.[157, 158] The protein is then transported to the plasma membrane. *Trans* binding of a membrane bound protein ligand from a neighboring cell to the extracellular EGF domain of the Notch protein[150] triggers a trans-endocytosis of the Notch-bound ligand.[179] This induces a force on the NOTCH ECD that mechanically extends the negative regulatory region of the protein including residues 1449-1731.[156] This force exposes the previously buried S2 cut site (Figure 3.2B) to the ADAM 10/17 metalloprotease,[182-184] which cleaves the protein to release its ECD in the committed step of the signaling pathway.

While the exact order of the subsequent processing, trafficking, and cleavage steps is still being investigated, Notch is endocytosed and cleaved in its TMD by γ-secretase,[160] releasing a small extracellular peptide (Nβ)[161] and the large Notch

[2] This chapter consists of work adapted from Deatherage CL, Lu Z, Kim JH, Sanders CR. Notch Transmembrane Domain: Secondary Structure and Topology. Biochemistry. 2015 Jun 16;54(23):3565-8. doi: 10.1021/acs.biochem.5b00456.

intracellular domain (NICD).[92, 162-164] After translocation to the nucleus, the NICD forms a transcriptional activator complex with CSL[168] and mastermind (MAML in mammals)[185] that targets a number of different genes.[186, 187] The signaling cascade is terminated when the NICD C-terminal PEST domain is phosphorylated by CDK8 and targeted for polyubiquitination and proteosomal degradation.[171, 176, 177] Researchers have explored the structure of the water- soluble domains of Notch protein associated proteins.[156, 159, 169, 198-202] However, the NOTCH TM and flanking juxtamembrane (TM/JM) domains have not been examined.

As noted, cleavage of this domain is an essential step in the Notch signaling pathway and the prevention of this event can cause significant dysregulation and disease.[203, 204] Moreover, toxicity caused by inhibition of gamma-secretase cleavage of the NOTCH TMD has stymied efforts to prevent or treat Alzheimer's disease by inhibiting gamma-secretase cleavage of the amyloid precursor protein.[110] In this paper, we present the purification and preliminary structural characterization of the combined Notch TM/JM domains.

Materials and Methods

Cloning of the Combined Notch1 Transmembrane and Juxtamembrane (TM/JM) Domains. Three segments of the Notch1 gene were synthesized (1721-1764, 1721-1815, and 1721-1850). (Eurofins Genomics Huntsville, AL). To construct the N-terminally MGHHHHHH-tagged constructs the Notch1 each gene segment was ligated into a pTrcHis vector as an NcoI-HindIII fragment. The synthesized 1721-1850 construct was further modified using standard site-directed mutagenesis to produce additional N-

terminal His_6-tagged constructs of varying lengths by the insertion of a stop codon at different positions (1759, 1765, 1772, and 1791).

Expression of Notch1 in E. coli. Vectors were transformed into *E. coli* BL21(DE3)star cells, which were plated onto ampicillin LB-agar plates and then incubated overnight at 37°C. A single colony was used to inoculate an 8 ml starter culture of LB media containing 100μg/ml of ampicillin. The starter culture was grown overnight at 37°C. A 1 L culture of M9 minimal media was prepared using $^{15}NH_4Cl$ for isotopic labeling. The media was split between two 2.8L Fernbach culture flasks, each with 500ml. The medium for large-scale growth also included 100μg/ml ampicillin, 4mg/ml glucose, MEM vitamins, 0.1 mM $CaCl_2$, and 1 mM $MgSO_4$. Starter culture (4 ml) was added directly to the 0.5L culture and the cells were grown at 37°C until the OD_{600} reached 0.8, at which point protein expression was induced using 1 mM IPTG and the temperature was dropped to 25°C. The cells were harvested by centrifugation 20 hours after induction. Expression of the recombinant Notch was confirmed by Western blotting using a monoclonal anti-5XHis mouse antibody (Cell Signaling Technology, Danvers, MA).

Purification of N-Terminal His_6-Tagged Notch1 TM/JM (1721-1771). The harvested cells were weighed and lysed in 20 ml of lysis buffer (75 mM Tris, 300 mM NaCl, 0.2 mM EDTA, pH 7.8) per gram of cells. To this was added MgAcetate to 5 mM, 2 mg/ml of lysozyme, 0.2 mg/ml DNase and RNase, and 1mM PMSF, as well as 50 μl of a protease inhibitor cocktail (Sigma-Aldrich, P8849), per gram of cells. The suspension was tumbled for 30 minutes at 4°C. Powdered DTT was then added to a concentration

of 1mM before cells were further disrupted by five-minute probe sonication with a 50% duty cycle at approximately 57 watts using a Misonix (Farmingdale, NY) sonicator. Notch, in both membranes and inclusion bodies, was then fully solubilized by the addition of Empigen detergent to 3% and tumbling at 4°C for at least 30 minutes. The lysate was then centrifuged at 30,000*xg* in a JA 25.5 rotor (Beckman-Coulter, Indianapolis, IN) to remove any remaining insoluble precipitate and unsolubilized membranes.

Ni-NTA resin (~0.5ml for every 2 liters of culture) was equilibrated with buffer A (40 mM HEPES, 300 mM NaCl pH 7.8) plus 1 mM fresh DTT. The volume of resin is based on the relatively low expression level of the Notch1 TM/JM; by keeping the resin volume low, total non-specific binding of other proteins (relative to tagged TM/JM) to the resin is minimized. The equilibrated resin was then added to the supernatant and the slurry was tumbled overnight at 4°C. The resin was loaded into a column connected to an A_{280} detector and washed with 10 bed volumes of buffer A containing 3% Empigen plus 1 mM fresh DTT, followed by a wash with buffer A containing 1.5% Empigen (% v/v) plus 1 mM fresh DTT to rinse all unbound proteins from the resin as judged by the return of eluate A_{280} to a baseline value. Empigen was then exchanged out for the detergent lyso-myristoylphosphatidylcholine (LMPC) by re-equilibrating with 12X1 column volumes (CV) of buffer A with 0.2% LMPC (%w/v) plus 1 mM fresh DTT. The column was then washed with successive imidazole washes with buffer A, 0.2% LMPC, 25 mM imidazole, and 1 mM DTT, followed by buffer A, 0.2% LMPC, 65 mM imidazole, and 1 mM DTT. These washes were conducted until the eluate A_{280} returned to a constant value in each case. The LMPC was then exchanged for

dihexanoylphosphatidylcholine (DH_6PC) with an 8XCV wash of 0.7% DH_6PC. The DH_6PC exchange was followed by a 4XCV exchange step with a 2% DMPC/ DH_6PC bicelle mixture q=0.33 (DMPC = dimyristoylphosphatidylcholine). The protein was then eluted in batch mode by mixing 2.5 ml of elution buffer (2% DMPC/ DH_6PC bicelle mixture, 300mM imidazole) with the resin and incubating. No DTT is included in these buffers due to its weak absorbance at 280 nm, which might introduce error in subsequent determination of the protein concentration. The resin was then spun down at 500*xg* in a tabletop centrifuge and the supernatant was collected. This batch mode elution method was used because prolonged contact between resin and elution buffer resulted in higher yield elution. Alternatively column elution with high yield can also be obtained provided the resin and the elution buffer are allowed to equilibrate briefly in the column (no flow) before the elution is allowed to proceed. After elution, the protein concentration was determined by measuring A_{280} and using an extinction coefficient of ε=6990 $M^{-1}cm^{-1}$. 10 mM DTT was added to the sample to reduce any disulfide bonds. The molecular weight of the tagged Notch1 TM/JM domain 1721-1771 is 6836 g/mol.

Purification was monitored by SDS-PAGE gel electrophoresis. Electrophoresis experiments were carried out using an Invitrogen (Grand Island, NY) Novex-Mini Gel system and NuPAGE 4-12% Bis-Tris polyacrylamide gels and MES running buffer.

Preparation of Notch1 for NMR Spectroscopy. After purification, the Notch1 TM/JM sample is in a 2% bicelle solution, pH 7.8, with 300mM imidazole plus 10 mM free DTT. The sample was concentrated by centrifugation at 3700*xg* using an Amicon Centrifugal Filter unit with a molecular weight cut-off of 10,000 Da (Millipore, Billerica, MA). When

the volume reached 0.5 ml, 15mM DH_6PC in 50 mM $NaPO_4$, pH 6.5 was added, returning the volume to 2ml. EDTA was then added to 1mM, and D_2O was added to 10%. This step reduces the imidazole concentration from 300 mM to approximately 65mM, and DTT to ~2mM. The inclusion of a ca. critical micelle concentration level of DH_6PC in the buffer serves to replenish the free DH_6PC that passes through the ultrafiltration membrane during concentration. The pH was then reduced from 7.8 to pH 5.5 using acetic acid and the solution was then centrifugally concentrated 10X to a volume of 0.2 ml and transferred to an NMR tube. Unless otherwise noted, all NMR experiments were conducted using 3mm NMR tubes. The final NMR conditions are ~0.5 mM Notch1 TM/JM, 15% DMPC/DH_6PC bicelles (q=0.33), 20 mM $NaPO_4$, 65 mM imidazole, 2 mM DTT, and 1 mM EDTA, pH 5.5, and 10% D_2O

Isotopic Labeling of Notch1 TM/JM. Minimal medium was prepared using 1g/L $^{15}NH_4Cl$ for simple U-^{15}N isotope labeling. For U-^{15}N,^{13}C samples 1g/L of $^{15}NH_4Cl$ was used along with 2 g/L of glucose (U-$^{13}C6$, 99%) (Cambridge Isotope Laboratories, Andover MA). Isotopically labeled cells were induced, harvested and lysed as described above. In addition to preparing uniformly-labeled samples, we also prepared samples to facilitate NMR resonance assignments using an amino acid-selective labeling scheme. For this an auxotrophic *E. Coli* cell strain CT19 was used,[205, 206] which has genetic lesions in the aspC, avtA, ilvE, trpB, and tyrB genes. These lesions inhibit cell capacity to synthesize branched chain and aromatic amino acids. Briefly, cells were grown in 1L of minimal media supplemented with 0.5 g each of unlabeled Ala, Asp, Leu, Ile, Phe, Val, and Tyr, and 0.1g of Trp as well as 10mg/L ampicillin, 20mg/L kanamycin and

tetracycline. The unlabeled amino acids are required for the healthy growth of the cells. The use of this auxotrophic cell strain allows for selective labeling of specific amino acids while minimizing isotopic scrambling. The cultures were then grown at 37°C, as described above until the OD_{600}=~0.85. The cultures were then harvested through centrifugation at 3,000*xg* for 15 minutes. The cells were re-suspended in identical media as above except for the inclusion of 0.2 g of ^{15}N-labled valine, leucine or phenylalanine in place the corresponding unlabeled amino acid. The cultures were then returned to 37°C and allowed to grow for 15 minutes, followed by induction with 1 mM IPTG and reduction of the temperature to 25°C. The induction time was reduced from the usual 20 hours to 10 hours to minimize residual isotopic scrambling. The cells were then harvested and lysed as above.

A reverse labeling scheme was also employed to confirm the identities of arginine and histidine peaks. In this scheme, normal U-^{15}N minimal media was prepared and inoculated with the regular TM/JM-expressing BL21(DE3) star cell strain as described above; however, just prior to induction, 1g/L of unlabled arginine or histidine was added to the medium. The TROSY NMR spectrum of the resulting ^{15}N- labeled protein contains all the usual peaks except those of arginine or histidine.

Notch1 Backbone Resonance Assignments. NMR spectra were collected at 318K (45°C) on a 900 MHz Bruker Avance spectrometer equipped with a cryoprobe. Uniformly double-labeled ^{15}N-^{13}C-Notch1 TM/JM was prepared in 15%DMPC/DH_6PC bicelles, q=0.33, pH 5.5, 500mM imidazole 5mM DTT, 1 mM EDTA and 10% D_2O. The high imidazole had been used to ensure complete elution of the Notch1 TM/JM.

Additional preparations with a reduced (65 mM) imidazole concentration in the final samples were later prepared. It was seen that there were no significant spectral differences between the low and high imidazole samples. The following three-dimensional (3D)-TROSY based experiments were carried out: HNCACB, HNCO and HNCA.[35, 207, 208]

Selective labeling experiments to resolve backbone assignment ambiguities were conducted on 800MHz or 900MHz Bruker Avance spectrometers equipped with cryoprobes. Two-dimensional ^{1}H-^{15}N (2D)-TROSY spectra were collected at 318K. Samples contained 15% DMPC/DH_6PC bicelle, q=0.33, 20 mM $NaPO_4$, pH 5.5, 65 mM imidazole, 2 mM DTT, 1 mM EDTA and 10% D_2O.

All NMR spectra were processed with NMRPipe[209] and analyzed with either NMRView software[210] or Sparky. Secondary structure was estimated using backbone chemical shift data and both Talos-N analysis[211] and chemical shift indexing.[212]

Notch1 Relaxation and Backbone Dynamics Experiments. NMR relaxation experiments were conducted on a 900MHz Bruker Avance spectrometer at 318K. Samples contained 15% DMPC/DH_6PC bicelles, q=0.33, 20 mM $NaPO_4$, pH 5.5, 65 mM imidazole, 2 mM DTT, 1mM EDTA, and 10% D_2O, with approximately 0.5 mM U-^{15}N-TM/JM. HSQC-based pulse sequences from the Bruker standard library: hsqct1etf3gpsi3d (avance-version 12/01/11), hsqct2etf3gpsi3d (avance-version 12/01/11), and hsqcnoetf3gpsi (avance-version 12/01/11), were used to determine T1, T2, and heteronuclear NOE values. T1 values were extracted from a series of inversion recovery experiments with 0.1, 0.25, 0.5, 0.8, 1.2, 2, 4, and 8-second relaxation delays.

T2 values were determined using the Carr-Purcell-Meiboom-Gill (CPMG) sequence with 0.016, 0.032, 0.048, 0.064, 0.080, 0.112, 0.144, and 0.192 second delays. The steady-state heteronuclear NOE values were determined from peak intensity ratios between spectra collected with and without 3 second presaturation.[206] All the spectra were processed with NMRPipe and analyzed using Sparky.

Paramagnetic Probe Accessibility NMR Experiments. This set of experiments measure the accessibility of protein backbone amide sites to water-soluble (Gd(III)-diethylenetriaminepentaacetic acid) and lipid soluble (16 DOXYL-stearic acid, 16-DSA, Aldrich, Milwaukee, WI) probes, as quantitated based on peak intensity reductions due to amide site exposure to these paramagnetic probes. A pair of matched ^{15}N-labeled TM/JM NMR samples were prepared with 15% DMPC/DH_6PC bicelles, q=0.33, 20 mM $NaPO_4$, pH 5.5, 65 mM imidazole, 2 mM DTT, 1 mM EDTA, and 10% D_2O with ~0.5 mM U-^{15}N Notch 1 TM/JM. A 2D-TROSY was taken of the probe-free reference sample. After the reference 900 MHz TROSY was collected, Gd(III)-diethylenetriaminepentaacetic acid (Gd-DTPA, Aldrich, Milwaukee, WI) was added from a 100 mM stock to a final concentration of 2 mM. Another 2D TROSY spectrum was collected using the same acquisition parameters, including number of scans per increment. The peak intensities of each resonance were measured and compared to the corresponding peak intensities from the probe-free reference sample. The peak intensities were plotted (Figure 3) as an indicator of site access to Gd(III)-DTPA.

Using the remaining matched NMR sample, we also assessed site accessibilities to the lipophilic probe. For this, 2.5 mM of 16- DOXYL-steric acid (16-DSA) in methanol

was dried in a glass vial, followed by addition of the second 0.2 ml U-^{15}N-TM/JM sample and vortexing in the vial until the 16-DSA completely dissolved. This was then transferred to a 3 mm NMR tube and a TROSY spectrum was collected using the same parameters as for the reference (no probe) and Gd-DTPA samples (above). Peak intensities for the 16-DSA sample were compared to the intensities from the reference sample and plotted in Figure 3.5.

The TM/bicelle interface was probed using 3-cyano-PROXYL (Aldrich, Milwaukee, WI), a weakly apolar stable nitroxide free radical. As described above, paired samples were prepared with 15% DMPC/DH_6PC bicelles, q=0.33, 20 mM $NaPO_4$, pH 5.5, 65 mM imidazole, 2 mM DTT, 1 mM EDTA, and 10% D_2O with ~0.8 mM U-^{15}N Notch 1 TM/JM. 25 mM of 3-cyano-PROXYL in methanol was dried in a glass vial and then half of the matched sample was added to the vial and mixed until all the 3-cyano-PROXYL was dissolved. This was then transferred to a 3 mm NMR tube and a ^{15}N-^{1}H TROSY-HSQC spectrum was collected using the same parameters as for the reference (no probe). The peak intensities of the 3-cyano-PROXYL sample were compared to the intensities from the reference sample and the intensity ratios were plotted in Figure 3.5.

Water-Amide Hydrogen Exchange. This NMR experiment measured the proton exchange rate between the amide backbone residues and water using the CLEANEX-PM pulse sequence, which eliminates artifacts such as intramolecular NOEs.[213] The readout for this this experiment is an HSQC (or TROSY) spectrum in which peaks are seen only for amide sites that undergo hydrogen exchange with water that is rapid

compared to a delay (τ) that is part of the pulse sequence. A sample was prepared as above, with 15% DMPC/DH_6PC bicelles, q=0.33, 20 mM $NaPO_4$, pH 5.5, 65 mM imidazole, 2 mM DTT, 1 mM EDTA, and 10% D_2O with ~0.8 mM U-^{15}N Notch 1 TM/JM. An HSQC-based pulse program was used with a τ of 25 msec. The CLEANEX-PM-FHSQC peak intensities were compared to the intensities of an identical FHSQC experiment.

Results and Discussion

A number of constructs were explored to determine the best-behaving and most informative construct. Initially, a construct extending from Notch 1 residues 1721 (S2 cut site) through site 1815 (approximately halfway through the RAM domain) was expressed and purified. This construct was found to be unsuitable due to significant expression problems. A new series of constructs were then expressed and purified, all starting at site 1721 and terminating at: 1758, 1764, 1771, and 1790. These constructs expressed more favorably. An N-terminally His_6-tagged construct of human Notch 1 residues 1721 (S2 cleavage site) to 1771 was selected for study (Figure 3.2C) based on the facts that it includes both N- and C-terminal juxtamembrane regions, that it expresses well in *E. coli*, and that it yields a well-resolved NMR spectrum in bicelle model membranes (Figure 3.2D). While the yield for this construct is not high compared to many other recombinant proteins (yield of approximately 1 mg pure protein per liter of M9 medium), it does have threefold higher expression than the 1815 construct.

There were distinct differences between the TROSY spectrum of the Notch1 TM/JM in detergent micelles (LMPC) compared to the spectrum in DMPC/DH_6PC bicelles (Figure 3.1), including many differences in peak positions. The bicelle spectrum

(red) includes a few more resonances than the spectrum from micelles (black). Moreover, in the micelle spectrum the single tryptophan sidechain (inset) seems to exist in two populations: a major population at ~10.2ppm and a minor population at ~10.15 ppm, suggestive of two conformations or environmental states, whereas only a single Trp sidechain resonance is seen in the bicelle case. Given the excellent quality of the TROSY spectrum of the TM/JM in bicelles, the increased peak number, the more optimal spectral dispersion, and the fact that bicelles are a closer membrane-mimetic than micelles, bicelles were selected for the experiments of this work. It was also seen that varying pH did not impact the Notch1 TROSY spectrum to a significant degree (data not shown).

As detailed in the methods above, whole *E. coli* cell lysates harboring this recombinant Notch1 TM/JM were mixed with the harsh zwitterionic detergent Empigen to solubilize all membrane proteins, followed by addition of Ni(II)-metal ion affinity resin and elution of all non-His_6-tagged proteins. The resin with pure bound Notch1 TM/JM was subsequently re-equilibrated with lyso-phospholipid micelles and then DMPC/DH_6PC bicelles to refold the protein, followed by elution of the pure Notch TM/JM in bicelles.

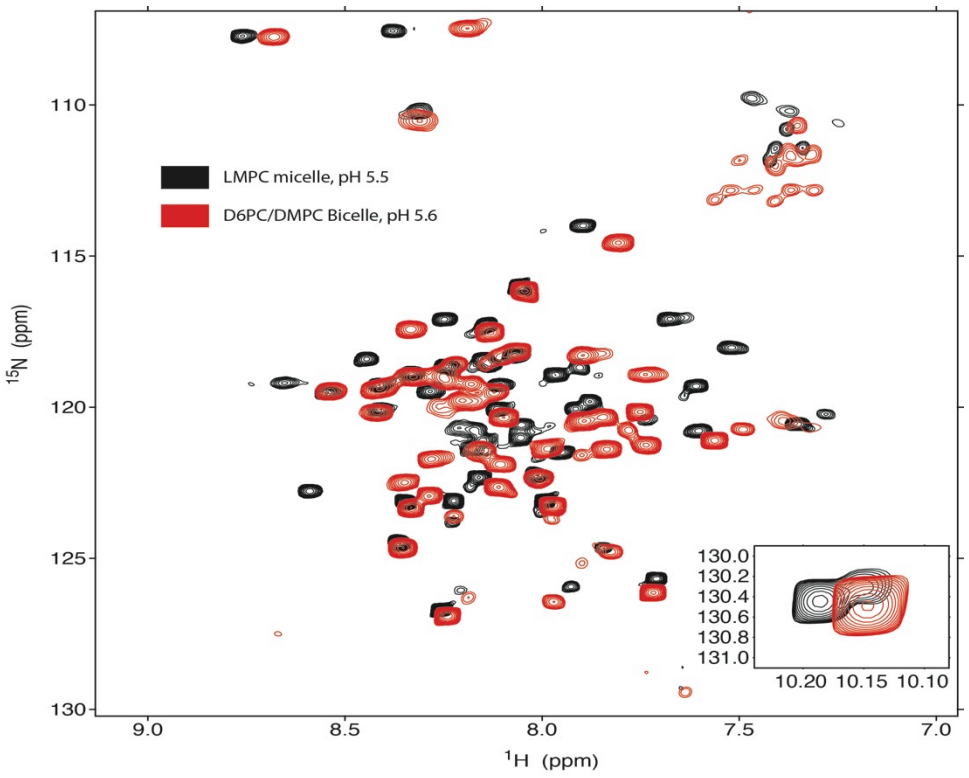

Figure 3.1. Notch 1 TM condition screening. ^{1}H-^{15}N TROSY-HSQC NMR spectra collected at 800MHz of the Notch1 TM/JM segment in LMPC micelles at pH 5.5 and 318K (black) overlaid with the spectrum of the same protein in 15% DMPC/DH$_6$PC bicelles, q=0.33 (red) at pH 5.6 and 318K. The inlay represents the peaks from the indole side chain of the single Trp residue present in the TM/JM.

Following screening (Figure 3.1), optimal NMR sample conditions were determined to be 0.5 mM TM/JM in 15% DMPC/ DH_6PC bicelle at q=0.33, pH 5.5, where the TM/JM-to-(DH_6PC+DMPC) mol:mol ratio is approximately 1:600. We then conducted NMR experiments at 900 MHz using standard TROSY-based 3D experiments (HNCA, HNCO, and HNCACB) in conjunction with both uniform and amino acid-selective labeling to accomplish nearly complete backbone and C_β resonance assignment for the TM/JM (Figure 3.2D; BioMagResBank (ID #26565). Exploiting the optimal resolution provided by the employment of TROSY-based NMR experiments and the modest size of the Notch1 TM construct, it was not necessary to perdeuterate the protein to obtain well-resolved 3D NMR data. To resolve any assignment ambiguities we used amino acid-selective labeling in order to determine the subset of TROSY peaks belonging to specific residue types. We used an auxotrophic cell line CT19 (see Methods) to selectively ^{15}N-label valine (6 residues), leucine (6 residues), and phenylalanine (5 residues) sites. Except for three of the prolines in the sequence, 100% of the peaks in the spectrum were assigned. Due to the nature of the HNCO and HNCACB experiments, we also have assignments for two of the five total proline residues.

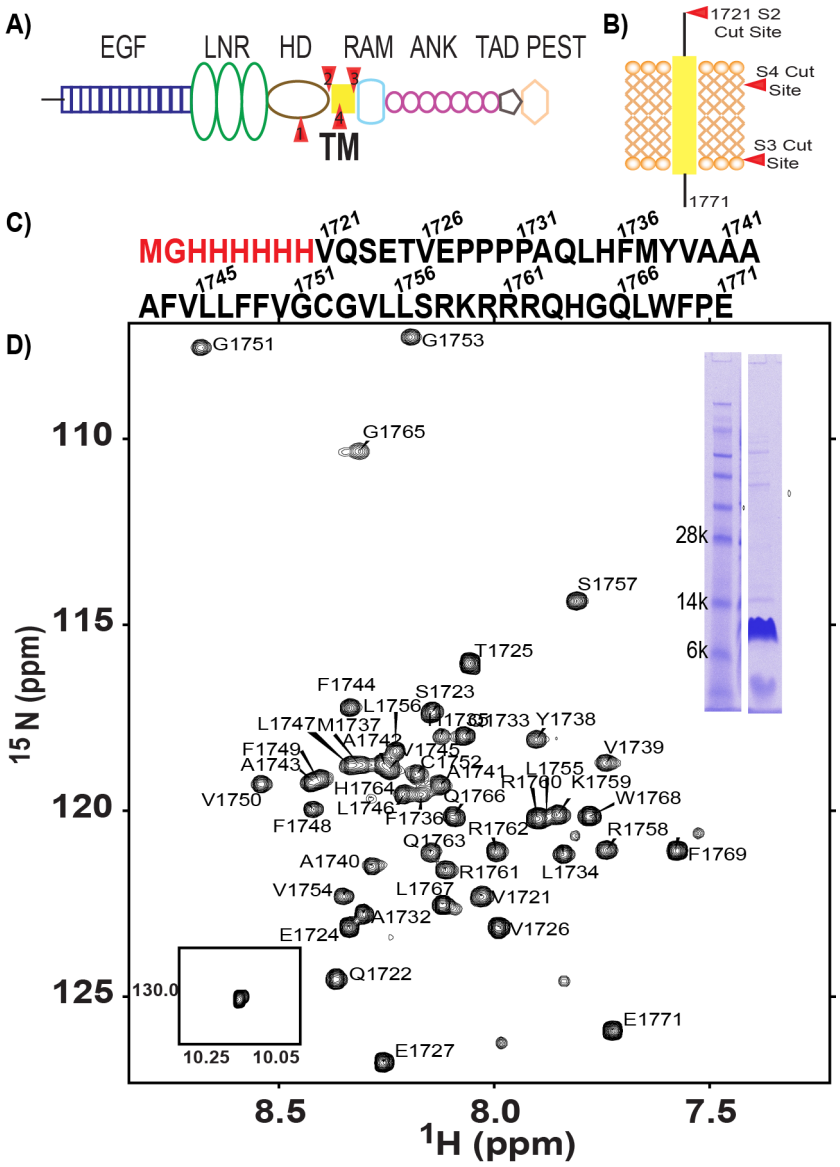

Figure 3.2. Notch 1 TM construct information and NMR spectrum. (A) Domain organization of full length Notch1. Sites of proteolysis are marked with red. (B) Notch1 TM/JM segment with proteolysis sites marked with red. S3 and S4 are γ-secretase cut sites. C) Sequence of the Notch1 TM/JM segment D) Assigned 900 MHz ^{15}N TROSY-HSQC spectrum of Notch1 TM segment in 15% DMPC/DH$_6$PC bicelles, q=0.33 at pH 5.5 and 318K. Backbone amide ^{1}H-^{15}N peaks have been assigned for all of the non-proline residues. The NMR sample included 2mM DTT, 10% D$_2$O, and 1mM EDTA. A sodium dodecylsulfate-polyacrylamide gel of the NMR sample and the single indole side chain ^{1}H-^{15}N peak are shown in the insets.

The secondary structure was then determined using both chemical shift index (CSI) and TALOS-N analyses of the chemical shifts.[211, 212, 214, 215] The secondary structure of the Notch TM/JM was mapped by analyzing the measured Cα, Cβ, and CO ^{13}C chemical shifts using the program Talos-N (Figure 3.3, upper panel).[211] Predominately α-helical segments were also evident via CSI analysis from plotting the chemical shift difference between the Notch1 TM segments Cα, Cβ, and CO chemical shift values and standard random coil shift values (Figure 3.3, bottom three panels). It appears that most of the TM domain is encompassed by an α-helix that extends from residues 1732-1761, with a point of uncertainty being the secondary structure of the tetra-proline motif preceding this segment. The flanking JM segments appear to have little regular secondary structure (see Figure 3.3).

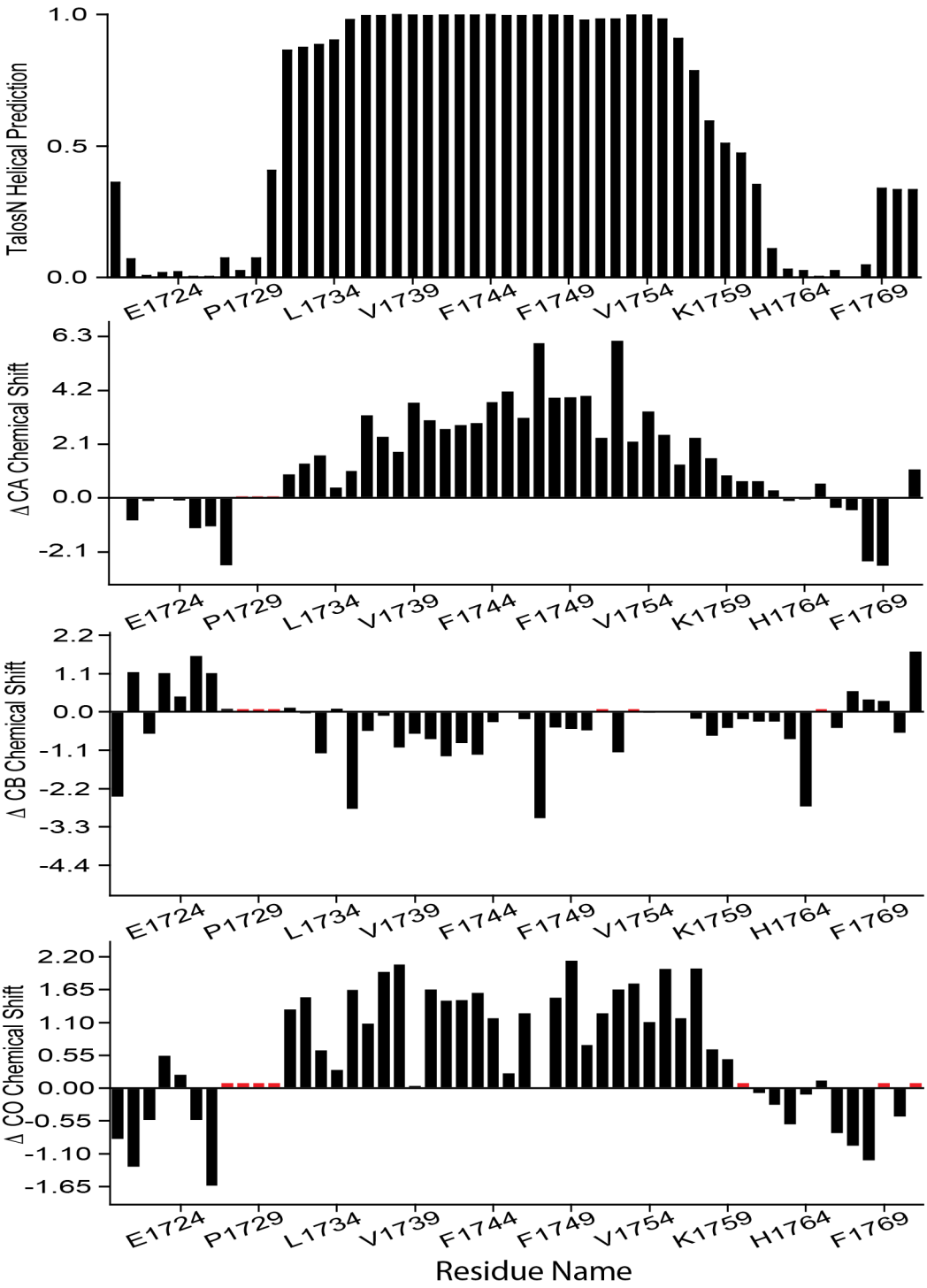

Figure 3.3. Notch 1 TM chemical shift indexing. Upper Panel- Results of using TALOS+ to determine the probability of α-helicity for sites in the Notch1 TM/JM under bicelle conditions based on analysis of backbone chemical shifts, as determined in this work. The lower three panels illustrate the differences between the observed chemical shifts and random coil values. The red bars indicate places where there is no chemical shift data or prediction.

We also collected NMR R_1, R_2, and HN-nuclear Overhauser effect (NOE) data, which provide insight into the flexibility of the Notch1 TM/JM (Figure 3.4). Low $R_1 \cdot R_2$ and NOE values indicate that sites in the N- terminal JM segment of the protein are very flexible, appears to be somewhat more ordered than the N- terminus. The elevated R_2 value for Val1754 is suggestive of local intermediate time scale motions at this site, which is interesting given that γ-secretase cleaves Notch between sites 1753 and 1754.[19, 44] Interestingly even in the $R_1 * R_2$ plot (Figure 3.4); which should eliminate anisotropy contributions, the V1754 has an anomalously higher $R_1 R_2$ value. This indicates that this site likely is involved in intermediate time scale motions. This residue is next to a G-C-G sequence, possibly explaining why it may be subject to such motions.

The overall correlation time of the Notch1 TM/JM protein in bicelles does seem high especially based on the theoretical values proposed for a similarly sized system.[216] The accuracy of the data acquisition and the fit were confirmed however so it is possible that the difference is due to either additional motion or exchange of the helix within the bicelle or a systemic factor of 2 error in the dataset.

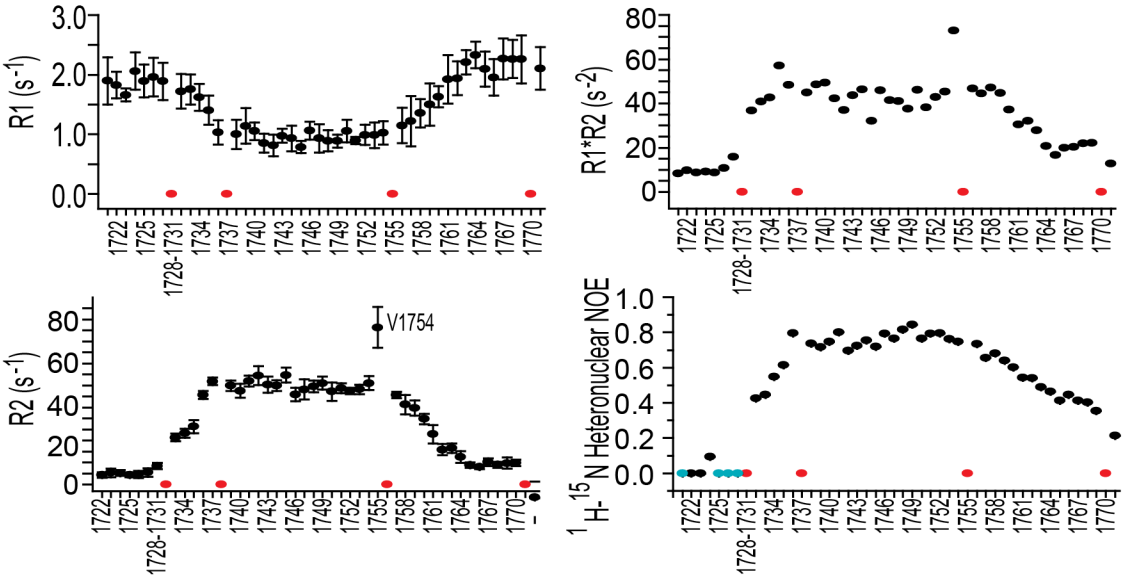

Figure 3.4. ^{15}N NMR relaxation measurements. Measurements collected on a 900MHz magnet reveal the global dynamics of the Notch1 TM/JM segment in 15% DMPC/DH_6PC bicelles, q=0.33 at pH 5.5 and 318K. R_1 is the longitudinal relaxation rate and R_2 is the transverse relaxation rate. Error bars give the uncertainty associated with the fits of the relaxation decays to yield the reported values. Sites with cyan circles represent peaks with negative values; red circles represent either proline sites or instances where extensive peak overlap prevented the determination of a reliable value.

We next examined the topology of the TM/JM domain in its bicelle environment. A water soluble paramagnetic probe, Gd(III)-DTPA, a lipid soluble probe, 16-DSA, and a weakly apolar probe, 3-cyano-PROXYL (that prefers the water-membrane interface), were added to bicellar Notch TM/JM samples and the paramagnet-induced intensity changes in the TROSY resonances were quantitated. From these data (Figure 3.5) it is clear that the TM domain ends at the cluster of basic residues starting at R1758.

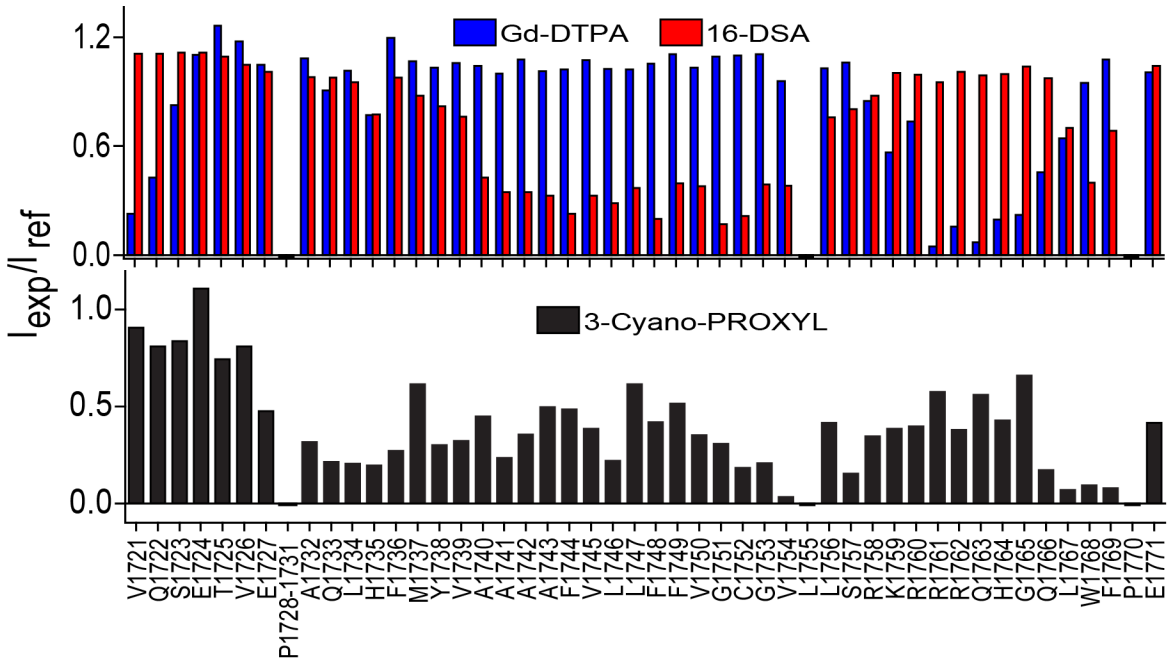

Figure 3.5. Notch 1 TM Membrane Topology. Membrane topology was probed for the ^{15}N Notch1 TM/JM segment in 15% DMPC/DH$_6$PC bicelles, q=0.33 at pH 5.5 and 318K. A plot of the ratio of site-specific peak intensities from samples containing a paramagnet vs. those from a diamagnetic reference sample reveals the probe-accessibility of each residue. The Gd(III)-DTPA accessibility is in blue and the 16-DSA accessibility is in red. The bottom panel represents a similar plot using 3-cyano-PROXYL. Sites with negative bars represent either proline residues or instances where extensive peak overlap prevented reliable analysis.

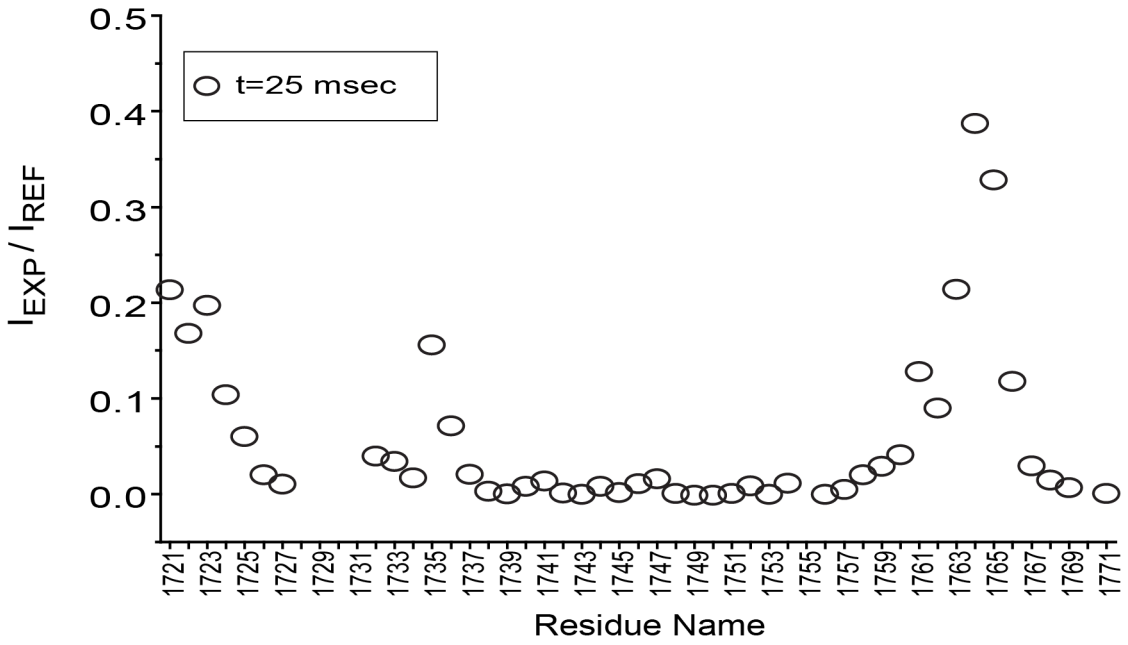

Figure 3.6. CLEANEX-PM water exchange experiment. Open circles represent the I_{EXP}/I_{REF} of each residue at a mixing time of 25 msec demonstrating areas where the amide backbone undergoes exchange with water. Exchange data indicates that there is a reduced level of exchange just prior to the tetra-proline residues (1728-1731).

The topology near the start of the transmembrane helix at 1732 seems to be more complex. The 3-cyano-PROXYL probe (Fig. 3.5) and NMR CLEANEX-PM water/amide hydrogen exchange data (Figure 3.6) indicate that the 1st turn of the TM helix at residues 1732-1736 is located at the water-bilayer interface. Moreover, a spike in the hydrogen exchange rates at residues 1735-1736 suggests local instability of the TM helix. The results of this experiment (Figure 3.6) elucidate and support the conclusions drawn about the Notch1 TM/JM topological orientation in this work. The N-terminal (1721-1725) residues display rapid exchange with water indicating the residues are solvent-exposed. Interestingly, the residues just N-terminal of the tetra-proline motif exhibit little-to-no exchange with water occurring on the order of 25 msec or faster. This suggests that these residues sit at or slightly below the water-bilayer interface. The exchange rate is also seen to be elevated at sites 1735 and 1736, indicating both that these sites are located near the water-membrane interface and that there must be some local helical instability at these sites, which are part of the TM helix (see Figure 3.3). As expected, the rest of the transmembrane domain exhibits little-to-no hydrogen exchange with water until the membrane-cytosol interface is approached, starting near site 1758. The intracellular juxtamembrane loop (1759-1768) exhibits fast exchange, followed by a dramatic reduction in the exchange rate that is associated with the Leu-Trp-Phe segment (1767-1769), which appears to be surface-associated, as supported by the paramagnetic probe data shown in Figure 3.5. While the tetraproline segment located at site 1728-1731 was not observed in our NMR spectra the fact that the amide sites flanking this segment are hydrogen exchange-resistant and inaccessible to all three paramagnetic probes might be interpreted to suggest some tertiary structure involving

the tetraproline motif and the preceding 1724-1727 segment. However, it is difficult to reconcile ordered tertiary structure with the high dynamics observed for the 1724-1727 segment (Figure 3.4). A more plausible explanation is that the Gd(III)-DTPA data for this segment is anomalous for a not-yet-determined reason. If this data is disregarded, all other measurements are consistent with a model in which the N-terminus is disordered and located in the aqueous phase, but is anchored to the membrane surface by the tetra-proline motif, which sits in the water-bilayer interface, oriented 90° with respect to the transmembrane domain.

The short C-terminal JM segment from R1758 to Q1766 is seen to be solvent-exposed. However, this segment is followed by residues that are significantly broadened by 16-DSA and 3-cyano-PROXYL but not by Gd(III)-DTPA, indicating that the end of the C-terminal JM segment actually dips back into the membrane as a consequence of the Leu-Trp-Phe sequence located near the C-terminus. This model is strongly supported by the water exchange data (Figure 3.6).

Even at the very rough level of resolution (Figure 3.7) provided by the data of this work it appears that the NOTCH TM/JM is structurally very different from the corresponding domain of the APP,[35, 36] also a gamma-secretase substrate. APP has a kinked TM domain and a C-terminal JM domain that interacts with the membrane surface only after a disordered and water-exposed 40-residue segment connecting its TM domain to a distal C-terminal amphipathic helix. These features differ from the apparently unbroken helix of the NOTCH TM and the short (9-residue) connecting to the membrane-interacting C-terminal JM Leu-Trp-Phe segment. While both APP and Notch have N-terminal JM segments that interact with the membrane surface, APP has a

surface-bound helix followed by a soluble connecting loop to the TMD, whereas the Notch TM helix appears to be preceded by an interfacial tetraproline segment, with no connecting water-exposed loop. While a more complete compare-and-contrast analysis of the structures of APP and Notch1 TM/JM domains will await completion of the Notch1 TM/JM structure, this work suggests that there are significant differences in their structures. These differences might be exploited in strategies to inhibit cleavage of APP by γ-secretase while still permitting normal (healthy) processing of NOTCH.

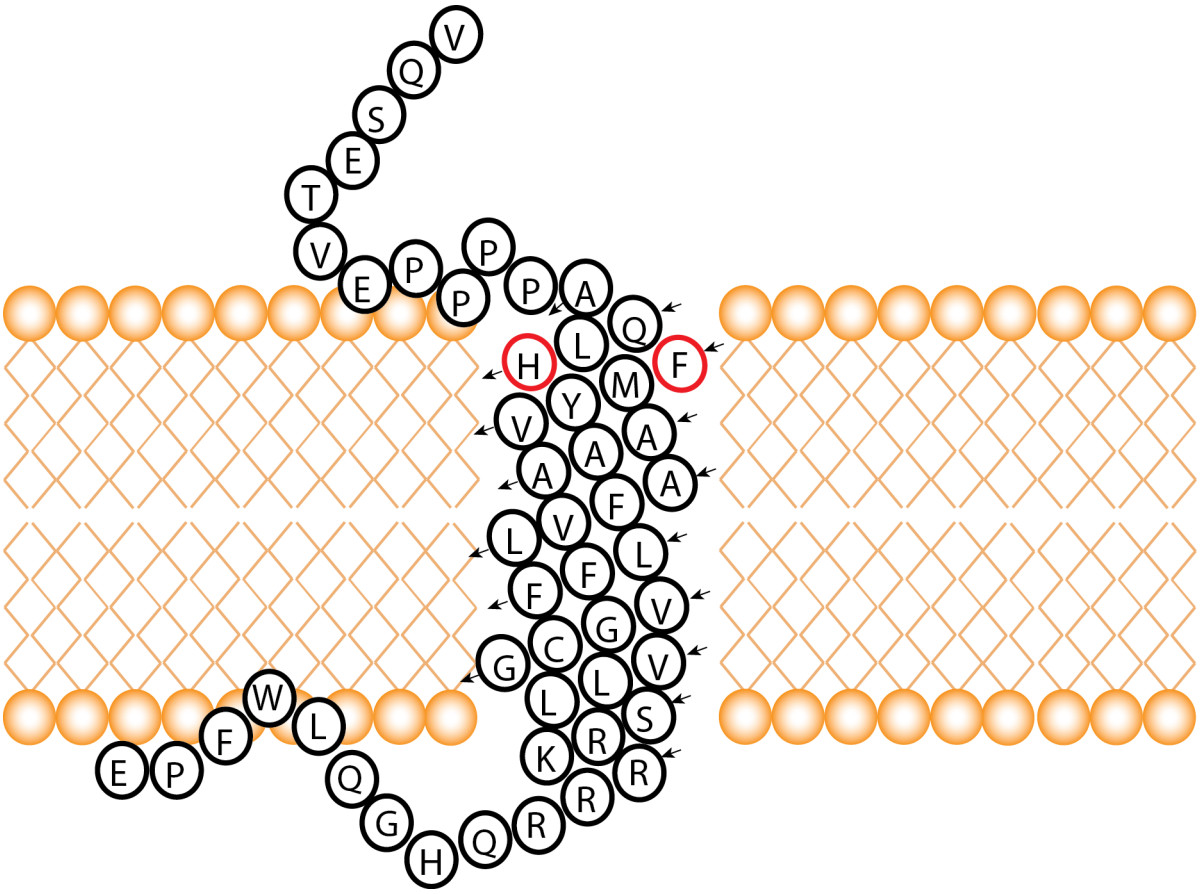

Figure 3.7. Notch 1 TM/JM preliminary structural/topological model. A basic structural and topological plot of the Notch1 TM/JM segment is constructed using the experimental data described in Chapter 3. The residues that experienced enhanced exchange in the water exchange experiment are ringed with red.

IV. The Notch 1 TM Segment is Structurally and Biochemically Distinct From C99.

Introduction

Alzheimer's disease is a devastating neurodegenerative disorder that affects millions of people worldwide. According to reports by the Alzheimer's Association, it is thought that by 2050, the number of people AD will triple in the United States alone.[1] Symptoms of AD are generally characterized by a gradual progression of mild cognitive impairment and minor physical limitations towards dementia.[1] First described in 1907, the etiology or mechanism of action of this deadly and devastating disease is still controversial. Historically, AD diagnosis occurred after a post-mortem autopsy. The presence of extracellular aggregated protein deposits called "amyloid plaques" and severe brain vascularization and atrophy characterize late stage AD. Amyloid plaques consist of fibrilized proteins the major component being Aβ, the proteolysis product of the amyloid precursor protein.[3, 4]

The most prominent model for AD etiology posits that the production and oligomerization/aggregation of the Aβ peptide in the brain is the central cause of the neuronal damage seen in AD.[26-33] APP is proteolytically processed in an "amyloidogenic pathway," where the β-secretase BACE1 excises the extracellular domain of APP. The membrane bound enzyme complex γ-secretase then proceeds to cleave the APP TM segment (C99) in the membrane to release the Aβ peptide and the APP intracellular domain (AICD).[8] Due to the promiscuous nature of the γ-secretase complex,[13] there are multiple cleavage products of C99. Processive cleavage results in Aβ peptide of differing lengths. The initial cut occurs near residue 720 with subsequent cleavage

proceeding up the helix every three to four residues, until one of Aβ peptides of varying lengths dissociates from the active site.[14, 15] The most abundant form of the Aβ peptide is the $A\beta_{40}$ with $A\beta_{42/38}$ being less prevalent. The $A\beta_{42}$ form is more prone to aggregation.[24] It is widely thought that the early stage soluble oligomers/aggregates are responsible for the neurotoxicity seen in the disease with the end stage aggregates being less toxic.[25]

One avenue to prevent Aβ formation would be to inhibit γ-secretase and stop proteolysis. Semagacestat, an allosteric inhibitor of γ-secretase, made it to Phase 3 clinical trials before cancellation.[111] Trial participants experienced a wealth of physical issues, but perhaps the most troubling was a decline in cognitive capabilities. It was determined that the inhibition of Notch signaling was the likely culprit. Notch is one of the many known γ-secretase substrates. For another cohort of inhibitors that were thought to be "Notch sparing," clinical trials had to be halted due to Notch induced toxicity.[112]

Given the drug development bottleneck that the Notch family of proteins precipitates[98, 100, 101, 111, 112] closer examination of this protein in the context of AD may provide new insights into AD drug development. The NOTCH gene(s) and notch signaling occur in all vertebrate organisms.[127-130] Notch signaling has been implicated in an array of developmental patterning choices.[131-134] Notch signaling also controls neurogenesis, axon and dendrite growth, and synapse plasticity, as well as neuronal death.[135-143]

Similar to C99, Notch undergoes a series of proteolysis steps that prepare the protein, prime for signaling and signal activation. Notch begins in the ER as a

holoprotein, and trafficks to the Golgi, where the protein is glycosylated and a furin-like convertase cuts the protein leaving a dimer of two non-covalently linked domains.[156, 158] The heterodimer is trafficked to the plasma membrane where signal activation can occur. In general, the canonical signaling pathway is initiated when mature Notch at the plasma membrane has a *trans* binding interaction with a membrane bound protein ligand from a neighboring cell to the extracellular EGF domain of the Notch protein.[150] This binding event triggers trans-endocytosis of the Notch-bound ligand.[179] The endocytosis induces a force on the Notch extracellular domain that mechanically extends the negative regulatory region of the protein (residues 1449-1731).[156] This force exposes the previously buried S2 cut site to the ADAM 10/17 metalloprotease,[182-184] which cleaves the protein to release the extracellular domain in the committed step of the signaling pathway. After the Notch extracellular domain has been cleaved at S2, the ectodomain is endocytosed into the signal-donor cell.[179, 181]

After γ-secretase cleavage in the TMD,[160] the large Notch intracellular domain (NICD)[92, 162-164] and a small extracellular peptide (Nβ)[161] are released. The NICD translocates to the nucleus where it forms a transcriptional activator complex with CSL[168] and MAML[185] that targets a number of different genes.[186, 187] The exact mechanism of γ-secretase cleavage and cellular compartment is unknown and is an active area of research.

The γ-secretase substrate C99 has recently been the subject of much study. Information regarding the backbone protein dynamics and the positioning of C99 relative to the membrane has been reported.[35] The structure of C99 in detergent micelles has been determined and it was discovered that C99 directly and specifically

forms a 1:1 complex with cholesterol.[36] Further work has shown that C99 is likely monomeric under physiological conditions.[37] Finally, it has been shown that changes in membrane bilayer thickness do not change the overall structure and dynamics of C99 but does affect membrane topology.[38] This extensive list of structural, biochemical, and biophysical characteristics has only been collected for C99. We present a complete set of data that will allow for a direct comparison of two gamma secretase substrates. In this work we present the experimentally determined structure of the Notch 1 TM segment in bicelles, test for possible Notch 1 cholesterol binding, and explore its structural and topological tolerance of changes in lipid composition. These data complement a previously published data set for C99. These data strongly suggest that there are significant differences between the Notch 1 TM segment and C99, which can and should be exploited in the search for AD therapeutics.

Materials and Methods

Expression of Notch1 in E. coli. Expression of Notch 1 was performed as described in Deatherage et. al. 2015.[217] Briefly, an expression vector was transformed into *E. coli* BL21(DE3)star cells, and a single colony was used to inoculate a starter culture of LB. The starter culture was grown overnight at 37°C. The starter culture (4 ml) was added directly to the large-scale culture media grown at 37°C until the OD_{600} reached 0.8. Expression was induced for 20hrs at 25°C, before harvesting.

Purification of N-Terminal His_6-Tagged Notch1 TM/JM (1721-1771). The purification of Notch1 was performed as previously described.[217] In brief, lysed cells were solubilized by the addition of Empigen detergent to 3% and tumbling at 4°C for at least 30 minutes. The solubilized lysate was cleared with centrifugation before being combined with

equilibrated resin and tumbled overnight at 4°C. The resin slurry was loaded into a column connected to an A_{280} detector and washed with a stepwise decrease in Empigen before an exchange with the detergent LMPC. The column was washed with two imidazole solutions at 25 mM and 65 mM, both containing LMPC. LMPC was then exchanged out for the bicelle component DH_6PC. The DH_6PC exchange was followed by a 4XCV exchange step with a 2% DMPC/ DH_6PC bicelle mixture q=0.33 (DMPC = dimyristoylphosphatidylcholine), before elution with 300 mM imidazole plus bicelles. After elution, the protein concentration was determined before 10 mM DTT was added to the sample to reduce any disulfide bonds.

Preparation of Notch1 for NMR Spectroscopy. General NMR conditions of Notch 1 TM segment were previously published.[217] Purified Notch1 TM/JM sample is in a 2% bicelle solution, pH 7.8, with 300 mM imidazole plus 10 mM free DTT was concentrated by centrifugation in a buffer exchange step where 15 mM DH_6PC in 50 mM $NaPO_4$, pH 6.5 was added and EDTA was then added to 1 mM. This was concentrated to the desired volume for approximately 15% bicelle. The pH was then reduced from 7.8 to pH 5.5 using acetic acid and transferred to a 3 mm NMR tube. The final NMR conditions are ~0.5 mM Notch1 TM/JM, 15% DMPC/DH_6PC bicelles (q=0.33), 20 mM $NaPO_4$, 65 mM imidazole, 2 mM DTT, and 1 mM EDTA, pH 5.5, and 10% D_2O.

Sidechain Assignments. U-^{15}N-^{13}C samples were prepared as previously published.[217] Samples were concentrated as described above. A H(CCO)NH[218, 219] and a TROSY-based C(CO)NH experiment were run on a Bruker 600MHz magnet. The final NMR buffer contained 100% D_2O for the HCCH-TOCSY experiment.[220, 221] All NMR spectra were processed with NMRPipe[209] and analyzed with Sparky. Assignments in TROSY-

HSQC were matched to side-chain carbon and hydrogen chemical shifts. HCCH-TOCSY was used to correlate side-chain carbon and hydrogen chemical shifts to get assignments of side-chain residues in non-deuterated bicelle.

Cholesterol Titration. These samples were prepared as previously described.[36] In brief, Cholesterol containing bicelles were prepared by dissolving DMPC and cholesterol in chloroform at the desired molar ratio before removing all solvent during lyophilization (Labconco, Kansas City, MO). A bicelle solution was then prepared by mixing the cholesterol and lipid film with DH_6PC and water to form a stock solution of 15mol% cholesterol. The stock was heated before undergoing freeze-thaw cycles until a clear solution was formed. This stock was used to make identical bicelle solutions that contained 0, 2.5, 5, and 10mol% cholesterol. This buffer was used to elute Notch from the resin. All samples for NMR were prepared as above with approximately 0.35 mM protein in each NMR sample. A ^{15}N-^{1}H TROSY was collected at 318 K for each point on a Bruker 900 MHz magnet.

Membrane Thickness. Membrane accessibility in both DMPC bicelles and in thicker bicelles is a method that has been previously described.[38, 217] In brief, DMPC, MSM, and ESM were weighed in solid form in glass vials at the desired molar ratio. The lipid mixtures were then solubilized with <1 ml 95:5 benzene:ethanol stock and lyophilized overnight to yield a white powder. After solvent removal, a 2% bicelle solution was generated by combining the appropriate amount of DH_6PC and water to form a q=1/3 bicelle mixture. Samples were purified as described above, concentrated to final NMR sample form and split in thirds. Three TROSY-HSQC spectra were collected for each bicelle condition. The first sample was a paramagnet free reference sample. The

second contained 2 mM Gd-DTPA, a water-soluble paramagnet (Santa Cruz Biotechnology, Dallas, TX) from a 0.1 M pH 5.5 stock. The third sample contained 2.5 mM 16-DSA (Santa Cruz Biotechnology, Dallas, TX). 2.5 mM of a 16-DSA stock in methanol was dried overnight, the Notch sample was added to the dried film and vortexed until the 16-DSA was completely incorporated. All three samples were transferred to NMR tubes and subjected to NMR on a 900MHz Bruker NMR spectrometer. The peak intensities of each resonance were measured and compared to the corresponding peak intensities from the matched probe-free reference sample. The peak intensities were plotted as an indicator of site access.

Paramagnetic Relaxation Enhancement Measurements as Distance Restraints. Wild type Notch 1 has one cysteine residue present in the amino acid sequence. For PRE measurements two sites were spin labeled. The first was the native cysteine. A second site was engineered with site-directed mutagenesis, where the native cysteine C1752 was mutated to serine and F1744 was mutated to cysteine in the Cys-less background. The cysteine mutant was prepared as described. The protein was purified into 0.2% DPC. The protein in 0.2%DPC was spin-labeled as described previously.[36] In brief, each cysteine mutant was concentrated to 0.5 mM and the pH was lowered to 6.5 before being reduced with 2.5mM DTT. Spin-labeling proceeded with the addition of the thiol-reactive probe, MTSL (Toronto Research Chemicals, Toronto, Canada). A twenty-fold excess of MTSL was added to a ~0.5 mM Notch 1 sample (buffer: 65 mM imidazole, 2 mM EDTA, 2.5 mM DTT, 0.2% DPC, pH 6.5). The labeled sample was incubated overnight before buffer exchange to prepare for chromatography. The solution was mixed overnight with Ni-NTA resin overnight and the resin was then washed with 25 CV

of 50mM phosphate, 0.2% DPC, pH 7.8 to remove excess MTSL. The spin-labeled Notch was then eluted using the above purification conditions. Spin label sites cover the full transmembrane segment and are in generally rigid regions.

PRE data was acquired at 900 MHz with sample and parameter matched paramagnetic-diamagnetic ^{1}H-^{15}N TROSY-HSQC experiments for the two spin-labeled samples. The matched diamagnetic sample was acquired following the addition of 20 mM ascorbic acid to reduce the paramagnet. Spectra were identically processed using NMRPipe [209] and analyzed in SPARKY[222] to determine the intensity ratio of the paramagnetic versus diamagnetic samples. The intensity ratios and the diamagnetic sample linewidths were used to obtain distance restraints as previously described.[36, 223, 224]

NIH-XPLOR Structure Calculation. Restraints used in structure calculations included using PRE-derived distances, backbone torsion angles derived from chemical shifts and NOE distancerestraints. Backbone C_{α}, C_{β}, CO, and N chemical shifts (published previously[217]) were input into TALOS+ [225] to generate dihedral angle restraints. Chemical shift index (CSI) analysis was also used to generate hydrogen bond restraints for the TM segment.[226] A 3-dimensional (^{1}H,^{1}H,^{15}N)-TROSY-NOESY experiment was carried out on U-^{15}N-Notch1 (100 ms mixing time) in DHPC/DMPC bicelles in the standard NMR conditions mentioned above to obtain 339 short-, and medium-range NOE restraints used in structure calculations. The PRE restraints where employed as previously described.[227] Briefly, these restraints were classified as close in space if the paramagnetic/diamagnetic intensity ratios were less than 0.15 and assigned as being between 2 Å to 19 Å apart. Resonances with ratios between 0.15 and 0.85 where

converted to distances [223] and given generous uncertainties of ±7 Å. Resonances that exhibited little to no PRE effects (intensity ratios greater than 0.85) were loosely restrained to be between 19 Å and 100 Å apart. The PRE restraints were implemented as NOE-like restraints from the spin label to the backbone amide hydrogen.[227, 228]

Structure calculations were conducted using XPLOR-NIH v2.24[229] and performed similar to previously published structure calculations.[36] [Kroncke, B.M. *e.t al*, unpublished] Simulated annealing was carried out with 15000 steps at 3500 K with cooling to 100 K. During the temperature-cooling ramp, the VDW force constant was varied from 0.004 to 4 kcal•mol-1•Å-4 increased Van der Waals (VDW) interaction potentials. Similarly, force constants were increased for the NOE, and PRE restraints from 1.0 to 30.0 kcal•mol^{-1}•Å^{-2}. High temperature simulated annealing was followed by torsion angle and full-atom minimization steps.

Structure Refinement with AMBER Molecular Dynamics Simulation. The refinement was carried out as previously described. [Kroncke, B.M. *e.t al,* unpublished] In brief, ten of the top 1%-scoring Xplor-NIH-generated Notch 1 structures were selected for further structural refinement in an explicit membrane bilayer using restrained molecular dynamics (rMD). The starting structures were chosen subjectively such that only the TM region Notch1 is located within the membrane bilayer. These ten selected structures were solvated in an explicit DMPC bilayer using the CHARMM-GUI server.[230, 231] Using GPU-accelerated AMBER14[232], we began with restrained minimization of each representative structure for 30000 steps using steepest descent followed by 30000 steps of conjugate gradient, with protein atoms restrained to initial positions. Following restrained minimization, structures were minimized without restraints with 1500 steps each of a steep descent

gradient followed by a conjugate gradient. With Notch still restrained to initial Xplor-NIH coordinates, heating of lipid and water to 10K over 500 steps was performed using constant volume boundary conditions and Langevin dynamics with a rapid collision frequency (10000 ps^{-1}) to ensure that forces/velocities remained stable. The system was then heated to 100K over 2500 steps. The time step was increased from 1fs to 2fs for system heating to 318K over 100 ps with constant pressure dynamics and anisotropic pressure scaling while the protein and lipid bilayer were restrained. The system was equilibrated for 5 ns with NMR restraints applied with a weight of 100%. Production rMD at 318K followed for 60 ns, using constant pressure periodic boundary conditions, anisotropic pressure scaling, and NMR restraint weight set to 100%. A representative structure for each of the ten production trajectories was selected by determining which frame contains the Notch structure closest to the mean structure for that trajectory. Determining these average structures as well as calculating water penetrance and side-chain/lipid interactions employed CPPTRAJ for processing of atomic positions across time.[233]

Results

Cholesterol Titration. The importance of cholesterol in AD has been firmly established, and it has been proposed that the interaction between C99 and cholesterol may be an essential part of the proteolysis of the C99 molecule in lipid rafts.[36, 234] The direct and specific interaction between C99 and cholesterol suggested an important role for cholesterol in partitioning C99 from the bulk plasma membrane into lipid rafts where γ-secretase cleaves. The role cholesterol plays in Notch biology/biochemistry may well be limited and has not been a major research focus of the field. We tested if Notch binds

cholesterol. Five samples were prepared with increasing mol% of cholesterol (0 mol%, 2.5 mol%, 5 mol%, 10 mol% and 15 mol%). HSQC spectra were collected at each titration point and were overlaid to monitor chemical shift changes. The overlay is shown in Figure 4.1. There were no significant shifts seen in the spectra. After plotting the minor chemical shift changes relative to mol% cholesterol, the plots were nearly exclusively linear and no residue reached a point of saturation. The minor shifts seen are also not restricted to residues in the membrane suggesting the shifts are indicative of a more rigid bicelle and a change in the local chemical environment, as opposed to a binding event.

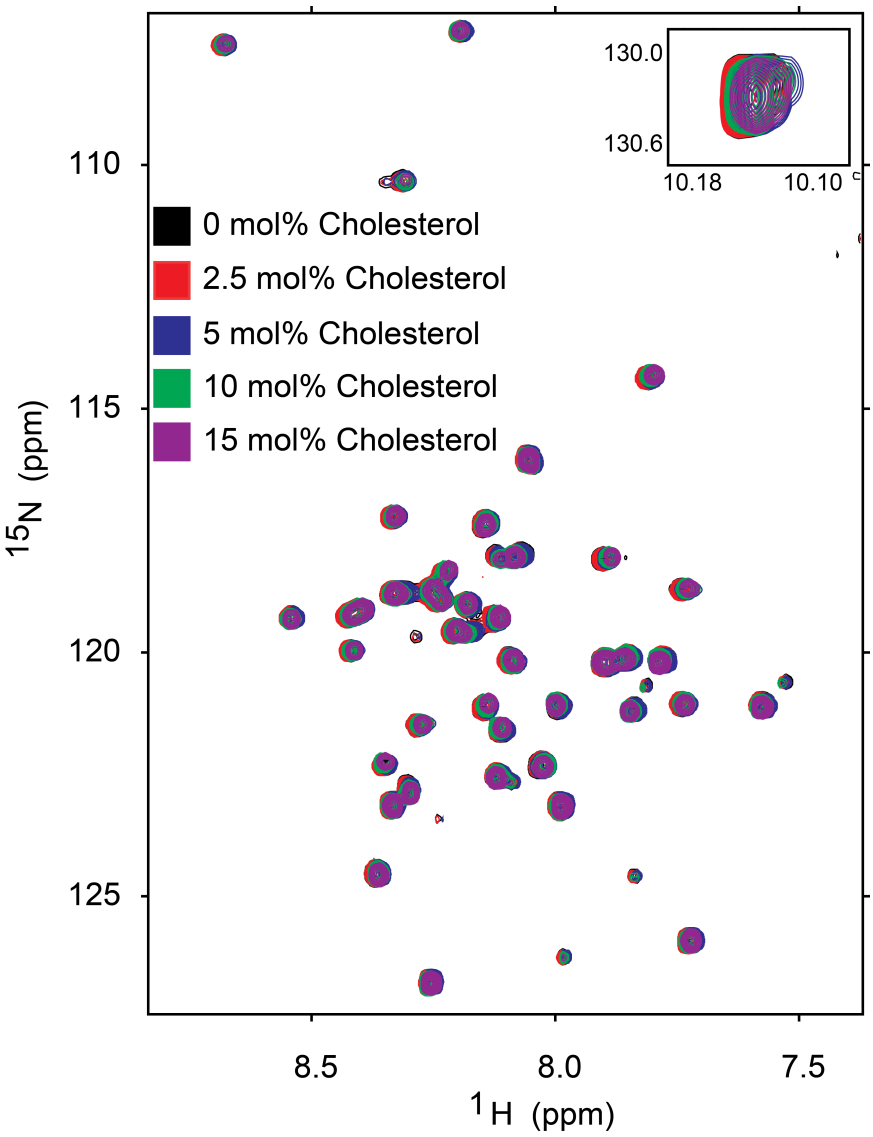

Figure 4.1. Notch 1 TM cholesterol titration. NMR samples were prepared with increasing mol% cholesterol (0, 2.5, 5, 10, and 15 mol% cholesterol). Sample contained ~0.35 mM protein, 15% DMPC/Cholesterol/DH6PC bicelle. The experiment was run on a 900 MHz magnet with match experimental conditions for each sample. There are no significant chemical shift perturbations that would suggest direct binding.

Impact of Varying Membrane Thickness on Notch Structure and Topology. The positioning of C99 relative to the membrane in detergent micelles was published in 2008[35] and in bicelles of varying thickness in 2014.[38] The positioning of C99 relative to the membrane changed with membrane thickness, and the changes were focused on the n-terminal (extracellularly) end of the TM helix. The C-terminal end of the helix was un-changed in terms of its location with respect to the membrane surface with increasing membrane thickness possibly due to a proposed membrane termination/anchor sequence of 3 positively charged lysine residues.[38] Topological changes induced by membrane thickness may regulate γ-secretase cleavage in both C99 and Notch processing. This led us to explore how Notch membrane topology is affected by changes in membrane thickness. We prepared three matched samples in 3 conditions. The first condition was in DMPC bicelles, relatively thin bicelles in which the lipid component has two 14-carbon chains; the second was in ESM bicelles, where the lipid has two 16-carbon chains; and the third was MSM bicelles, in which the lipid component has both a 16- and a 23- carbon chain. The changes in acyl chain length significantly increase the bilayer thickness. HSQC spectra of each condition were collected and the peak intensity of paramagnetic probe (water- and lipid-soluble) over reference intensity was plotted against residue number.

The plots of the three membrane thicknesses can be seen in Figure 4.2. These plots indicate that the Notch 1 TM segment is structurally tolerant to different bilayer thicknesses. The two solid lines represent the helix. There are no significant accessibility pattern differences at the C-terminal (intracellular) end of the TM helix and the juxtamembrane region as the bilayer thickness is varied. For this segment, probe

access patterns are conserved despite the increase in the bilayer thickness. In contrast, there are qualitatively different patterns of probe access in the N-terminal region of the helix between the bicelle conditions. The thicker bilayer condition is associated with greater access to the extracelluar N-terminal end of the TM helix by the lipophilic probe 16-DSA. The Gd-DTPA effect is more diverse, thus suggesting that the bilayer thickness does change only the N-terminal helix positioning not the C-terminal portion. This dataset is similar to the results for C99 as presented in 2014.[38] Like C99, Notch 1 also has a series of positive residues (R-K-R-R-R) at the juxtamembrane interface. These residues may serve as the Notch 1 membrane anchor sequence. In order to confirm the change of bicelle thickness didn't change conformational structure, differences between observed and random coil backbone amide peak chemical shift values are plotted in Figure 4.3. There were no significant changes in secondary structure in the differing bicelle thicknesses.

Side-Chain Assignments. Obtaining side chain assignments for membrane proteins can be challenging due the size of the protein/lipid mimetic complex and the enhanced rate of relaxation.[35] Generally, either special labeling schemes are performed to label the methyl groups of branched chain amino acids, or expensive deuterated detergents are purchased to reduce the proton peak intensity of the lipid chain. In the non-deuterated DMPC/DH_6PC bicelles used in the Notch1 TM studies there are 75 peaks in the aliphatic region that are from the bicelle. These signals can easily overwhelm the intensity of the side-chain chemical shifts. Using a combination of H(CCO)NH, C(CO)NH and HCCH-TOCSY NMR experiments, the chemical shift assignments were made for each backbone residue. The HCCH-TOCSY was used to coordinate the

identity of the carbon and proton and resulted in 95% of the non-proline side-chain atoms being assigned. The two residues left unassigned were either preceding proline residues or had a signal too weak to be reliable. The HCCH-TOCSY experiment was also used to determine the all trans orientation of the tetra-proline stretch based on the chemical shift of the Cβ and the Cγ.[235] This all-trans orientation suggests new structural information about the tetra-proline motif that in part made up for not being able to do more traditional ^{13}C-NOESY experiments to obtain structural restraints for the proline residues.

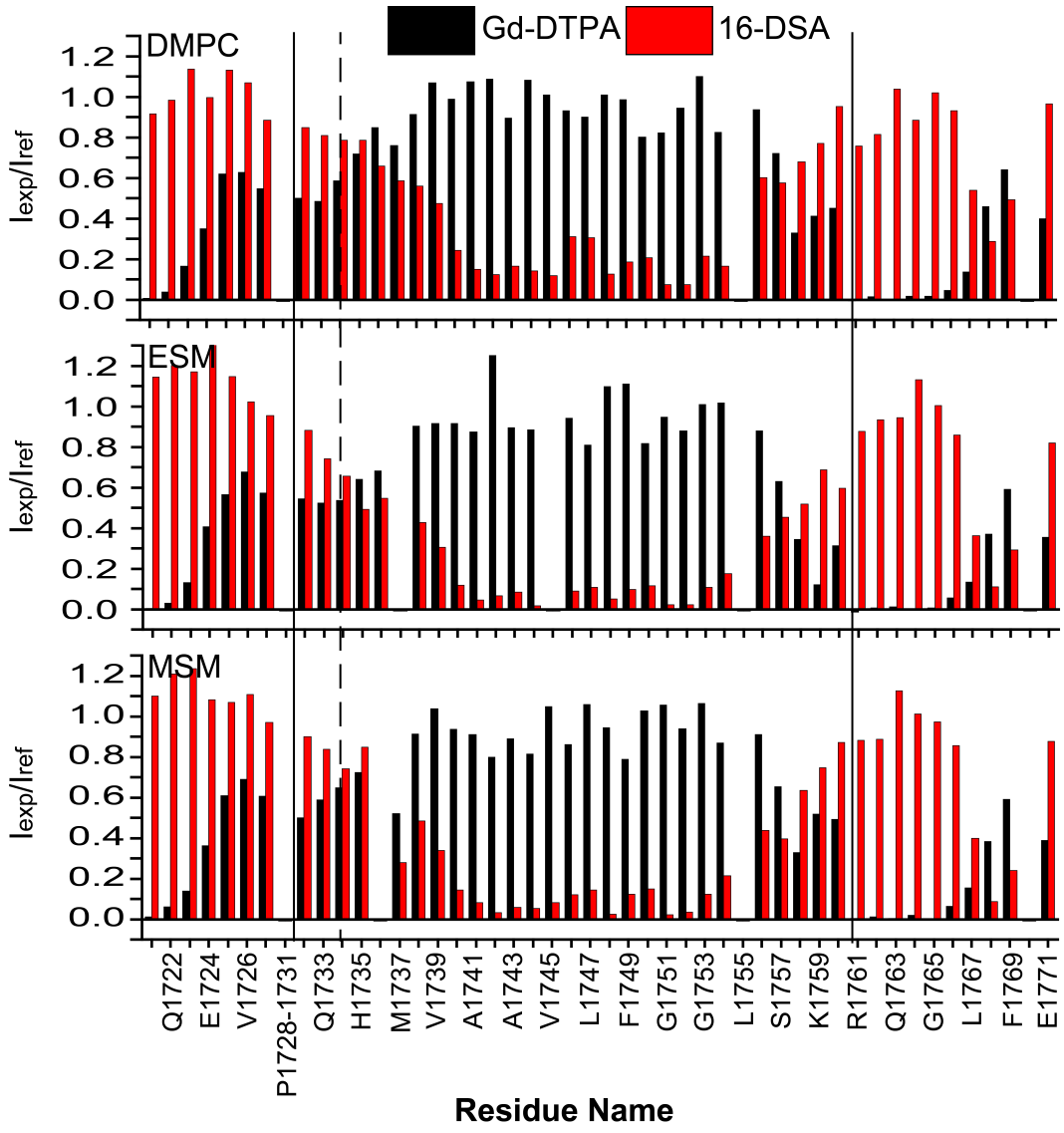

Figure 4.2- Membrane Thickness. Notch 1 TM segment was prepared in bicelles with 14, 16 or 22 carbons per chain varying the membrane thickness. Water (Gd-DTPA) or lipid (16-DSA) soluble paramagnetic probes were added and the paramagnetic induced change in intensity was monitored per residue in the different thicknesses. The solid lines indicate the length of the helix while the dotted line marks the region with the most changes in different bicelle thicknesses.

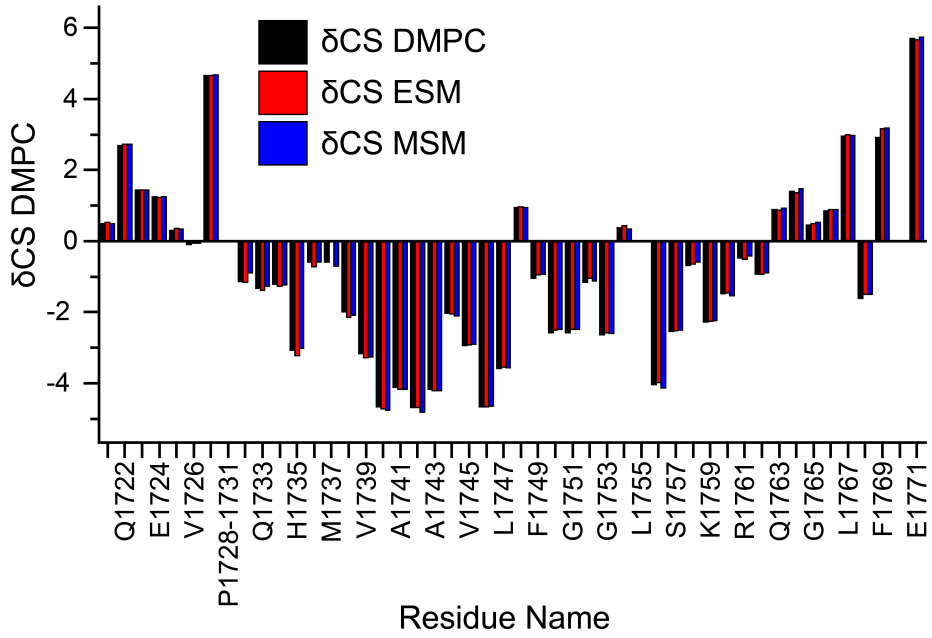

Figure 4.3- Secondary structure changes. The change in the ^{15}N chemical shift of Notch 1 residues compared to random coil was plotted for each bicelle condition. There are no significant differences between conditions.

The near complete assignment of backbone and side-chain residues was useful in assigning the 1H-1H-15N NOESY-TROSY spectrum, as required for structural restraints. The number of backbone-backbone NOE peaks in the NOESY was sparse although the side-chain NOE's were better represented. Using our side-chain and backbone assignments, a total of 337 NOEs were assigned with a high degree of confidence despite the (obscuring) contributions of lipid-detergent to side-chain NOES present owing to the use of non-deuterated bicelles. These NOEs were used as distance constraints during structure calculations.

Structure Determination. A combination of NMR restraints was used to determine the bicelle-associated structure of the transmembrane segment of Notch 1. Matched spin labeled sample was used to collect a paramagnetic HSQC and a diamagnetic HSQC and the difference in the peak intensity was used to obtain distance restraints as described in the methods. The NOEs described above and dihedral angles calculated from the backbone chemical shift values[211, 236] were also used in preliminary structure calculation. After initial calculations, a final calculation of 2,000 structures was completed and had reasonable convergence. The helical Notch1 TM segment is fairly straight, although a non-ideal α-helix. The N-terminal soluble loop samples space extensively (Figure 4.4). The C-terminus is far more constrained, at least in part due to a kink at the L-W-F motif that is membrane reentrant.[217] From the top 1% lowest energy models, ten models that did not have soluble domains occupying space where the bilayer would be were selected to undergo further refinement in a 60 ns AMBER molecular dynamics simulation. Both the X-Plor structures and the Amber refinement structures were validated by Procheck.[237] A list of restraints, violations and statistics can

seen in Table 4.1. When the Notch structures were inserted in the DMPC bilayer prior to rMD refinement the tryptophan side-chain were clearly intercalated in the lipid bilayer (Figure 4.5). In the refined structure, there is a distorted helix turn at the center of the intracellular surface. In Figure 4.6, an example X-PLOR model is compared to the refined model. Specific residues are shaded and demonstrate that despite being similarly aligned at the start of the helix (A1732), the distortion essentially initiates an un-winding of the helix at L1747 shifting the register of the entire second half of the helix, which is near the primary γ-secretase cut site (V1754). Interestingly, the overall convergence of the structures was not impeded.

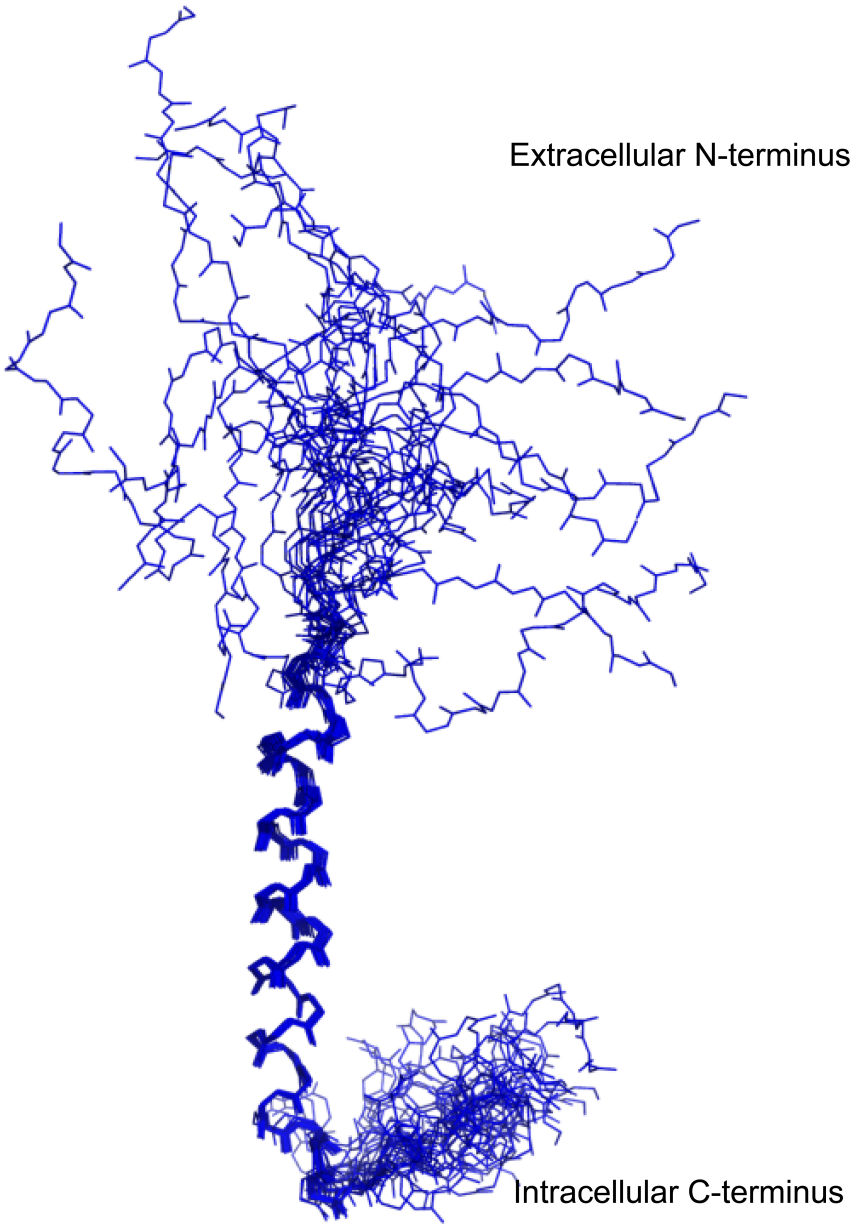

Figure 4.4- Top 1% of 2,000 structures. The TM helix tightly converges although there is significant divergence at the soluble N- and C-terminal segments.

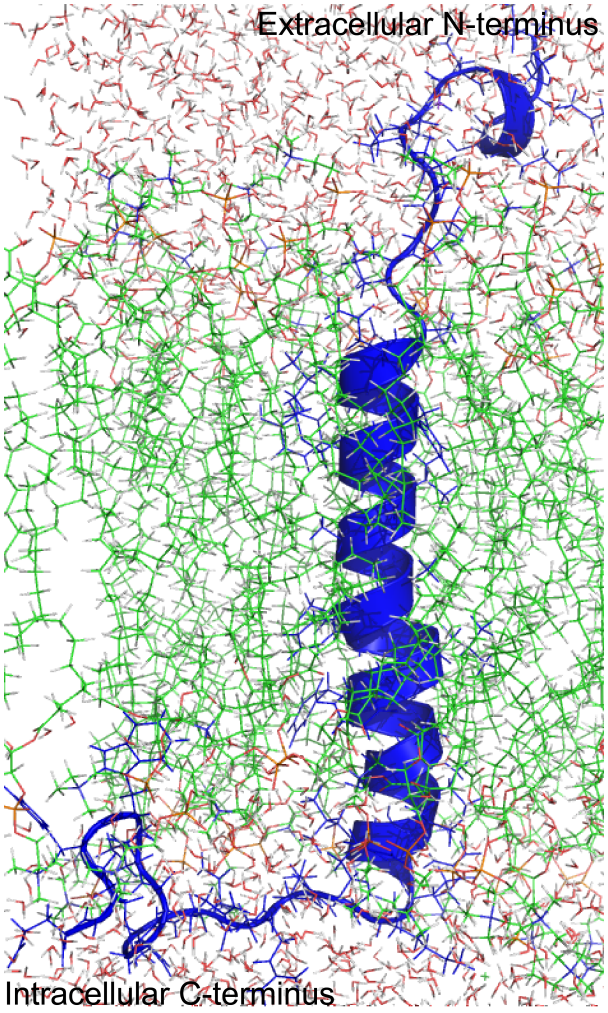

Figure 4.5- Average structure of Notch 1 TM during rMD simulation. An example of Notch 1 TM structure during 60ns molecular dynamics simulation. There is fraying in the C-terminal part of the helix starting with a pronounced helical distortion. The re-entrant tryptophan is firmly imbedded in the lipid bilayer. Overall, the Notch 1 TM segment is a straight, although, non-ideal α-helix.

Table 4.1- Statistics of structural quality. The statistics for restraints, structural calculations, and structural quality for 10 lowest energy structures of 2000 calculated using XPlor and further refined in Amber.

NMR Distance and dihedral constraints

Distance Constraints

Total NOE	337
Intra-residue	85
Inter-residue	244
Ambiguous	8
PRE restraints**	81
Total dihedral angle restraints	70

Structure Statistics*

	X-plor	**AMBER**
Violations		
Distance constraints (Å)	0.067±0.001	0.121±0.11
Dihedral angle constraints (°)	1.129±0.064	9.067±1.131
Average backbone pairwise r.m.s.d. (Å)***	0.088	0.723
Ramachandran plot (%)		
Most favored regions	90%	90.9%
Additionally allowed regions	10%	9.1%
Generous allowed regions	0%	0%
Disallowed regions	0%	0%

*10 NMR structures from the top 1% were used in the calculations.
**PRE restraints came from F1744C (39) and C1752 (42).

AMBER Simulation. The 60 ns simulation refined the X-Plor structure and provided a computational model of water entry to the lipid bilayer and Notch 1 TM side-chain-lipid interactions. An analysis of the atomic positions over time allowed an average calculation of duration of close proximity of each residue with either water or with the acyl chain of a DMPC molecule. In Figure 4.7 the average contacts for all ten models are plotted for each residue. There is a high level of contact between residues and acyl chains in the TM span (1737-1756) (Figure 4.7a). Interestingly, we see a shoulder on the curve from residues P1730-F1736. This plot also shows increased contact with lipid acyl chains for the re-entrant sequence L-W-F (residues 1767-1769). The result for water contact shows the TM segment (1737-1754) is nearly totally devoid of water (Figure 4.7b). Interestingly, there is a peak representing water contact at position 1753, this would position a water molecule very close to the γ-secretase cleavage site that releases the NICD from the membrane.

Discussion

One challenge that arises when trying to develop AD drugs is a lack of understanding of the γ-secretase mechanism of action and how this enzyme differentiates C99 and Notch as substrates. The data presented in this paper will help to clarify some details regarding the differences and possibly inform on whether the γ-secretase mechanism of action has a substrate conformational structural requirement.

Role of Cholesterol in AD vs. Notch Signaling

The interaction and importance of cholesterol in AD has been extensively studied.[23, 52, 92, 234] Cholesterol is thought to play important roles in AD progression. Our

observed lack interaction between the Notch 1 TM segment and cholesterol was not surprising. The majority of research examining lipids and lipid requirements in Notch signaling has been focused on cellular trafficking and endocytosis rather than an interaction between Notch and cholesterol. Research has shown that non-cannonical Notch signaling can be stimulated by endocytosis and initiated by an E3 ligase with an unknown mechanism.[238] Further, depending on the endosomal stage, levels of this basal, non-canonical signaling can be tuned.[239] In 2014, the Baron group reported that cholesterol added or depleted from culture media was able to change the cellular location of Notch activation in this non-canonical signaling pathway.[240] They did not posit a mechanism of how cholesterol was changing Notch signaling, but based on our titration results it is likely an indirect effect, unlike the C99-cholesterol relationship. It is possible that changing the membrane cholesterol levels may alter clathrin and AP-3 endocytosis[241] and thus change Notch trafficking.

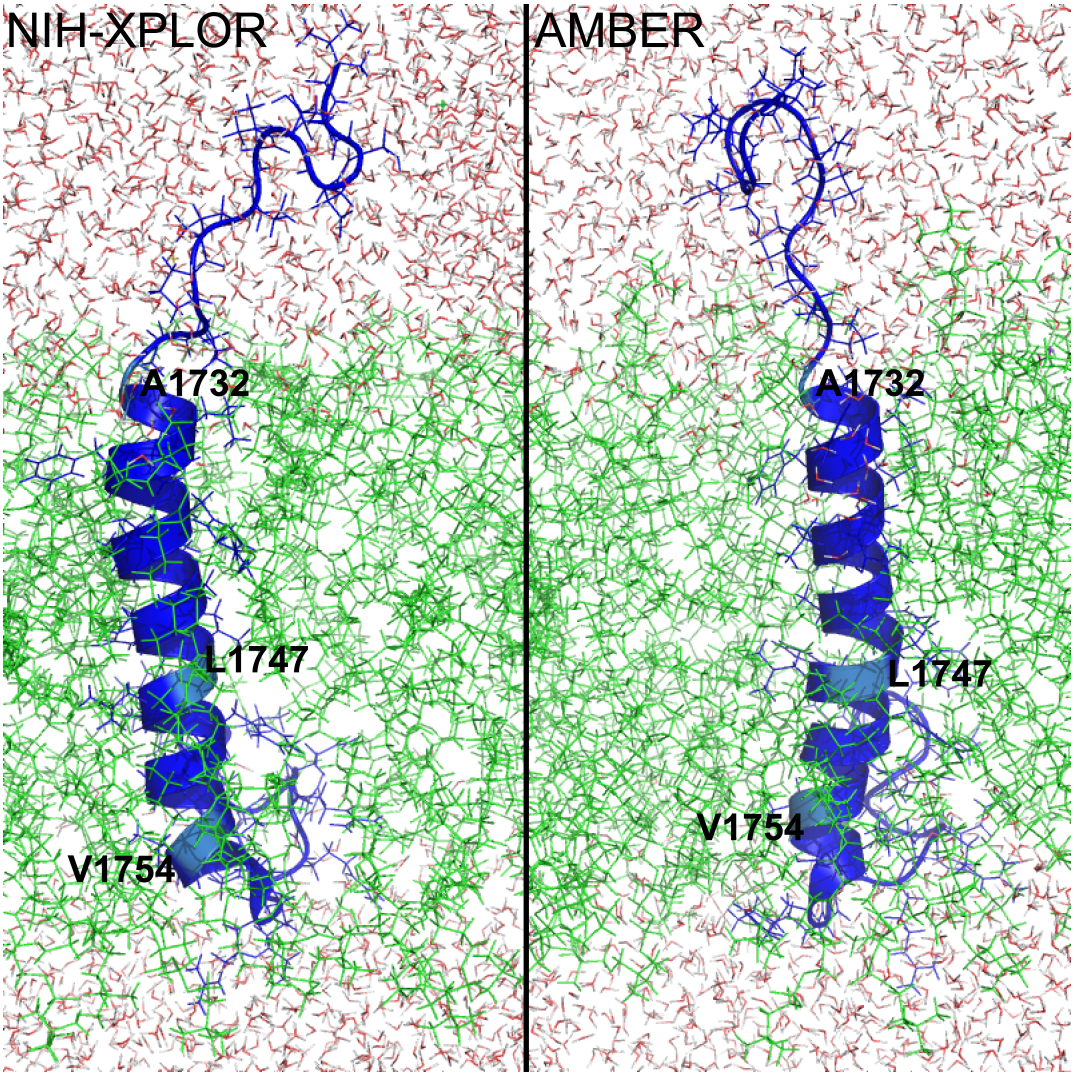

Figure 4.6- X-plor vs. AMBER comparison. Comparison of the starting X-PLOR determined structure to the AMBER refinement average structure. Specific residues are labeled and shaded lighter blue to emphasize the changes in the refined structure. Notice the shift in helical register starting at L1747 not present in A1732.

Membrane Thickness

It is known that the production of Aβ is controlled by the function and regulation of γ-secretase. This membrane bound complex is sensitive to pH,[242, 243] membrane thickness, chain length, saturation and lipid head group.[92-94] Because of this, the lipid microenvironment and the cellular compartment that γ-secretase is occupying at the time of enzyme/substrate interaction may regulate function. Based on previously published data it is easy to speculate that the kink in the C99 structure provides flexibility that allows C99 to straighten out in thicker membranes without changing the c-terminal membrane anchor position, a mechanism that would explain the changes in paramagnetic accessibility with changing membrane thickness. This would likely change the position of C99 in the active site of γ-secretase. This may be one potential way to regulate proteolysis. The straighter and more rigid helix of Notch[217] does not have this capability. During the course of the AMBER simulations, the TM segment seems to laterally diffuse through the membrane, sitting at an angle within the membrane as opposed to the perpendicular orientation relative to the plane of the membrane. This angled positioning would allow for a greater membrane thickness tolerance as the angle of the helix could adjust with changing bilayer thickness. It is also possible that some of the accessibility ambiguity comes from multiple populations of Notch1 at different angles within the bicelle resulting in an average accessibility seen in Figure 4.2 as opposed to a single conformational accessibility. This Notch flexibility would suggest that a therapeutic that would prevent C99 from entering the preferred cellular compartment for γ-secretase cleavage, or that prevents C99 from adjusting to the bilayer thickness, thus changing γ-secretase cleavage, would not have a major impact on Notch processing.

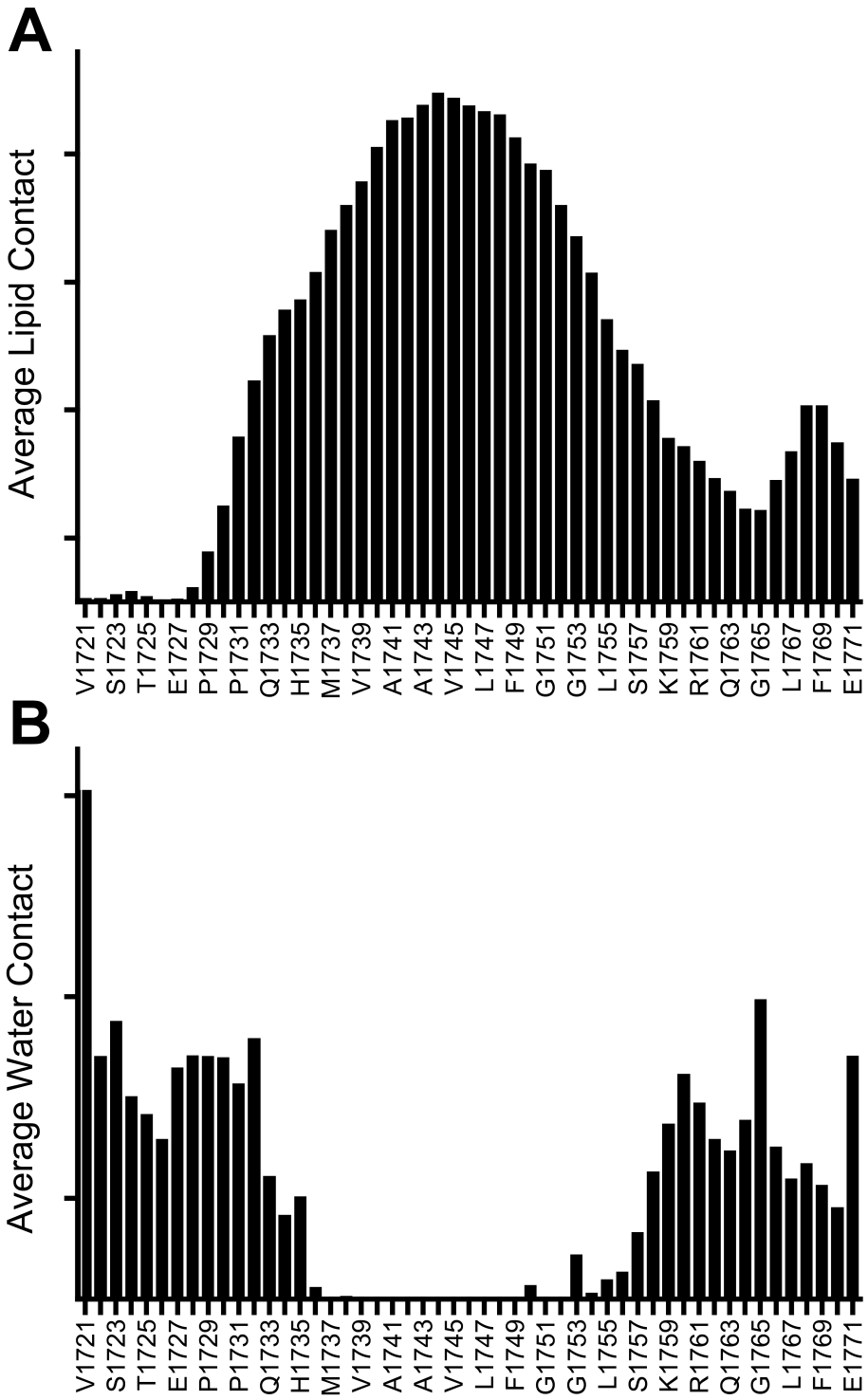

Figure 4.7- AMBER analysis. Analysis of residue contact with lipid acyl chain (A) and water (B) during 40 ns rMD simulation.

Amber Model

The average Notch helix after the rMD refinement is a non-ideal helix. Largely remaining a straight helix, the distortion around residues 1746-1748 seemingly tightens the N-terminal portion of the helix leaving a frayed or unwound C-terminal portion. This helical distortion gives the appearance of a bend or a kink in the helix. Interestingly, this may better help to position Notch at the active site of γ-secretase and limit steric clashes between the straight Notch helix and the loop between presenilin helix 3 and 4 surrounding the active site. The presence of water seen in the membrane during the rMD simulation suggests an unstable helix. The water molecule at position 1753 water could serve to solvate the helix after proteolysis or to compensate for broken hydrogen bonding that may result from the distorted helical turn. The clustering of waters around the N-terminal helix at least partially supports the water exchange data previously published.[217] The differences seen are likely due to the difference in timescale (ns vs. ms).[217] The near consistent close proximity of the tryptophan residue to the lipid chains of the bilayer in the simulation suggest that the membrane penetrance by the re-entrant L-W-F sequence is energetically reasonable and supports the membrane accessibility data presented previously.[217] Interestingly, the shoulder seen in Figure 4.7a is the same region of the TM helix that has an ambiguous data in Figure 4.2. This region is the most N-terminal portion of the helix, and there is a level of ambiguity regarding positioning within the membrane. This simulation confirms earlier hypotheses that these residues sit very near the surface of the membrane and may also sample outside of the membrane.

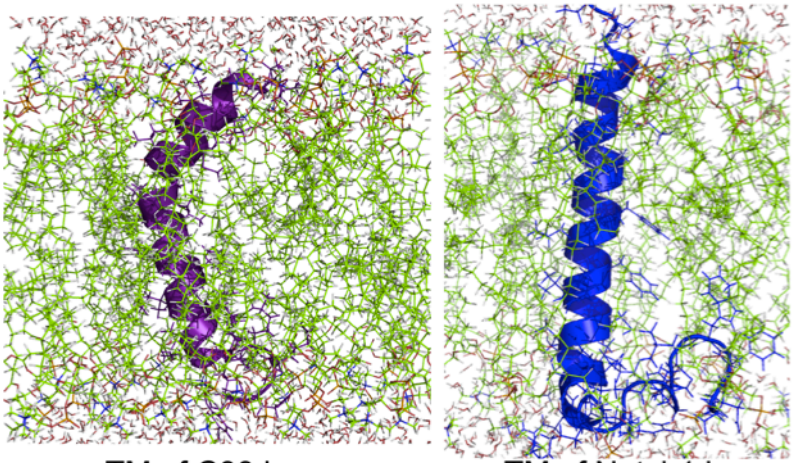

Figure 4.8- Comparison of C99 and Notch 1 TM in DMPC bilayer. C99 and Notch 1 have distinctly different structures.

Conclusion

The biochemistry of Notch and C99 is very different. The work presented in this paper further demonstrates this by showing Notch has no interaction with cholesterol and seems to have a totally different mechanism for adjusting to different membrane compositions/thicknesses than C99. Furthermore, the structures of Notch and C99 are very different. Comparing the two experimentally determined structures from simulated annealing (Figure 4.8), the significant differences in the transmembrane segment are apparent. C99 has a pronounced kink centered around 708/709 and decided surfaces. The Notch structure is a straight helix with a distortion in the helix seen in the rMD simulation that shifts the register of the helix near C-terminal end of the helix. The DeGrado lab has designed peptides that can bind specific integrin TM segments and small molecule inhibitors that can recognize mutations.[244, 245] These methodologies could potentially be used to capitalize on the distinct differences between C99 and Notch and that should be sufficient to engineer small molecule drugs that can specifically recognize proteins based on minor structural differences. In the case of differentiating Notch and C99, the differences are more than minor. With the completion of this work, there is now a complete dataset for the Notch 1 TM segment that compliments the accumulated data already known about the protein C99. With the complete datasets for both Notch 1 and C99, there should now be sufficient information to draw new insights into not just how γ-secretase functions, but also inform possible drug therapies that can specifically target APP and C99 while sparing the essential function of Notch.

V. Discussion and Future Directions

γ-Secretase Activating Protein

Ultimately, despite initial optimism, the GSAP work of the Sanders lab did not progress beyond the published manuscript described in Chapter 2 due to the unexpected challenges in working with recombinant GSAP. The overall instability of the protein and the unexpected requirement of detergent, despite being a soluble protein led us to question the stability and folded-ness of the protein. In the imatinib pull-down assays in which GSAP was discovered, it is possible that were other protein factors, that are essential for GSAP folding or functionality. Given that the entire panel of pull-down results were not published in He *et. al.,*[123] it is possible another protein co-factor was pulled down and was simply missed in the original screen. This would suggest that the *in vitro* protein that was purified was lacking an essential component that is needed for stability and possibly for the interaction with or the efficacy of the imatinib interaction. Given the detergent requirement in the purification (Deatherage *et. al.*)[246], it is also possible that GSAP is a lipid binding protein and there is a lipid co-factor.

Lipid binding proteins carry out a great number of different functions.[247-249] Since GSAP was expected to be a soluble protein, even if it binds lipids, it would be similar to other members of the lipid binding family. Folding upon lipid binding could make sense mechanistically given that APP and γ-secretase are generally considered to be associated with lipid rafts.[234] Lipid binding may be how GSAP is able to localize to its binding partners. GSAP does have a cholesterol-binding (CRAC) motif.[250, 251] If the CRAC motif does truly bind cholesterol, then the localization of APP and γ-secretase to

cholesterol rich microdomains would support GSAP being in close proximity to the other proteins.

As a future direction, obtaining a stable folded protein is essential. It would potentially be worthwhile to pursue condition testing that focuses on having lipids present. It would be interesting to see if the presence of cholesterol, sphingomyelin, phosphoethanolamine, or synthetic phosphocholine or phosphglycerine in a lipid bilayer mimetic would make a difference in the protein stability, activity or folded state. If it made a difference, it would suggest that the lipid presence makes a significant difference in protein stability.

GSAP Follow-up Research and Controversy

Following the 2012 Sanders Lab publication, subsequent papers came out that cast the GSAP story in a new light. In 2013, a *Journal of Biological Chemistry* paper was published that sought to further characterize the role of GSAP in imatinib regulation of γ-secretase.[252] In this paper, the researchers sought first to reproduce the finding of the original GSAP paper,[123] and then to extrapolate further. As in the original paper, siRNA knockdown of endogenous GSAP resulted in a reduction of Aβ levels. When the researcher hypothesized that overexpression of GSAP should increase Aβ levels, they were surprised that the results in different cell lines did not bear this hypothesis out. They found over expression of full-length GSAP and the reported 16kDa form reduced the levels of Aβ in some cells, but in N2a cells (used in He *et. al.*), GSAP did not change Aβ levels.[252]

In the original GSAP paper, the authors postulated that GSAP has a direct and specific interaction with the C-terminal domain of APP, called C99. Similar to the result

described in Chapter 2,[246] the authors performed a GSAP IP that failed to pull down either C99 or any components of γ-secretase. The reverse C99 IP did pull down γ-secretase components, but not GSAP.[252] These researchers also purified recombinant GSAP, which had a detergent in the final buffer, similar to the purification described in Chapter 2. They used this recombinant protein in an *in vitro* γ-secretase assay, where the addition of purified GSAP had no impact on the levels of either Aβ or the AICD.[252] Due to the inconsistencies the researchers saw between *in vitro* assays and *in vivo* assays and between their data and the data published in the original paper, the authors suggested that the GSAP story was more complicated than it originally seemed, consistent with our results.

In 2014, another paper, this time from the lab of Kai Blennow, shifted the focus back to imatinib as a possible drug compound lead. These researchers noticed that the GSAP paper and the Netzger paper used animal models and cellular assays; there was no exploration of how imatinib would change Aβ levels in human patients. They then collected plasma samples from >20 patients with either chronic myeloid leukemia (CML) or AD. The CML patients were about to begin a one-year treatment course with either 400 or 600 mg of imatinib. Plasma samples were drawn regularly over the course of the year, at 3, 6, 9 and 12 months. The AD patients had plasma drawn at the baseline time point and at the year mark.[253] In the CML cohort which had very low Aβ levels, the Blennow group saw an increase in Aβ levels at the 3 month time point which then normalized for the remainder of the year. This was the same in both the low (400 mg) and the high dose (600 mg) patients. The AD patients had steady levels of Aβ from baseline to the 12-month time point.[253] The researchers also saw no change in Aβ

levels with increased dosage of imatinib in cultured cells. This led the researchers to conclude that, in humans, imatinib was not significantly impacting Aβ levels and therefore, both imatinib and GSAP are unlikely to be good targets for AD therapeutics.[253]

It is important to briefly discuss that even before the GSAP theory was advanced in 2010, there were at least two opposing theories regarding how imatinib was able to lower Aβ levels. The first theory, published by the Wolfe group in 2005, investigated the role that nucleotides played in γ-secretase activity. They found that the purity of the Gleevac drug changed how the γ-secretase activity was inhibited. Fully purified Gleevac did not inhibit γ-secretase activity. They reported a number of additional compounds found in commercially available Gleevac, and suggested that one of these molecules was the actual inhibitory molecule.[254] In 2007, the Kilger group published a different theory. They reported that the effects of imatinib are independent of γ-secretase inhibition.[255] In this publication, the Kilger group presented a model where Gleevac was able to reduce Aβ through the action of neprilysin, a metalloprotein that degrades Aβ.[256] The Kilger group proposed that Gleevac increased the AICD by slowing the peptide turnover. This increase enhances neprilysin expression and the increased protein levels are then able to clear more Aβ, thus lowering the overall amount without changing γ-secretase activity or affecting Notch processing.[255] These theories are very different from the mechanism laid out in the GSAP paper.

The contradictions and inconsistencies between different groups investigating imatinib and GSAP led to a report covering the issue in Alzforum, in early 2014.[257] In this article the author reported at least 8 groups attempted to reproduce the original

GSAP work, and none were successful. Paul Greengard, the corresponding author of the original paper suggested that the real problem with the failed attempts was that other researchers were not exactly duplicating experimental conditions and this was where the contradictions came from.[257] This opened a discussion regarding scientific reproducibility and how closely labs should have to follow original methods to get identical results. Another question arose regarding the dissemination of negative or contradictory data. The original paper was published in the journal *Nature,* which has a large impact factor and a powerful reputation. The three papers that contradicted this work were published in *Biochemistry*, *Journal of Biological Chemistry*, and *Alzheimer's & Dementia.* These journals have excellent reputations but are not as widely cited or read as *Nature*. According to the Alzforum report, Blennow attempted to publish his imatinib study in *Nature* as a BCA (Brief Communication Arising), but after consulting with the original authors, *Nature* elected not to publish the paper. This leads to interesting questions about journal's roles in being impartial and disseminating negative data or opposing research. To paraphrase a quote from the Alzforum report by a leading AD researcher Bart deStrooper "…negative or contradictory data is important and needs to be published at the same level as the original paper…"[257]

Despite the controversy discussed in this section and the contradictory papers published in 2012, 2013, and 2014, GSAP is still mentioned as a viable drug target in reviews, and people are still trying to learn more about this molecule. In fact, new papers have been published that explore the GSAP/imatinib relationship. One such paper suggested that in mice, imatinib acts in GSAP expression and lowers Aβ and tau phosphorylation.[258] Another paper explored GSAP degradation and determined that

GSAP is ubiqutinated and degraded by the proteasome.[259] Another publication proposed that Caspase 3 modulates GSAP.[260] These new papers don't render the contradictory papers moot, and the controversy regarding GSAP will likely remain until either a lab is able to replicate the results seen in the original paper or GSAP is determined to be unimportant to AD pathology.

Notch 1

Structure

The Notch 1 TM segment structure detailed in Chapter 4 is the first transmembrane segment structure that has been determined in the Notch field. There are four Notch family members and the Notch family ligands; Jagged and DSL, are also type 1 membrane proteins. Prior to the Notch 1 TM studies, the bulk of the structural work being done has been on the soluble domains of these proteins. A summary of the structures published as of 2008 was published in the *Journal of Cell Science*.[169] One avenue of future research will be to determine the structures of the missing TM segments using the purification strategies detailed in Chapter 3.[217] A table of possible structural targets can be seen in Table 5.1. It would also worthwhile to determine if computational methods could be used to model a reconstructed version of full length Notch using the published structures as a way to better model and visualize the proteolytic processing that occurs during Notch signaling.

Table 5.1- New TM segment targets

Target Name	Uniprot ID	Approximate TM Span*
Notch 2	Q04721	1678-1696
Notch 3	Q9UM47	1644-1664
Notch 4	Q99466	1448-1468
Jagged 1	P78504	1068-1093
Jagged 2	Q9Y219	1081-1101
Delta-like protein 1 (Dll1)	O00548	546-568

*Proposed TM span from Uniprot entry.

Notch and Disease

Beyond the confounding role that Notch plays in AD pathogenesis, Notch and associated signaling have been implicated in a number of different serious diseases. The loss of Notch function, either due to mutation in the Notch ligand binding domain or in the ligand itself can cause an array of developmental disorders including Alagille Syndrome, and heritable congenital heart defects.[261-264] In the case of stroke or traumatic brain injury, the ischemic neuronal injury/death prognosis can be worsened by Notch activation worsening inflammation.[265] Notch signaling controls tumor progression.[204, 266, 267] There have been preclinical studies that use γ-secretase inhibitors suggesting that changing Notch signaling may be a way to disrupt cancer progression.[268, 269] Mutation in the NRR of Notch can cause T-cell acute lymphoblastic leukemia (T-ALL) by deregulating Notch signaling.[159, 270, 271] There is even evidence to suggest that there is hyperactivation of Notch signaling in AD and Pick's disease.[272]

There is now a wealth of biochemical and structural data that are known about the Notch 1 TM segment and the soluble domains. A future research endeavor should be to design a small drug or peptide that would bind specifically to the TM segment to inhibit γ-secretase cleavage and could be used immediately after stroke and during cancer chemotherapy treatment to prevent damaging inflammation and tumor metastasis. There is evidence that small changes to a TM helix structure are sufficient for drug specificity.[244, 245] As such, a drug could be made to prevent incidences of illness where overactive Notch signaling causes disease without necessarily inhibiting the Notch signaling otherwise required for functionality.

Figure 5.1- Clustal sequence alignment of the human Notch family transmembrane segments. The level of conservation is marked by darker shade. Arrows mark the absolute conservation of the S2 cut site, the "membrane anchor" sequence, and the re-entrant tryptophan sequence.

Notch Family Sequence Conservation

The Notch 1 TM segment characterization work described in Chapters 3 and 4 is the first time structural and biophysical characteristics of the transmembrane segment of a member of the Notch family has been investigated in depth. Only the TM segment of Notch 1 has been determined, so it is challenging to assess how many structural and biochemical similarities can be inferred for the other members of the Notch family. As mentioned in Chapter 1, Notch 1-4 vary in both the number of EGF repeats and in the presence of the transcriptional activation domain (TAD). These proteins also have different TM segments. A Clustal W[273] sequence alignment of the four human Notch proteins can be seen in Figure 5.1. There are three sites of absolute conservation across the family. The first is at the S2 cut site.

The second site of conservation is at the membrane anchor arginine(s) at the juxtamembrane (discussed in Chapter 4). This conservation of both arginine positioning and overall charge state in the same position support the hypothesis that this positive charge serves to anchor the C-terminal position of the helix relative to the membrane. This would help to position the helix at the approximate position to be cleaved by γ-secretase. Changes to the charge state of this stretch of positively charged residues would possibly change the positioning of the molecule in the membrane shifting the γ-secretase cut site and thus the NICD. It has already been reported that mutating Lysine1759 to arginine shifts the S3 cute site and forms an unstable NICD with weaker signaling.[274] The data in Chapter 4 (Figure 4.2) shows changes to membrane thickness only change the N-terminal helix topology pattern not the C-terminal. It is possible that disrupting the membrane anchor would change the C-terminal positioning and alter γ-

secretase cleavage. This would be an avenue for future research to pursue: determining how lipid composition (and thus cellular compartment[95]) would change Notch topology and NICD generation across that Notch family, which could serve to better our understanding of Notch signaling.

The third site of absolute conservation is in the intracellular juxtamembrane region. In Notch 1 there is a L-W-F sequence. The L-W is conserved and the third position is conserved for residues with strongly similar chemical properties. This stretch of residues has been shown to re-enter the lipid bilayer (discussed in Chapter 3).[217] The molecular dynamics refinement in AMBER (Chapter 4, Figure 4.7a) also shows a distinct kink at those residues, and the tryptophan residue is firmly inserted in the bilayer and does not leave the membrane during the 60ns simulation. It is likely that the other Notch family members have a similar re-entrant kink. This part of the protein is technically part of the RAM domain. Determining what function this amphipathic region has, and whether mutating it would alter the ability of the RAM domain to bind the transcription factor-binding partners would allow us to better understand what physiological role this amphipathic region has and why it would be conserved. It is also possible that these residues position the intracellular NICD domain away from γ-secretase during cleavage by serving as an anchor position distal to the active site. Determining if mutagenesis of these residues changes γ-secretase cleavage would assess whether these residues are more important to Notch and notch signaling than had previously been considered.

The remainder of the helix has regions where the sequence is moderately conserved, namely in overall chemical properties (see Figure 5.1), especially in the

center of the helix. Given that the Notch 1 structure is a generally straight helix (although not an ideal α-helix), it would be valuable to determine the structure of the other three Notch proteins to see if the structure of the other three would resemble Notch, or if they would demonstrate curvature, a kink, or dynamic flexibility like C99.[35, 36] Determining the structure of the different members of the Notch family would help to assess the γ-secretase-substrate interaction in different cell types due to variable Notch family tissue expression.

Docking and Molecular Dynamics Analysis of γ-Secretase and Substrate Interactions

Until late 2015 there was no atomic resolution structure of the complete γ-secretase complex. With the new γ-secretase structures and the experimentally determined structures of C99 and Notch, docking studies can be done to interrogate the differences in the substrate cleavage. Future docking studies could also be performed as more γ-secretase substrate structures are published. The Sanders group has structures of 2 members of the KCNE modulatory protein family. These proteins were listed as a substrate in Table 1.1, but γ-secretase cleavage is not a big part of the literature. It would be worthwhile to pursue the docking to determine if the docking of these predicted substrate would resemble the docking of the better known substrates Notch and C99.

Additional and more comprehensive studies should be performed to model the γ-secretase processivity that characterizes the proteolysis. It would also be interesting to determine if molecular dynamics simulations could reproduce the different confirmations that the Shi group found in their cryo-EM structural analysis of γ-secretase.[97]

Additionally, a simulation could map the helical trajectories that underlie the conformational changes that γ-secretase must undergo to bring the active site aspartate residues close enough to perform chemistry.

The connection between γ-secretase and lipid rafts has been well established.[234] Another research question to pursue with molecular dynamics simulations would be to assess the role that lipid rafts and cholesterol play in the organization and flexibility of the γ-secretase complex. Bai *et. al*. used careful cryo-EM reconstructions to show multiple confirmations of the γ-secretase active site.[97] They did not explore what the membrane organization and plasticity would do to moderate the flexibility of the γ-secretase complex. Figure 5.2 is a cartoon model of how the γ-secretase complex with substrate may be different in the bulk plasma membrane (top) and how the complex may change in lipid raft where the cholesterol and the sphingmyelin molecules serve to organize and rigidify the membrane (bottom).

It is possible that the flexibility of the bulk membrane allows for the multiple confirmations seen in the Bai *et. al.* paper. This flexibility also suggests that the active site confirmation could shift and change depending on the allowances of the membrane. Further, since it has been shown that in thicker membranes, only the n-terminal part of the helix is changed in C99[38] and in Notch (Chapter 4), this may suggest a concomitant change in γ-secretase. By first docking γ-secretase and the substrate to fully sample the conformational space, the models could then be computationally inserted into membranes enriched with cholesterol and sphingomyelin. The positioning of the substrate C-terminal residues could be enforced and molecular dynamics simulations could be run to explore the membrane induced conformational changes. These

simulations would not only further explore the γ-secretase active site, but would also provide information on the functional difference of γ-secretase in lipid rafts and outside of them that could be correlated to experimental data.

Another potentially helpful avenue of future research would be to use computational mutagenesis targeting how familial AD mutations in both C99 and in presenilin[275, 276] impact the structure and interactions of both C99 and γ-secretase. It is possible that these mutations induce structural changes that alter γ-secretase function. Determining the feasibility of an *in silico* drug screen to investigate small molecule compounds that might mitigate AD processing may also be a promising avenue of research that could result in a therapeutic possibility.

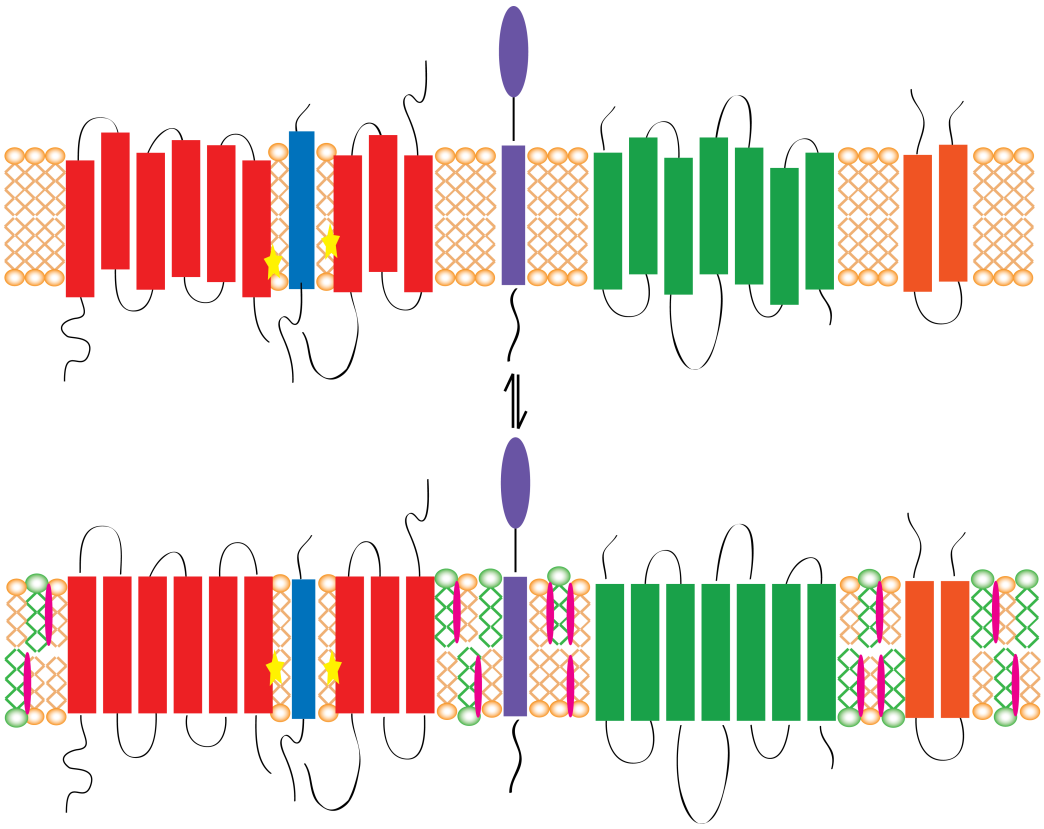

Figure 5.2- Lipid raft induced structural perturbations. It is possible that there are differences in the structural organization of γ-secretase in the bulk membrane (top) and in the ordered lipid rafts (bottom). The thicker and more rigid membrane may not only position the substrate differently but may change the orientation of the active site. Green lipid=sphingomyelin, pink=cholesterol, star=active site, blue=substrate.

Significance and Impact

The goal of this doctoral thesis project has been to explore and characterize the etiology of Alzheimer's disease. Multiple roads of inquiry were undertaken, but ultimately, this dissertation has detailed the work done towards characterizing proteins that are related to Alzheimer's disease. The characterization of GSAP, originally thought to regulate the processing of C99, in Chapter 2 clearly laid out the biochemical and preliminary structural characterization of the GSAP protein as well as why the project was terminated. The GSAP discussion in Chapter 5 further details problems with GSAP research that arose after the characterization was published. This details how issues of reproducibility and conflicts in the field have stymied the progress towards targeting GSAP as a viable AD therapeutic and how these issues need to be resolved before genuine progress can be made.

The lack of knowledge about biochemical and structural characteristics of the Notch protein, which has significantly confounded Alzheimer's disease drug development, led to the second major project described in this dissertation. Chapter 3 details the cloning, expression, purification, and initial NMR characterization of the transmembrane segment of the human Notch 1 protein. Chapter 4 details the structure determination process, Notch tolerance to bilayer thickness, cholesterol binding and a molecular dynamics simulation of the Notch molecule. The Notch structural studies add new knowledge on how to further differentiate Notch and C99 during the treatment of Alzheimer's disease and open new pathways of research towards drug development. Previously there was little to no structural or biochemical information about the Notch 1

TM segment. The work presented here provides the first structural information regarding the TM segment, which will will allow for better and more carefully designed studies in the future that can rely on the structural datasets.

In general, one challenge in the AD field is that there are disparate bodies of knowledge regarding disease pathology and etiology, but that are rarely merged or thought about in the context of planning for further study. In this work I present a potential new way to approach the AD field, in which real focus and attention are devoted to bridging disparate bodies of knowledge (i.e., regarding C99 and Notch) and creating a more broadly integrated body of knowledge for both datasets. This approach provides new information regarding the biochemical and structural differences between C99 and Notch 1, which may provide a new platform for the development of C99-specific therapeutics.

REFERENCES

[1] (2015) 2015 Alzheimer's disease facts and figures, *Alzheimer's & dementia : the journal of the Alzheimer's Association 11*, 332-384.

[2] Goedert, M., Crowther, R. A., and Garner, C. C. (1991) Molecular characterization of microtubule-associated proteins tau and MAP2, *Trends in neurosciences 14*, 193-199.

[3] Glenner, G. G., and Wong, C. W. (1984) Alzheimer's disease: initial report of the purification and characterization of a novel cerebrovascular amyloid protein, *Biochemical and biophysical research communications 120*, 885-890.

[4] Kang, J., Lemaire, H. G., Unterbeck, A., Salbaum, J. M., Masters, C. L., Grzeschik, K. H., Multhaup, G., Beyreuther, K., and Muller-Hill, B. (1987) The precursor of Alzheimer's disease amyloid A4 protein resembles a cell-surface receptor, *Nature 325*, 733-736.

[5] Tanzi, R. E., Gusella, J. F., Watkins, P. C., Bruns, G. A., St George-Hyslop, P., Van Keuren, M. L., Patterson, D., Pagan, S., Kurnit, D. M., and Neve, R. L. (1987) Amyloid beta protein gene: cDNA, mRNA distribution, and genetic linkage near the Alzheimer locus, *Science 235*, 880-884.

[6] Lott, I. T., and Head, E. (2001) Down syndrome and Alzheimer's disease: a link between development and aging, *Mental retardation and developmental disabilities research reviews 7*, 172-178.

[7] Zigman, W. B., Schupf, N., Sersen, E., and Silverman, W. (1996) Prevalence of dementia in adults with and without Down syndrome, *American journal of mental retardation : AJMR 100*, 403-412.

[8] Nunan, J., and Small, D. H. (2000) Regulation of APP cleavage by alpha-, beta- and gamma-secretases, *FEBS letters 483*, 6-10.

[9] Konietzko, U. (2012) AICD nuclear signaling and its possible contribution to Alzheimer's disease, *Current Alzheimer research 9*, 200-216.

[10] Dislich, B., and Lichtenthaler, S. F. (2012) The Membrane-Bound Aspartyl Protease BACE1: Molecular and Functional Properties in Alzheimer's Disease and Beyond, *Frontiers in physiology 3*, 8.

[11] Nikolaev, A., McLaughlin, T., O'Leary, D. D., and Tessier-Lavigne, M. (2009) APP binds DR6 to trigger axon pruning and neuron death via distinct caspases, *Nature 457*, 981-989.

[12] Kheradmand, F., and Werb, Z. (2002) Shedding light on sheddases: role in growth and development, *BioEssays : news and reviews in molecular, cellular and developmental biology 24*, 8-12.

[13] Beel, A. J., and Sanders, C. R. (2008) Substrate specificity of gamma-secretase and other intramembrane proteases, *Cellular and molecular life sciences : CMLS 65*, 1311-1334.

[14] Kukar, T. L., Ladd, T. B., Robertson, P., Pintchovski, S. A., Moore, B., Bann, M. A., Ren, Z., Jansen-West, K., Malphrus, K., Eggert, S., Maruyama, H., Cottrell, B. A., Das, P., Basi, G. S., Koo, E. H., and Golde, T. E. (2011) Lysine 624 of the

amyloid precursor protein (APP) is a critical determinant of amyloid beta peptide length: support for a sequential model of gamma-secretase intramembrane proteolysis and regulation by the amyloid beta precursor protein (APP) juxtamembrane region, *The Journal of biological chemistry 286*, 39804-39812.

[15] Takami, M., Nagashima, Y., Sano, Y., Ishihara, S., Morishima-Kawashima, M., Funamoto, S., and Ihara, Y. (2009) gamma-Secretase: successive tripeptide and tetrapeptide release from the transmembrane domain of beta-carboxyl terminal fragment, *The Journal of neuroscience : the official journal of the Society for Neuroscience 29*, 13042-13052.

[16] Yoshiike, Y., Chui, D. H., Akagi, T., Tanaka, N., and Takashima, A. (2003) Specific compositions of amyloid-beta peptides as the determinant of toxic beta-aggregation, *The Journal of biological chemistry 278*, 23648-23655.

[17] Hellstrom-Lindahl, E., Viitanen, M., and Marutle, A. (2009) Comparison of Abeta levels in the brain of familial and sporadic Alzheimer's disease, *Neurochemistry international 55*, 243-252.

[18] Kuperstein, I., Broersen, K., Benilova, I., Rozenski, J., Jonckheere, W., Debulpaep, M., Vandersteen, A., Segers-Nolten, I., Van Der Werf, K., Subramaniam, V., Braeken, D., Callewaert, G., Bartic, C., D'Hooge, R., Martins, I. C., Rousseau, F., Schymkowitz, J., and De Strooper, B. (2010) Neurotoxicity of Alzheimer's disease Abeta peptides is induced by small changes in the Abeta42 to Abeta40 ratio, *The EMBO journal 29*, 3408-3420.

[19] Pauwels, K., Williams, T. L., Morris, K. L., Jonckheere, W., Vandersteen, A., Kelly, G., Schymkowitz, J., Rousseau, F., Pastore, A., Serpell, L. C., and Broersen, K. (2012) Structural basis for increased toxicity of pathological abeta42:abeta40 ratios in Alzheimer disease, *The Journal of biological chemistry 287*, 5650-5660.

[20] Borchelt, D. R., Thinakaran, G., Eckman, C. B., Lee, M. K., Davenport, F., Ratovitsky, T., Prada, C. M., Kim, G., Seekins, S., Yager, D., Slunt, H. H., Wang, R., Seeger, M., Levey, A. I., Gandy, S. E., Copeland, N. G., Jenkins, N. A., Price, D. L., Younkin, S. G., and Sisodia, S. S. (1996) Familial Alzheimer's disease-linked presenilin 1 variants elevate Abeta1-42/1-40 ratio in vitro and in vivo, *Neuron 17*, 1005-1013.

[21] Zawia, N. H., Lahiri, D. K., and Cardozo-Pelaez, F. (2009) Epigenetics, oxidative stress, and Alzheimer disease, *Free radical biology & medicine 46*, 1241-1249.

[22] Pratico, D. (2008) Evidence of oxidative stress in Alzheimer's disease brain and antioxidant therapy: lights and shadows, *Annals of the New York Academy of Sciences 1147*, 70-78.

[23] Reid, P. C., Urano, Y., Kodama, T., and Hamakubo, T. (2007) Alzheimer's disease: cholesterol, membrane rafts, isoprenoids and statins, *Journal of cellular and molecular medicine 11*, 383-392.

[24] Snyder, S. W., Ladror, U. S., Wade, W. S., Wang, G. T., Barrett, L. W., Matayoshi, E. D., Huffaker, H. J., Krafft, G. A., and Holzman, T. F. (1994) Amyloid-beta aggregation: selective inhibition of aggregation in mixtures of amyloid with different chain lengths, *Biophysical journal 67*, 1216-1228.

[25] Walsh, D. M., and Selkoe, D. J. (2007) A beta oligomers - a decade of discovery, *Journal of neurochemistry 101*, 1172-1184.

[26] Hardy, J. A., and Higgins, G. A. (1992) Alzheimer's disease: the amyloid cascade hypothesis, *Science 256*, 184-185.
[27] Broersen, K., Rousseau, F., and Schymkowitz, J. (2010) The culprit behind amyloid beta peptide related neurotoxicity in Alzheimer's disease: oligomer size or conformation?, *Alzheimer's research & therapy 2*, 12.
[28] Karran, E., Mercken, M., and De Strooper, B. (2011) The amyloid cascade hypothesis for Alzheimer's disease: an appraisal for the development of therapeutics, *Nature reviews. Drug discovery 10*, 698-712.
[29] Hardy, J., and Selkoe, D. J. (2002) The Amyloid Hypothesis of Alzheimer's Disease: Progress and Problems on the Road to Therapeutics, *Science 297*, 353-356.
[30] Mudher, A., and Lovestone, S. (2002) Alzheimer's disease-do tauists and baptists finally shake hands?, *Trends in neurosciences 25*, 22-26.
[31] McGeer, P. L., and McGeer, E. G. (2013) The amyloid cascade-inflammatory hypothesis of Alzheimer disease: implications for therapy, *Acta neuropathologica 126*, 479-497.
[32] Herrup, K. (2015) The case for rejecting the amyloid cascade hypothesis, *Nature neuroscience 18*, 794-799.
[33] Puzzo, D., Gulisano, W., Arancio, O., and Palmeri, A. (2015) The keystone of Alzheimer pathogenesis might be sought in Aβ physiology, *Neuroscience 307*, 26-36.
[34] Lee, H. G., Casadesus, G., Zhu, X., Takeda, A., Perry, G., and Smith, M. A. (2004) Challenging the amyloid cascade hypothesis: senile plaques and amyloid-beta as protective adaptations to Alzheimer disease, *Annals of the New York Academy of Sciences 1019*, 1-4.
[35] Beel, A. J., Mobley, C. K., Kim, H. J., Tian, F., Hadziselimovic, A., Jap, B., Prestegard, J. H., and Sanders, C. R. (2008) Structural studies of the transmembrane C-terminal domain of the amyloid precursor protein (APP): does APP function as a cholesterol sensor?, *Biochemistry 47*, 9428-9446.
[36] Barrett, P. J., Song, Y., Van Horn, W. D., Hustedt, E. J., Schafer, J. M., Hadziselimovic, A., Beel, A. J., and Sanders, C. R. (2012) The amyloid precursor protein has a flexible transmembrane domain and binds cholesterol, *Science 336*, 1168-1171.
[37] Song, Y., Hustedt, E. J., Brandon, S., and Sanders, C. R. (2013) Competition Between Homodimerization and Cholesterol Binding to the C99 Domain of the Amyloid Precursor Protein, *Biochemistry 52*, 5051-5064.
[38] Song, Y., Mittendorf, K. F., Lu, Z., and Sanders, C. R. (2014) Impact of bilayer lipid composition on the structure and topology of the transmembrane amyloid precursor C99 protein, *Journal of the American Chemical Society 136*, 4093-4096.
[39] Sparks, D. L., Scheff, S. W., Hunsaker, J. C., 3rd, Liu, H., Landers, T., and Gross, D. R. (1994) Induction of Alzheimer-like beta-amyloid immunoreactivity in the brains of rabbits with dietary cholesterol, *Experimental neurology 126*, 88-94.
[40] Sparks, D. L., Hunsaker, J. C., 3rd, Scheff, S. W., Kryscio, R. J., Henson, J. L., and Markesbery, W. R. (1990) Cortical senile plaques in coronary artery disease, aging and Alzheimer's disease, *Neurobiology of aging 11*, 601-607.

[41] Gibson Wood, W., Eckert, G. P., Igbavboa, U., and Muller, W. E. (2003) Amyloid beta-protein interactions with membranes and cholesterol: causes or casualties of Alzheimer's disease, *Biochimica et biophysica acta 1610*, 281-290.
[42] Puglielli, L., Tanzi, R. E., and Kovacs, D. M. (2003) Alzheimer's disease: the cholesterol connection, *Nature neuroscience 6*, 345-351.
[43] Burns, M. P., and Rebeck, G. W. (2010) Intracellular cholesterol homeostasis and amyloid precursor protein processing, *Biochimica et biophysica acta 1801*, 853-859.
[44] Posse de Chaves, E. (2012) Reciprocal regulation of cholesterol and beta amyloid at the subcellular level in Alzheimer's disease, *Canadian journal of physiology and pharmacology 90*, 753-764.
[45] Maulik, M., Westaway, D., Jhamandas, J. H., and Kar, S. (2013) Role of cholesterol in APP metabolism and its significance in Alzheimer's disease pathogenesis, *Molecular neurobiology 47*, 37-63.
[46] Ong, W. Y., Tanaka, K., Dawe, G. S., Ittner, L. M., and Farooqui, A. A. (2013) Slow excitotoxicity in Alzheimer's disease, *Journal of Alzheimer's disease : JAD 35*, 643-668.
[47] Silva, T., Teixeira, J., Remiao, F., and Borges, F. (2013) Alzheimer's disease, cholesterol, and statins: the junctions of important metabolic pathways, *Angew Chem Int Ed Engl 52*, 1110-1121.
[48] Allinquant, B., Clamagirand, C., and Potier, M. C. (2014) Role of cholesterol metabolism in the pathogenesis of Alzheimer's disease, *Current opinion in clinical nutrition and metabolic care 17*, 319-323.
[49] Wood, W. G., Li, L., Muller, W. E., and Eckert, G. P. (2014) Cholesterol as a causative factor in Alzheimer's disease: a debatable hypothesis, *Journal of neurochemistry 129*, 559-572.
[50] Bu, G. (2009) Apolipoprotein E and its receptors in Alzheimer's disease: pathways, pathogenesis and therapy, *Nature reviews. Neuroscience 10*, 333-344.
[51] Fan, J., Donkin, J., and Wellington, C. (2009) Greasing the wheels of Abeta clearance in Alzheimer's disease: the role of lipids and apolipoprotein E, *Biofactors 35*, 239-248.
[52] Martins, I. J., Berger, T., Sharman, M. J., Verdile, G., Fuller, S. J., and Martins, R. N. (2009) Cholesterol metabolism and transport in the pathogenesis of Alzheimer's disease, *Journal of neurochemistry 111*, 1275-1308.
[53] Tanzi, R. E., and Bertram, L. (2001) New frontiers in Alzheimer's disease genetics, *Neuron 32*, 181-184.
[54] Florent-Bechard, S., Desbene, C., Garcia, P., Allouche, A., Youssef, I., Escanye, M. C., Koziel, V., Hanse, M., Malaplate-Armand, C., Stenger, C., Kriem, B., Yen-Potin, F. T., Olivier, J. L., Pillot, T., and Oster, T. (2009) The essential role of lipids in Alzheimer's disease, *Biochimie 91*, 804-809.
[55] Cole, S. L., and Vassar, R. (2007) The Alzheimer's disease beta-secretase enzyme, BACE1, *Molecular neurodegeneration 2*, 22.
[56] Puglielli, L., Konopka, G., Pack-Chung, E., Ingano, L. A., Berezovska, O., Hyman, B. T., Chang, T. Y., Tanzi, R. E., and Kovacs, D. M. (2001) Acyl-coenzyme A: cholesterol acyltransferase modulates the generation of the amyloid beta-peptide, *Nature cell biology 3*, 905-912.

[57] Pierrot, N., Tyteca, D., D'Auria, L., Dewachter, I., Gailly, P., Hendrickx, A., Tasiaux, B., Haylani, L. E., Muls, N., N'Kuli, F., Laquerriere, A., Demoulin, J. B., Campion, D., Brion, J. P., Courtoy, P. J., Kienlen-Campard, P., and Octave, J. N. (2013) Amyloid precursor protein controls cholesterol turnover needed for neuronal activity, *EMBO molecular medicine 5*, 608-625.

[58] Wang, W., Mutka, A. L., Zmrzljak, U. P., Rozman, D., Tanila, H., Gylling, H., Remes, A. M., Huttunen, H. J., and Ikonen, E. (2014) Amyloid precursor protein alpha- and beta-cleaved ectodomains exert opposing control of cholesterol homeostasis via SREBP2, *FASEB journal : official publication of the Federation of American Societies for Experimental Biology 28*, 849-860.

[59] Liu, Q., Zerbinatti, C. V., Zhang, J., Hoe, H. S., Wang, B., Cole, S. L., Herz, J., Muglia, L., and Bu, G. (2007) Amyloid precursor protein regulates brain apolipoprotein E and cholesterol metabolism through lipoprotein receptor LRP1, *Neuron 56*, 66-78.

[60] Muller, T., Meyer, H. E., Egensperger, R., and Marcus, K. (2008) The amyloid precursor protein intracellular domain (AICD) as modulator of gene expression, apoptosis, and cytoskeletal dynamics-relevance for Alzheimer's disease, *Progress in neurobiology 85*, 393-406.

[61] Kandiah, N., and Feldman, H. H. (2009) Therapeutic potential of statins in Alzheimer's disease, *Journal of the neurological sciences 283*, 230-234.

[62] Sadowski, M., Pankiewicz, J., Scholtzova, H., Li, Y. S., Quartermain, D., Duff, K., and Wisniewski, T. (2004) Links between the pathology of Alzheimer's disease and vascular dementia, *Neurochemical research 29*, 1257-1266.

[63] Kim, S. I., Yi, J. S., and Ko, Y. G. (2006) Amyloid beta oligomerization is induced by brain lipid rafts, *Journal of cellular biochemistry 99*, 878-889.

[64] Lau, T. L., Gehman, J. D., Wade, J. D., Masters, C. L., Barnham, K. J., and Separovic, F. (2007) Cholesterol and Clioquinol modulation of A beta(1-42) interaction with phospholipid bilayers and metals, *Biochimica et biophysica acta 1768*, 3135-3144.

[65] Nicholson, A. M., and Ferreira, A. (2009) Increased membrane cholesterol might render mature hippocampal neurons more susceptible to beta-amyloid-induced calpain activation and tau toxicity, *The Journal of neuroscience : the official journal of the Society for Neuroscience 29*, 4640-4651.

[66] Qiu, L., Lewis, A., Como, J., Vaughn, M. W., Huang, J., Somerharju, P., Virtanen, J., and Cheng, K. H. (2009) Cholesterol modulates the interaction of beta-amyloid peptide with lipid bilayers, *Biophysical journal 96*, 4299-4307.

[67] Grimm, M. O., Grimm, H. S., Patzold, A. J., Zinser, E. G., Halonen, R., Duering, M., Tschape, J. A., De Strooper, B., Muller, U., Shen, J., and Hartmann, T. (2005) Regulation of cholesterol and sphingomyelin metabolism by amyloid-beta and presenilin, *Nature cell biology 7*, 1118-1123.

[68] Haag, M. D., Hofman, A., Koudstaal, P. J., Stricker, B. H., and Breteler, M. M. (2009) Statins are associated with a reduced risk of Alzheimer disease regardless of lipophilicity. The Rotterdam Study, *Journal of neurology, neurosurgery, and psychiatry 80*, 13-17.

[69] Fonseca, A. C., Resende, R., Oliveira, C. R., and Pereira, C. M. (2010) Cholesterol and statins in Alzheimer's disease: current controversies, *Experimental neurology 223*, 282-293.
[70] Wolfe, M. S., and Kopan, R. (2004) Intramembrane Proteolysis: Theme and Variations, *Science 305*, 1119-1123.
[71] Makinoshima, H., and Glickman, M. S. (2006) Site-2 proteases in prokaryotes: regulated intramembrane proteolysis expands to microbial pathogenesis, *Microbes and infection / Institut Pasteur 8*, 1882-1888.
[72] Lemberg, M. K., Menendez, J., Misik, A., Garcia, M., Koth, C. M., and Freeman, M. (2005) Mechanism of intramembrane proteolysis investigated with purified rhomboid proteases, *The EMBO journal 24*, 464-472.
[73] Martoglio, B., and Golde, T. E. (2003) Intramembrane-cleaving aspartic proteases and disease: presenilins, signal peptide peptidase and their homologs, *Human molecular genetics 12 Spec No 2*, R201-206.
[74] Pastorino, L., and Lu, K. P. (2006) Pathogenic mechanisms in Alzheimer's disease, *European journal of pharmacology 545*, 29-38.
[75] De Strooper, B. (2003) Aph-1, Pen-2, and Nicastrin with Presenilin generate an active gamma-Secretase complex, *Neuron 38*, 9-12.
[76] Shah, S., Lee, S. F., Tabuchi, K., Hao, Y. H., Yu, C., LaPlant, Q., Ball, H., Dann, C. E., 3rd, Sudhof, T., and Yu, G. (2005) Nicastrin functions as a gamma-secretase-substrate receptor, *Cell 122*, 435-447.
[77] Niimura, M., Isoo, N., Takasugi, N., Tsuruoka, M., Ui-Tei, K., Saigo, K., Morohashi, Y., Tomita, T., and Iwatsubo, T. (2005) Aph-1 contributes to the stabilization and trafficking of the gamma-secretase complex through mechanisms involving intermolecular and intramolecular interactions, *The Journal of biological chemistry 280*, 12967-12975.
[78] Luo, W. J., Wang, H., Li, H., Kim, B. S., Shah, S., Lee, H. J., Thinakaran, G., Kim, T. W., Yu, G., and Xu, H. (2003) PEN-2 and APH-1 coordinately regulate proteolytic processing of presenilin 1, *The Journal of biological chemistry 278*, 7850-7854.
[79] Thinakaran, G., Borchelt, D. R., Lee, M. K., Slunt, H. H., Spitzer, L., Kim, G., Ratovitsky, T., Davenport, F., Nordstedt, C., Seeger, M., Hardy, J., Levey, A. I., Gandy, S. E., Jenkins, N. A., Copeland, N. G., Price, D. L., and Sisodia, S. S. (1996) Endoproteolysis of presenilin 1 and accumulation of processed derivatives in vivo, *Neuron 17*, 181-190.
[80] Brunkan, A. L., Martinez, M., Walker, E. S., and Goate, A. M. (2005) Presenilin endoproteolysis is an intramolecular cleavage, *Molecular and cellular neurosciences 29*, 65-73.
[81] Sato, T., Diehl, T. S., Narayanan, S., Funamoto, S., Ihara, Y., De Strooper, B., Steiner, H., Haass, C., and Wolfe, M. S. (2007) Active gamma-secretase complexes contain only one of each component, *The Journal of biological chemistry 282*, 33985-33993.
[82] Prokop, S., Shirotani, K., Edbauer, D., Haass, C., and Steiner, H. (2004) Requirement of PEN-2 for stabilization of the presenilin N-/C-terminal fragment heterodimer within the gamma-secretase complex, *The Journal of biological chemistry 279*, 23255-23261.

[83] Haapasalo, A., and Kovacs, D. M. (2011) The many substrates of presenilin/gamma-secretase, *Journal of Alzheimer's disease : JAD 25*, 3-28.
[84] Dickey, S. W., Baker, R. P., Cho, S., and Urban, S. (2013) Proteolysis inside the membrane is a rate-governed reaction not driven by substrate affinity, *Cell 155*, 1270-1281.
[85] Hebert, S. S., Serneels, L., Dejaegere, T., Horre, K., Dabrowski, M., Baert, V., Annaert, W., Hartmann, D., and De Strooper, B. (2004) Coordinated and widespread expression of gamma-secretase in vivo: evidence for size and molecular heterogeneity, *Neurobiology of disease 17*, 260-272.
[86] Shirotani, K., Edbauer, D., Prokop, S., Haass, C., and Steiner, H. (2004) Identification of distinct gamma-secretase complexes with different APH-1 variants, *The Journal of biological chemistry 279*, 41340-41345.
[87] Vetrivel, K. S., Cheng, H., Kim, S. H., Chen, Y., Barnes, N. Y., Parent, A. T., Sisodia, S. S., and Thinakaran, G. (2005) Spatial segregation of gamma-secretase and substrates in distinct membrane domains, *The Journal of biological chemistry 280*, 25892-25900.
[88] Kakuda, N., Shoji, M., Arai, H., Furukawa, K., Ikeuchi, T., Akazawa, K., Takami, M., Hatsuta, H., Murayama, S., Hashimoto, Y., Miyajima, M., Arai, H., Nagashima, Y., Yamaguchi, H., Kuwano, R., Nagaike, K., and Ihara, Y. (2012) Altered gamma-secretase activity in mild cognitive impairment and Alzheimer's disease, *EMBO molecular medicine 4*, 344-352.
[89] Matsumura, N., Takami, M., Okochi, M., Wada-Kakuda, S., Fujiwara, H., Tagami, S., Funamoto, S., Ihara, Y., and Morishima-Kawashima, M. (2014) gamma-Secretase associated with lipid rafts: multiple interactive pathways in the stepwise processing of beta-carboxyl-terminal fragment, *The Journal of biological chemistry 289*, 5109-5121.
[90] Vetrivel, K. S., Cheng, H., Lin, W., Sakurai, T., Li, T., Nukina, N., Wong, P. C., Xu, H., and Thinakaran, G. (2004) Association of gamma-secretase with lipid rafts in post-Golgi and endosome membranes, *The Journal of biological chemistry 279*, 44945-44954.
[91] Lingwood, D., and Simons, K. (2010) Lipid rafts as a membrane-organizing principle, *Science 327*, 46-50.
[92] Osenkowski, P., Ye, W., Wang, R., Wolfe, M. S., and Selkoe, D. J. (2008) Direct and potent regulation of gamma-secretase by its lipid microenvironment, *The Journal of biological chemistry 283*, 22529-22540.
[93] Holmes, O., Paturi, S., Ye, W., Wolfe, M. S., and Selkoe, D. J. (2012) Effects of membrane lipids on the activity and processivity of purified gamma-secretase, *Biochemistry 51*, 3565-3575.
[94] Winkler, E., Kamp, F., Scheuring, J., Ebke, A., Fukumori, A., and Steiner, H. (2012) Generation of Alzheimer disease-associated amyloid beta42/43 peptide by gamma-secretase can be inhibited directly by modulation of membrane thickness, *The Journal of biological chemistry 287*, 21326-21334.
[95] van Meer, G., Voelker, D. R., and Feigenson, G. W. (2008) Membrane lipids: where they are and how they behave, *Nature reviews. Molecular cell biology 9*, 112-124.

[96] Bai, X. C., Yan, C., Yang, G., Lu, P., Ma, D., Sun, L., Zhou, R., Scheres, S. H., and Shi, Y. (2015) An atomic structure of human gamma-secretase, *Nature 525*, 212-217.
[97] Bai, X. C., Rajendra, E., Yang, G., Shi, Y., and Scheres, S. H. (2015) Sampling the conformational space of the catalytic subunit of human gamma-secretase, *eLife 4*.
[98] Salloway, S., Sperling, R., and Brashear, H. R. (2014) Phase 3 trials of solanezumab and bapineuzumab for Alzheimer's disease, *The New England journal of medicine 370*, 1460.
[99] Salloway, S., Sperling, R., Fox, N. C., Blennow, K., Klunk, W., Raskind, M., Sabbagh, M., Honig, L. S., Porsteinsson, A. P., Ferris, S., Reichert, M., Ketter, N., Nejadnik, B., Guenzler, V., Miloslavsky, M., Wang, D., Lu, Y., Lull, J., Tudor, I. C., Liu, E., Grundman, M., Yuen, E., Black, R., and Brashear, H. R. (2014) Two phase 3 trials of bapineuzumab in mild-to-moderate Alzheimer's disease, *The New England journal of medicine 370*, 322-333.
[100] Doody, R. S., Farlow, M., and Aisen, P. S. (2014) Phase 3 trials of solanezumab and bapineuzumab for Alzheimer's disease, *The New England journal of medicine 370*, 1460.
[101] Doody, R. S., Thomas, R. G., Farlow, M., Iwatsubo, T., Vellas, B., Joffe, S., Kieburtz, K., Raman, R., Sun, X., Aisen, P. S., Siemers, E., Liu-Seifert, H., and Mohs, R. (2014) Phase 3 trials of solanezumab for mild-to-moderate Alzheimer's disease, *The New England journal of medicine 370*, 311-321.
[102] Karran, E., and Hardy, J. (2014) Antiamyloid therapy for Alzheimer's disease--are we on the right road?, *The New England journal of medicine 370*, 377-378.
[103] Golde, T. E., Koo, E. H., Felsenstein, K. M., Osborne, B. A., and Miele, L. (2013) gamma-Secretase inhibitors and modulators, *Biochimica et biophysica acta 1828*, 2898-2907.
[104] Wolfe, M. S., Xia, W., Moore, C. L., Leatherwood, D. D., Ostaszewski, B., Rahmati, T., Donkor, I. O., and Selkoe, D. J. (1999) Peptidomimetic probes and molecular modeling suggest that Alzheimer's gamma-secretase is an intramembrane-cleaving aspartyl protease, *Biochemistry 38*, 4720-4727.
[105] Esler, W. P., Kimberly, W. T., Ostaszewski, B. L., Diehl, T. S., Moore, C. L., Tsai, J. Y., Rahmati, T., Xia, W., Selkoe, D. J., and Wolfe, M. S. (2000) Transition-state analogue inhibitors of gamma-secretase bind directly to presenilin-1, *Nature cell biology 2*, 428-434.
[106] Li, Y. M., Xu, M., Lai, M. T., Huang, Q., Castro, J. L., DiMuzio-Mower, J., Harrison, T., Lellis, C., Nadin, A., Neduvelil, J. G., Register, R. B., Sardana, M. K., Shearman, M. S., Smith, A. L., Shi, X. P., Yin, K. C., Shafer, J. A., and Gardell, S. J. (2000) Photoactivated gamma-secretase inhibitors directed to the active site covalently label presenilin 1, *Nature 405*, 689-694.
[107] Shearman, M. S., Beher, D., Clarke, E. E., Lewis, H. D., Harrison, T., Hunt, P., Nadin, A., Smith, A. L., Stevenson, G., and Castro, J. L. (2000) L-685,458, an aspartyl protease transition state mimic, is a potent inhibitor of amyloid beta-protein precursor gamma-secretase activity, *Biochemistry 39*, 8698-8704.
[108] Kreft, A. F., Martone, R., and Porte, A. (2009) Recent advances in the identification of gamma-secretase inhibitors to clinically test the Abeta oligomer

hypothesis of Alzheimer's disease, *Journal of medicinal chemistry 52*, 6169-6188.

[109] Dovey, H. F., John, V., Anderson, J. P., Chen, L. Z., de Saint Andrieu, P., Fang, L. Y., Freedman, S. B., Folmer, B., Goldbach, E., Holsztynska, E. J., Hu, K. L., Johnson-Wood, K. L., Kennedy, S. L., Kholodenko, D., Knops, J. E., Latimer, L. H., Lee, M., Liao, Z., Lieberburg, I. M., Motter, R. N., Mutter, L. C., Nietz, J., Quinn, K. P., Sacchi, K. L., Seubert, P. A., Shopp, G. M., Thorsett, E. D., Tung, J. S., Wu, J., Yang, S., Yin, C. T., Schenk, D. B., May, P. C., Altstiel, L. D., Bender, M. H., Boggs, L. N., Britton, T. C., Clemens, J. C., Czilli, D. L., Dieckman-McGinty, D. K., Droste, J. J., Fuson, K. S., Gitter, B. D., Hyslop, P. A., Johnstone, E. M., Li, W. Y., Little, S. P., Mabry, T. E., Miller, F. D., and Audia, J. E. (2001) Functional gamma-secretase inhibitors reduce beta-amyloid peptide levels in brain, *Journal of neurochemistry 76*, 173-181.

[110] De Strooper, B., and Chavez Gutierrez, L. (2015) Learning by failing: ideas and concepts to tackle gamma-secretases in Alzheimer's disease and beyond, *Annual review of pharmacology and toxicology 55*, 419-437.

[111] Doody, R. S., Raman, R., Farlow, M., Iwatsubo, T., Vellas, B., Joffe, S., Kieburtz, K., He, F., Sun, X., Thomas, R. G., Aisen, P. S., Siemers, E., Sethuraman, G., and Mohs, R. (2013) A phase 3 trial of semagacestat for treatment of Alzheimer's disease, *The New England journal of medicine 369*, 341-350.

[112] Coric, V., van Dyck, C. H., Salloway, S., Andreasen, N., Brody, M., Richter, R. W., Soininen, H., Thein, S., Shiovitz, T., Pilcher, G., Colby, S., Rollin, L., Dockens, R., Pachai, C., Portelius, E., Andreasson, U., Blennow, K., Soares, H., Albright, C., Feldman, H. H., and Berman, R. M. (2012) Safety and tolerability of the gamma-secretase inhibitor avagacestat in a phase 2 study of mild to moderate Alzheimer disease, *Archives of neurology 69*, 1430-1440.

[113] Kounnas, M. Z., Danks, A. M., Cheng, S., Tyree, C., Ackerman, E., Zhang, X., Ahn, K., Nguyen, P., Comer, D., Mao, L., Yu, C., Pleynet, D., Digregorio, P. J., Velicelebi, G., Stauderman, K. A., Comer, W. T., Mobley, W. C., Li, Y. M., Sisodia, S. S., Tanzi, R. E., and Wagner, S. L. (2010) Modulation of gamma-secretase reduces beta-amyloid deposition in a transgenic mouse model of Alzheimer's disease, *Neuron 67*, 769-780.

[114] Rogers, K., Felsenstein, K. M., Hrdlicka, L., Tu, Z., Albayya, F., Lee, W., Hopp, S., Miller, M. J., Spaulding, D., Yang, Z., Hodgdon, H., Nolan, S., Wen, M., Costa, D., Blain, J. F., Freeman, E., De Strooper, B., Vulsteke, V., Scrocchi, L., Zetterberg, H., Portelius, E., Hutter-Paier, B., Havas, D., Ahlijanian, M., Flood, D., Leventhal, L., Shapiro, G., Patzke, H., Chesworth, R., and Koenig, G. (2012) Modulation of gamma-secretase by EVP-0015962 reduces amyloid deposition and behavioral deficits in Tg2576 mice, *Molecular neurodegeneration 7*, 61.

[115] Gamerdinger, M., Clement, A. B., and Behl, C. (2007) Cholesterol-like effects of selective cyclooxygenase inhibitors and fibrates on cellular membranes and amyloid-beta production, *Molecular pharmacology 72*, 141-151.

[116] Kukar, T. L., Ladd, T. B., Bann, M. A., Fraering, P. C., Narlawar, R., Maharvi, G. M., Healy, B., Chapman, R., Welzel, A. T., Price, R. W., Moore, B., Rangachari, V., Cusack, B., Eriksen, J., Jansen-West, K., Verbeeck, C., Yager, D., Eckman, C., Ye, W., Sagi, S., Cottrell, B. A., Torpey, J., Rosenberry, T. L., Fauq, A.,

Wolfe, M. S., Schmidt, B., Walsh, D. M., Koo, E. H., and Golde, T. E. (2008) Substrate-targeting gamma-secretase modulators, *Nature 453*, 925-929.
[117] Beel, A. J., Barrett, P., Schnier, P. D., Hitchcock, S. A., Bagal, D., Sanders, C. R., and Jordan, J. B. (2009) Nonspecificity of binding of gamma-secretase modulators to the amyloid precursor protein, *Biochemistry 48*, 11837-11839.
[118] Richter, L., Munter, L. M., Ness, J., Hildebrand, P. W., Dasari, M., Unterreitmeier, S., Bulic, B., Beyermann, M., Gust, R., Reif, B., Weggen, S., Langosch, D., and Multhaup, G. (2010) Amyloid beta 42 peptide (Abeta42)-lowering compounds directly bind to Abeta and interfere with amyloid precursor protein (APP) transmembrane dimerization, *Proceedings of the National Academy of Sciences of the United States of America 107*, 14597-14602.
[119] Botev, A., Munter, L. M., Wenzel, R., Richter, L., Althoff, V., Ismer, J., Gerling, U., Weise, C., Koksch, B., Hildebrand, P. W., Bittl, R., and Multhaup, G. (2011) The amyloid precursor protein C-terminal fragment C100 occurs in monomeric and dimeric stable conformations and binds gamma-secretase modulators, *Biochemistry 50*, 828-835.
[120] Barrett, P. J., Sanders, C. R., Kaufman, S. A., Michelsen, K., and Jordan, J. B. (2011) NSAID-based gamma-secretase modulators do not bind to the amyloid-beta polypeptide, *Biochemistry 50*, 10328-10342.
[121] Greenfield, J. P., Tsai, J., Gouras, G. K., Hai, B., Thinakaran, G., Checler, F., Sisodia, S. S., Greengard, P., and Xu, H. (1999) Endoplasmic reticulum and trans-Golgi network generate distinct populations of Alzheimer beta-amyloid peptides, *Proceedings of the National Academy of Sciences of the United States of America 96*, 742-747.
[122] Netzer, W. J., Dou, F., Cai, D., Veach, D., Jean, S., Li, Y., Bornmann, W. G., Clarkson, B., Xu, H., and Greengard, P. (2003) Gleevec inhibits beta-amyloid production but not Notch cleavage, *Proceedings of the National Academy of Sciences of the United States of America 100*, 12444-12449.
[123] He, G., Luo, W., Li, P., Remmers, C., Netzer, W. J., Hendrick, J., Bettayeb, K., Flajolet, M., Gorelick, F., Wennogle, L. P., and Greengard, P. (2010) Gamma-secretase activating protein is a therapeutic target for Alzheimer's disease, *Nature 467*, 95-98.
[124] Artavanis-Tsakonas, S., and Muskavitch, M. A. (2010) Notch: the past, the present, and the future, *Current topics in developmental biology 92*, 1-29.
[125] Morgan, T. H. (1928) *The theory of the gene*, Enl. and rev. ed., Yale university press;
H. Milford Oxford university press, New Haven,
London,.
[126] Poulson, D. F. (1940) The effects of certain X-chromosome deficiencies on the embryonic development of Drosophila melanogaster, *Journal of Experimental Zoology 83*, 271-325.
[127] Artavanis-Tsakonas, S., Muskavitch, M. A., and Yedvobnick, B. (1983) Molecular cloning of Notch, a locus affecting neurogenesis in Drosophila melanogaster, *Proceedings of the National Academy of Sciences of the United States of America 80*, 1977-1981.

[128] Coffman, C., Harris, W., and Kintner, C. (1990) Xotch, the Xenopus homolog of Drosophila notch, *Science 249*, 1438-1441.
[129] Ellisen, L. W., Bird, J., West, D. C., Soreng, A. L., Reynolds, T. C., Smith, S. D., and Sklar, J. (1991) TAN-1, the human homolog of the Drosophila notch gene, is broken by chromosomal translocations in T lymphoblastic neoplasms, *Cell 66*, 649-661.
[130] Kidd, S., Lockett, T. J., and Young, M. W. (1983) The Notch locus of Drosophila melanogaster, *Cell 34*, 421-433.
[131] Lanford, P. J., Lan, Y., Jiang, R., Lindsell, C., Weinmaster, G., Gridley, T., and Kelley, M. W. (1999) Notch signalling pathway mediates hair cell development in mammalian cochlea, *Nature genetics 21*, 289-292.
[132] Robey, E., Chang, D., Itano, A., Cado, D., Alexander, H., Lans, D., Weinmaster, G., and Salmon, P. (1996) An activated form of Notch influences the choice between CD4 and CD8 T cell lineages, *Cell 87*, 483-492.
[133] van Es, J. H., van Gijn, M. E., Riccio, O., van den Born, M., Vooijs, M., Begthel, H., Cozijnsen, M., Robine, S., Winton, D. J., Radtke, F., and Clevers, H. (2005) Notch/gamma-secretase inhibition turns proliferative cells in intestinal crypts and adenomas into goblet cells, *Nature 435*, 959-963.
[134] Washburn, T., Schweighoffer, E., Gridley, T., Chang, D., Fowlkes, B. J., Cado, D., and Robey, E. (1997) Notch activity influences the alphabeta versus gammadelta T cell lineage decision, *Cell 88*, 833-843.
[135] Huppert, S. S., Le, A., Schroeter, E. H., Mumm, J. S., Saxena, M. T., Milner, L. A., and Kopan, R. (2000) Embryonic lethality in mice homozygous for a processing-deficient allele of Notch1, *Nature 405*, 966-970.
[136] Redmond, L., Oh, S. R., Hicks, C., Weinmaster, G., and Ghosh, A. (2000) Nuclear Notch1 signaling and the regulation of dendritic development, *Nature neuroscience 3*, 30-40.
[137] Presente, A., Andres, A., and Nye, J. S. (2001) Requirement of Notch in adulthood for neurological function and longevity, *Neuroreport 12*, 3321-3325.
[138] Lowell, S., Benchoua, A., Heavey, B., and Smith, A. G. (2006) Notch promotes neural lineage entry by pluripotent embryonic stem cells, *PLoS biology 4*, e121.
[139] Bigas, A., D'Altri, T., and Espinosa, L. (2012) The Notch pathway in hematopoietic stem cells, *Current topics in microbiology and immunology 360*, 1-18.
[140] Kopan, R., and Ilagan, M. X. (2009) The canonical Notch signaling pathway: unfolding the activation mechanism, *Cell 137*, 216-233.
[141] Bray, S. J. (2006) Notch signalling: a simple pathway becomes complex, *Nature reviews. Molecular cell biology 7*, 678-689.
[142] Ables, J. L., Breunig, J. J., Eisch, A. J., and Rakic, P. (2011) Not(ch) just development: Notch signalling in the adult brain, *Nature reviews. Neuroscience 12*, 269-283.
[143] Logeat, F., Bessia, C., Brou, C., LeBail, O., Jarriault, S., Seidah, N. G., and Israel, A. (1998) The Notch1 receptor is cleaved constitutively by a furin-like convertase, *Proceedings of the National Academy of Sciences of the United States of America 95*, 8108-8112.
[144] Larsson, C., Lardelli, M., White, I., and Lendahl, U. (1994) The human NOTCH1, 2, and 3 genes are located at chromosome positions 9q34, 1p13-p11, and

19p13.2-p13.1 in regions of neoplasia-associated translocation, *Genomics 24*, 253-258.
[145] Pilz, A., Prohaska, R., Peters, J., and Abbott, C. (1994) Genetic linkage analysis of the Ak1, Col5a1, Epb7.2, Fpgs, Grp78, Pbx3, and Notch1 genes in the region of mouse chromosome 2 homologous to human chromosome 9q, *Genomics 21*, 104-109.
[146] Sugaya, K., Fukagawa, T., Matsumoto, K., Mita, K., Takahashi, E., Ando, A., Inoko, H., and Ikemura, T. (1994) Three genes in the human MHC class III region near the junction with the class II: gene for receptor of advanced glycosylation end products, PBX2 homeobox gene and a notch homolog, human counterpart of mouse mammary tumor gene int-3, *Genomics 23*, 408-419.
[147] Ujike, H., Takehisa, Y., Takaki, M., Tanaka, Y., Nakata, K., Takeda, T., Kodama, M., Fujiwara, Y., Yamamoto, A., and Kuroda, S. (2001) NOTCH4 gene polymorphism and susceptibility to schizophrenia and schizoaffective disorder, *Neuroscience letters 301*, 41-44.
[148] Artavanis-Tsakonas, S., Rand, M. D., and Lake, R. J. (1999) Notch signaling: cell fate control and signal integration in development, *Science 284*, 770-776.
[149] Raya, A., Kawakami, Y., Rodriguez-Esteban, C., Ibanes, M., Rasskin-Gutman, D., Rodriguez-Leon, J., Buscher, D., Feijo, J. A., and Izpisua Belmonte, J. C. (2004) Notch activity acts as a sensor for extracellular calcium during vertebrate left-right determination, *Nature 427*, 121-128.
[150] Cordle, J., Redfieldz, C., Stacey, M., van der Merwe, P. A., Willis, A. C., Champion, B. R., Hambleton, S., and Handford, P. A. (2008) Localization of the delta-like-1-binding site in human Notch-1 and its modulation by calcium affinity, *The Journal of biological chemistry 283*, 11785-11793.
[151] Haines, N., and Irvine, K. D. (2003) Glycosylation regulates Notch signalling, *Nature reviews. Molecular cell biology 4*, 786-797.
[152] Vodovar, N., and Schweisguth, F. (2008) Functions of O-fucosyltransferase in Notch trafficking and signaling: towards the end of a controversy?, *Journal of biology 7*, 7.
[153] Henderson, S. T., Gao, D., Christensen, S., and Kimble, J. (1997) Functional domains of LAG-2, a putative signaling ligand for LIN-12 and GLP-1 receptors in Caenorhabditis elegans, *Molecular biology of the cell 8*, 1751-1762.
[154] Shimizu, K., Chiba, S., Kumano, K., Hosoya, N., Takahashi, T., Kanda, Y., Hamada, Y., Yazaki, Y., and Hirai, H. (1999) Mouse jagged1 physically interacts with notch2 and other notch receptors. Assessment by quantitative methods, *The Journal of biological chemistry 274*, 32961-32969.
[155] Wang, M. M. (2011) Notch signaling and Notch signaling modifiers, *The international journal of biochemistry & cell biology 43*, 1550-1562.
[156] Gordon, W. R., Vardar-Ulu, D., Histen, G., Sanchez-Irizarry, C., Aster, J. C., and Blacklow, S. C. (2007) Structural basis for autoinhibition of Notch, *Nature structural & molecular biology 14*, 295-300.
[157] Blaumueller, C. M., Qi, H., Zagouras, P., and Artavanis-Tsakonas, S. (1997) Intracellular cleavage of Notch leads to a heterodimeric receptor on the plasma membrane, *Cell 90*, 281-291.

[158] Rand, M. D., Grimm, L. M., Artavanis-Tsakonas, S., Patriub, V., Blacklow, S. C., Sklar, J., and Aster, J. C. (2000) Calcium depletion dissociates and activates heterodimeric notch receptors, *Molecular and cellular biology 20*, 1825-1835.
[159] Gordon, W. R., Roy, M., Vardar-Ulu, D., Garfinkel, M., Mansour, M. R., Aster, J. C., and Blacklow, S. C. (2009) Structure of the Notch1-negative regulatory region: implications for normal activation and pathogenic signaling in T-ALL, *Blood 113*, 4381-4390.
[160] Vooijs, M., Schroeter, E. H., Pan, Y., Blandford, M., and Kopan, R. (2004) Ectodomain shedding and intramembrane cleavage of mammalian Notch proteins is not regulated through oligomerization, *The Journal of biological chemistry 279*, 50864-50873.
[161] Chandu, D., Huppert, S. S., and Kopan, R. (2006) Analysis of transmembrane domain mutants is consistent with sequential cleavage of Notch by gamma-secretase, *Journal of neurochemistry 96*, 228-235.
[162] Okochi, M., Fukumori, A., Jiang, J., Itoh, N., Kimura, R., Steiner, H., Haass, C., Tagami, S., and Takeda, M. (2006) Secretion of the Notch-1 Abeta-like peptide during Notch signaling, *The Journal of biological chemistry 281*, 7890-7898.
[163] Okochi, M., Steiner, H., Fukumori, A., Tanii, H., Tomita, T., Tanaka, T., Iwatsubo, T., Kudo, T., Takeda, M., and Haass, C. (2002) Presenilins mediate a dual intramembranous gamma-secretase cleavage of Notch-1, *The EMBO journal 21*, 5408-5416.
[164] Wolfe, M. S., and Kopan, R. (2004) Intramembrane proteolysis: theme and variations, *Science 305*, 1119-1123.
[165] Mumm, J. S., and Kopan, R. (2000) Notch signaling: from the outside in, *Developmental biology 228*, 151-165.
[166] Tamura, K., Taniguchi, Y., Minoguchi, S., Sakai, T., Tun, T., Furukawa, T., and Honjo, T. (1995) Physical interaction between a novel domain of the receptor Notch and the transcription factor RBP-J kappa/Su(H), *Current biology : CB 5*, 1416-1423.
[167] Nam, Y., Weng, A. P., Aster, J. C., and Blacklow, S. C. (2003) Structural requirements for assembly of the CSL.intracellular Notch1.Mastermind-like 1 transcriptional activation complex, *The Journal of biological chemistry 278*, 21232-21239.
[168] Kovall, R. A. (2008) More complicated than it looks: assembly of Notch pathway transcription complexes, *Oncogene 27*, 5099-5109.
[169] Gordon, W. R., Arnett, K. L., and Blacklow, S. C. (2008) The molecular logic of Notch signaling--a structural and biochemical perspective, *Journal of cell science 121*, 3109-3119.
[170] Wilson, J. J., and Kovall, R. A. (2006) Crystal structure of the CSL-Notch-Mastermind ternary complex bound to DNA, *Cell 124*, 985-996.
[171] Fryer, C. J., Lamar, E., Turbachova, I., Kintner, C., and Jones, K. A. (2002) Mastermind mediates chromatin-specific transcription and turnover of the Notch enhancer complex, *Genes & development 16*, 1397-1411.
[172] Gerhardt, D. M., Pajcini, K. V., D'Altri, T., Tu, L., Jain, R., Xu, L., Chen, M. J., Rentschler, S., Shestova, O., Wertheim, G. B., Tobias, J. W., Kluk, M., Wood, A. W., Aster, J. C., Gimotty, P. A., Epstein, J. A., Speck, N., Bigas, A., and Pear, W.

S. (2014) The Notch1 transcriptional activation domain is required for development and reveals a novel role for Notch1 signaling in fetal hematopoietic stem cells, *Genes & development 28*, 576-593.
[173] Kurooka, H., and Honjo, T. (2000) Functional interaction between the mouse notch1 intracellular region and histone acetyltransferases PCAF and GCN5, *The Journal of biological chemistry 275*, 17211-17220.
[174] Kurooka, H., Kuroda, K., and Honjo, T. (1998) Roles of the ankyrin repeats and C-terminal region of the mouse notch1 intracellular region, *Nucleic acids research 26*, 5448-5455.
[175] Rogers, S., Wells, R., and Rechsteiner, M. (1986) Amino acid sequences common to rapidly degraded proteins: the PEST hypothesis, *Science 234*, 364-368.
[176] Fryer, C. J., White, J. B., and Jones, K. A. (2004) Mastermind recruits CycC:CDK8 to phosphorylate the Notch ICD and coordinate activation with turnover, *Molecular cell 16*, 509-520.
[177] Tsunematsu, R., Nakayama, K., Oike, Y., Nishiyama, M., Ishida, N., Hatakeyama, S., Bessho, Y., Kageyama, R., Suda, T., and Nakayama, K. I. (2004) Mouse Fbw7/Sel-10/Cdc4 is required for notch degradation during vascular development, *The Journal of biological chemistry 279*, 9417-9423.
[178] Sprinzak, D., Lakhanpal, A., Lebon, L., Santat, L. A., Fontes, M. E., Anderson, G. A., Garcia-Ojalvo, J., and Elowitz, M. B. (2010) Cis-interactions between Notch and Delta generate mutually exclusive signalling states, *Nature 465*, 86-90.
[179] Nichols, J. T., Miyamoto, A., Olsen, S. L., D'Souza, B., Yao, C., and Weinmaster, G. (2007) DSL ligand endocytosis physically dissociates Notch1 heterodimers before activating proteolysis can occur, *The Journal of cell biology 176*, 445-458.
[180] Le Borgne, R., Bardin, A., and Schweisguth, F. (2005) The roles of receptor and ligand endocytosis in regulating Notch signaling, *Development 132*, 1751-1762.
[181] Klueg, K. M., and Muskavitch, M. A. (1999) Ligand-receptor interactions and trans-endocytosis of Delta, Serrate and Notch: members of the Notch signalling pathway in Drosophila, *Journal of cell science 112 (Pt 19)*, 3289-3297.
[182] Brou, C., Logeat, F., Gupta, N., Bessia, C., LeBail, O., Doedens, J. R., Cumano, A., Roux, P., Black, R. A., and Israel, A. (2000) A novel proteolytic cleavage involved in Notch signaling: the role of the disintegrin-metalloprotease TACE, *Molecular cell 5*, 207-216.
[183] Lieber, T., Kidd, S., and Young, M. W. (2002) kuzbanian-mediated cleavage of Drosophila Notch, *Genes & development 16*, 209-221.
[184] Mumm, J. S., Schroeter, E. H., Saxena, M. T., Griesemer, A., Tian, X., Pan, D. J., Ray, W. J., and Kopan, R. (2000) A ligand-induced extracellular cleavage regulates gamma-secretase-like proteolytic activation of Notch1, *Molecular cell 5*, 197-206.
[185] Wu, L., Aster, J. C., Blacklow, S. C., Lake, R., Artavanis-Tsakonas, S., and Griffin, J. D. (2000) MAML1, a human homologue of Drosophila mastermind, is a transcriptional co-activator for NOTCH receptors, *Nature genetics 26*, 484-489.
[186] Iso, T., Kedes, L., and Hamamori, Y. (2003) HES and HERP families: multiple effectors of the Notch signaling pathway, *Journal of cellular physiology 194*, 237-255.

[187] Kageyama, R., and Ohtsuka, T. (1999) The Notch-Hes pathway in mammalian neural development, *Cell research 9*, 179-188.
[188] (2012) 2012 Alzheimer's disease facts and figures, *Alzheimer's & dementia : the journal of the Alzheimer's Association 8*, 131-168.
[189] Selkoe, D. J. (1991) The molecular pathology of Alzheimer's disease, *Neuron 6*, 487-498.
[190] Esler, W. P., Kimberly, W. T., Ostaszewski, B. L., Ye, W., Diehl, T. S., Selkoe, D. J., and Wolfe, M. S. (2002) Activity-dependent isolation of the presenilin–γ-secretase complex reveals nicastrin and a γ substrate, *Proceedings of the National Academy of Sciences 99*, 2720.
[191] Kimberly, W. T., LaVoie, M. J., Ostaszewski, B. L., Ye, W., Wolfe, M. S., and Selkoe, D. J. (2003) γ-Secretase is a membrane protein complex comprised of presenilin, nicastrin, Aph-1, and Pen-2, *Proceedings of the National Academy of Sciences 100*, 6382.
[192] Kopan, R., and Ilagan, M. X. (2004) Gamma-secretase: proteasome of the membrane?, *Nature reviews. Molecular cell biology 5*, 499-504.
[193] Satoh, J., Tabunoki, H., Ishida, T., Saito, Y., and Arima, K. (2011) Immunohistochemical characterization of gamma-secretase activating protein expression in Alzheimer's disease brains, *Neuropathology and applied neurobiology*.
[194] Sanders, C. R., and Sonnichsen, F. (2006) Solution NMR of membrane proteins: practice and challenges, *Magnetic resonance in chemistry : MRC 44 Spec No*, S24-40.
[195] LaVallie, E. R., DiBlasio, E. A., Kovacic, S., Grant, K. L., Schendel, P. F., and McCoy, J. M. (1993) A thioredoxin gene fusion expression system that circumvents inclusion body formation in the E. coli cytoplasm, *Biotechnology (N Y) 11*, 187-193.
[196] Sorensen, H. P., and Mortensen, K. K. (2005) Soluble expression of recombinant proteins in the cytoplasm of Escherichia coli, *Microbial cell factories 4*, 1.
[197] Louis-Jeune, C., Andrade-Navarro, M. A., and Perez-Iratxeta, C. (2011) Prediction of protein secondary structure from circular dichroism using theoretically derived spectra, *Proteins*.
[198] Vardar, D., North, C. L., Sanchez-Irizarry, C., Aster, J. C., and Blacklow, S. C. (2003) Nuclear magnetic resonance structure of a prototype Lin12-Notch repeat module from human Notch1, *Biochemistry 42*, 7061-7067.
[199] Ehebauer, M. T., Chirgadze, D. Y., Hayward, P., Martinez Arias, A., and Blundell, T. L. (2005) High-resolution crystal structure of the human Notch 1 ankyrin domain, *The Biochemical journal 392*, 13-20.
[200] Lubman, O. Y., Kopan, R., Waksman, G., and Korolev, S. (2005) The crystal structure of a partial mouse Notch-1 ankyrin domain: repeats 4 through 7 preserve an ankyrin fold, *Protein science : a publication of the Protein Society 14*, 1274-1281.
[201] Zweifel, M. E., Leahy, D. J., and Barrick, D. (2005) Structure and Notch receptor binding of the tandem WWE domain of Deltex, *Structure 13*, 1599-1611.

[202] Nam, Y., Sliz, P., Song, L., Aster, J. C., and Blacklow, S. C. (2006) Structural basis for cooperativity in recruitment of MAML coactivators to Notch transcription complexes, *Cell 124*, 973-983.
[203] Riccio, O., van Gijn, M. E., Bezdek, A. C., Pellegrinet, L., van Es, J. H., Zimber-Strobl, U., Strobl, L. J., Honjo, T., Clevers, H., and Radtke, F. (2008) Loss of intestinal crypt progenitor cells owing to inactivation of both Notch1 and Notch2 is accompanied by derepression of CDK inhibitors p27Kip1 and p57Kip2, *EMBO reports 9*, 377-383.
[204] Wong, G. T., Manfra, D., Poulet, F. M., Zhang, Q., Josien, H., Bara, T., Engstrom, L., Pinzon-Ortiz, M., Fine, J. S., Lee, H. J., Zhang, L., Higgins, G. A., and Parker, E. M. (2004) Chronic treatment with the gamma-secretase inhibitor LY-411,575 inhibits beta-amyloid peptide production and alters lymphopoiesis and intestinal cell differentiation, *The Journal of biological chemistry 279*, 12876-12882.
[205] Zhuang, T., Vishnivetskiy, S. A., Gurevich, V. V., and Sanders, C. R. (2010) Elucidation of inositol hexaphosphate and heparin interaction sites and conformational changes in arrestin-1 by solution nuclear magnetic resonance, *Biochemistry 49*, 10473-10485.
[206] Peng, D., Kim, J. H., Kroncke, B. M., Law, C. L., Xia, Y., Droege, K. D., Van Horn, W. D., Vanoye, C. G., and Sanders, C. R. (2014) Purification and structural study of the voltage-sensor domain of the human KCNQ1 potassium ion channel, *Biochemistry 53*, 2032-2042.
[207] Salzmann, M., Pervushin, K., Wider, G., Senn, H., and Wuthrich, K. (1998) TROSY in triple-resonance experiments: new perspectives for sequential NMR assignment of large proteins, *Proceedings of the National Academy of Sciences of the United States of America 95*, 13585-13590.
[208] Shenkarev, Z. O., Paramonov, A. S., Lyukmanova, E. N., Shingarova, L. N., Yakimov, S. A., Dubinnyi, M. A., Chupin, V. V., Kirpichnikov, M. P., Blommers, M. J., and Arseniev, A. S. (2010) NMR structural and dynamical investigation of the isolated voltage-sensing domain of the potassium channel KvAP: implications for voltage gating, *Journal of the American Chemical Society 132*, 5630-5637.
[209] Delaglio, F., Grzesiek, S., Vuister, G. W., Zhu, G., Pfeifer, J., and Bax, A. (1995) NMRPipe: a multidimensional spectral processing system based on UNIX pipes, *Journal of biomolecular NMR 6*, 277-293.
[210] Johnson, B. A. (2004) Using NMRView to visualize and analyze the NMR spectra of macromolecules, *Methods Mol Biol 278*, 313-352.
[211] Shen, Y., and Bax, A. (2013) Protein backbone and sidechain torsion angles predicted from NMR chemical shifts using artificial neural networks, *Journal of biomolecular NMR 56*, 227-241.
[212] Wishart, D. S., and Sykes, B. D. (1994) Chemical shifts as a tool for structure determination, *Methods in enzymology 239*, 363-392.
[213] Hwang, T. L., van Zijl, P. C., and Mori, S. (1998) Accurate quantitation of water-amide proton exchange rates using the phase-modulated CLEAN chemical EXchange (CLEANEX-PM) approach with a Fast-HSQC (FHSQC) detection scheme, *Journal of biomolecular NMR 11*, 221-226.

[214] Wishart, D. S., Sykes, B. D., and Richards, F. M. (1992) The chemical shift index: a fast and simple method for the assignment of protein secondary structure through NMR spectroscopy, *Biochemistry 31*, 1647-1651.
[215] Wishart, D. S. (2011) Interpreting protein chemical shift data, *Progress in nuclear magnetic resonance spectroscopy 58*, 62-87.
[216] Kneller, J. M., Lu, M., and Bracken, C. (2002) An effective method for the discrimination of motional anisotropy and chemical exchange, *Journal of the American Chemical Society 124*, 1852-1853.
[217] Deatherage, C. L., Lu, Z., Kim, J. H., and Sanders, C. R. (2015) Notch Transmembrane Domain: Secondary Structure and Topology, *Biochemistry 54*, 3565-3568.
[218] Grzesiek, S., Anglister, J., and Bax, A. (1993) Correlation of Backbone Amide and Aliphatic Side-Chain Resonances in 13C/15N-Enriched Proteins by Isotropic Mixing of 13C Magnetization, *Journal of Magnetic Resonance, Series B 101*, 114-119.
[219] Montelione, G. T., Lyons, B. A., Emerson, S. D., and Tashiro, M. (1992) An efficient triple resonance experiment using carbon-13 isotropic mixing for determining sequence-specific resonance assignments of isotopically-enriched proteins, *Journal of the American Chemical Society 114*, 10974-10975.
[220] Bax, A., Clore, G. M., and Gronenborn, A. M. (1990) 1Hashiro, M. (1992) An efficient triple reson magnetization, a new three-dimensional approach for assigning 1H and 13C spectra of 13C-enriched proteins, *Journal of Magnetic Resonance (1969) 88*, 425-431.
[221] Olejniczak, E. T., Xu, R. X., and Fesik, S. W. (1992) A 4D HCCH-TOCSY experiment for assigning the side chain 1H and 13C resonances of proteins, *Journal of biomolecular NMR 2*, 655-659.
[222] Kneller, T. D. G. a. D. G. Sparky 3, *University of California, San Francisco*.
[223] Battiste, J. L., and Wagner, G. (2000) Utilization of site-directed spin labeling and high-resolution heteronuclear nuclear magnetic resonance for global fold determination of large proteins with limited nuclear overhauser effect data, *Biochemistry 39*, 5355-5365.
[224] Solomon, I., and Bloembergen, N. (1956) Nuclear Magnetic Interactions in the HF Molecule, *The Journal of Chemical Physics 25*, 261-266.
[225] Shen, Y., Delaglio, F., Cornilescu, G., and Bax, A. (2009) TALOS plus : a hybrid method for predicting protein backbone torsion angles from NMR chemical shifts, *Journal of biomolecular NMR 44*, 213-223.
[226] Wishart, D. S., and Sykes, B. D. (1994) The C-13 Chemical-Shift Index - a Simple Method for the Identification of Protein Secondary Structure Using C-13 Chemical-Shift Data, *Journal of biomolecular NMR 4*, 171-180.
[227] Van Horn, W. D., Kim, H. J., Ellis, C. D., Hadziselimovic, A., Sulistijo, E. S., Karra, M. D., Tian, C. L., Sonnichsen, F. D., and Sanders, C. R. (2009) Solution Nuclear Magnetic Resonance Structure of Membrane-Integral Diacylglycerol Kinase, *Science 324*, 1726-1729.
[228] Kang, C., Tian, C., Sonnichsen, F. D., Smith, J. A., Meiler, J., George, A. L., Jr., Vanoye, C. G., Kim, H. J., and Sanders, C. R. (2008) Structure of KCNE1 and

implications for how it modulates the KCNQ1 potassium channel, *Biochemistry 47*, 7999-8006.
[229] Schwieters, C. D., Kuszewski, J. J., Tjandra, N., and Clore, G. M. (2003) The Xplor-NIH NMR molecular structure determination package, *J Magn Reson 160*, 65-73.
[230] Wu, E. L., Cheng, X., Jo, S., Rui, H., Song, K. C., Davila-Contreras, E. M., Qi, Y., Lee, J., Monje-Galvan, V., Venable, R. M., Klauda, J. B., and Im, W. (2014) CHARMM-GUI Membrane Builder toward realistic biological membrane simulations, *Journal of computational chemistry 35*, 1997-2004.
[231] Jo, S., Kim, T., Iyer, V. G., and Im, W. (2008) CHARMM-GUI: a web-based graphical user interface for CHARMM, *Journal of computational chemistry 29*, 1859-1865.
[232] Case, D. A., Cheatham, T. E., 3rd, Darden, T., Gohlke, H., Luo, R., Merz, K. M., Jr., Onufriev, A., Simmerling, C., Wang, B., and Woods, R. J. (2005) The Amber biomolecular simulation programs, *Journal of computational chemistry 26*, 1668-1688.
[233] Roe, D. R., and Cheatham, T. E., 3rd. (2013) PTRAJ and CPPTRAJ: Software for Processing and Analysis of Molecular Dynamics Trajectory Data, *Journal of chemical theory and computation 9*, 3084-3095.
[234] Beel, A. J., Sakakura, M., Barrett, P. J., and Sanders, C. R. (2010) Direct binding of cholesterol to the amyloid precursor protein: An important interaction in lipid-Alzheimer's disease relationships?, *Biochimica et biophysica acta 1801*, 975-982.
[235] Schubert, M., Labudde, D., Oschkinat, H., and Schmieder, P. (2002) A software tool for the prediction of Xaa-Pro peptide bond conformations in proteins based on 13C chemical shift statistics, *Journal of biomolecular NMR 24*, 149-154.
[236] Shen, Y., Delaglio, F., Cornilescu, G., and Bax, A. (2009) TALOS+: a hybrid method for predicting protein backbone torsion angles from NMR chemical shifts, *Journal of biomolecular NMR 44*, 213-223.
[237] Laskowski, R. A., Rullmannn, J. A., MacArthur, M. W., Kaptein, R., and Thornton, J. M. (1996) AQUA and PROCHECK-NMR: programs for checking the quality of protein structures solved by NMR, *Journal of biomolecular NMR 8*, 477-486.
[238] Hori, K., Sen, A., Kirchhausen, T., and Artavanis-Tsakonas, S. (2011) Synergy between the ESCRT-III complex and Deltex defines a ligand-independent Notch signal, *The Journal of cell biology 195*, 1005-1015.
[239] Baron, M. (2012) Endocytic routes to Notch activation, *Seminars in cell & developmental biology 23*, 437-442.
[240] Shimizu, H., Woodcock, S. A., Wilkin, M. B., Trubenova, B., Monk, N. A., and Baron, M. (2014) Compensatory flux changes within an endocytic trafficking network maintain thermal robustness of Notch signaling, *Cell 157*, 1160-1174.
[241] Wilkin, M., Tongngok, P., Gensch, N., Clemence, S., Motoki, M., Yamada, K., Hori, K., Taniguchi-Kanai, M., Franklin, E., Matsuno, K., and Baron, M. (2008) Drosophila HOPS and AP-3 complex genes are required for a Deltex-regulated activation of notch in the endosomal trafficking pathway, *Developmental cell 15*, 762-772.
[242] Urra, S., Escudero, C. A., Ramos, P., Lisbona, F., Allende, E., Covarrubias, P., Parraguez, J. I., Zampieri, N., Chao, M. V., Annaert, W., and Bronfman, F. C.

(2007) TrkA receptor activation by nerve growth factor induces shedding of the p75 neurotrophin receptor followed by endosomal gamma-secretase-mediated release of the p75 intracellular domain, *The Journal of biological chemistry 282*, 7606-7615.

[243] Pasternak, S. H., Bagshaw, R. D., Guiral, M., Zhang, S., Ackerley, C. A., Pak, B. J., Callahan, J. W., and Mahuran, D. J. (2003) Presenilin-1, nicastrin, amyloid precursor protein, and gamma-secretase activity are co-localized in the lysosomal membrane, *The Journal of biological chemistry 278*, 26687-26694.

[244] Caputo, G. A., Litvinov, R. I., Li, W., Bennett, J. S., Degrado, W. F., and Yin, H. (2008) Computationally designed peptide inhibitors of protein-protein interactions in membranes, *Biochemistry 47*, 8600-8606.

[245] Wang, J., Ma, C., Fiorin, G., Carnevale, V., Wang, T., Hu, F., Lamb, R. A., Pinto, L. H., Hong, M., Klein, M. L., and DeGrado, W. F. (2011) Molecular dynamics simulation directed rational design of inhibitors targeting drug-resistant mutants of influenza A virus M2, *Journal of the American Chemical Society 133*, 12834-12841.

[246] Deatherage, C. L., Hadziselimovic, A., and Sanders, C. R. (2012) Purification and Characterization of the Human gamma-Secretase Activating Protein, *Biochemistry 51*, 5153-5159.

[247] Alva, V., and Lupas, A. N. (2016) The TULIP superfamily of eukaryotic lipid-binding proteins as a mediator of lipid sensing and transport, *Biochimica et biophysica acta*.

[248] Gilbert, R. J. (2015) Protein-lipid interactions and non-lamellar lipidic structures in membrane pore formation and membrane fusion, *Biochimica et biophysica acta*.

[249] Bailo, R., Bhatt, A., and Ainsa, J. A. (2015) Lipid transport in Mycobacterium tuberculosis and its implications in virulence and drug development, *Biochemical pharmacology 96*, 159-167.

[250] Epand, R. M. (2008) Proteins and cholesterol-rich domains, *Biochimica et biophysica acta 1778*, 1576-1582.

[251] Li, H., Yao, Z., Degenhardt, B., Teper, G., and Papadopoulos, V. (2001) Cholesterol binding at the cholesterol recognition/ interaction amino acid consensus (CRAC) of the peripheral-type benzodiazepine receptor and inhibition of steroidogenesis by an HIV TAT-CRAC peptide, *Proceedings of the National Academy of Sciences of the United States of America 98*, 1267-1272.

[252] Hussain, I., Fabregue, J., Anderes, L., Ousson, S., Borlat, F., Eligert, V., Berger, S., Dimitrov, M., Alattia, J. R., Fraering, P. C., and Beher, D. (2013) The role of gamma-secretase activating protein (GSAP) and imatinib in the regulation of gamma-secretase activity and amyloid-beta generation, *The Journal of biological chemistry 288*, 2521-2531.

[253] Olsson, B., Legros, L., Guilhot, F., Stromberg, K., Smith, J., Livesey, F. J., Wilson, D. H., Zetterberg, H., and Blennow, K. (2014) Imatinib treatment and Abeta42 in humans, *Alzheimer's & dementia : the journal of the Alzheimer's Association 10*, S374-380.

[254] Fraering, P. C., Ye, W., LaVoie, M. J., Ostaszewski, B. L., Selkoe, D. J., and Wolfe, M. S. (2005) gamma-Secretase substrate selectivity can be modulated

directly via interaction with a nucleotide-binding site, *The Journal of biological chemistry 280*, 41987-41996.
[255] Eisele, Y. S., Baumann, M., Klebl, B., Nordhammer, C., Jucker, M., and Kilger, E. (2007) Gleevec increases levels of the amyloid precursor protein intracellular domain and of the amyloid-beta degrading enzyme neprilysin, *Molecular biology of the cell 18*, 3591-3600.
[256] Carson, J. A., and Turner, A. J. (2002) Beta-amyloid catabolism: roles for neprilysin (NEP) and other metallopeptidases?, *Journal of neurochemistry 81*, 1-8.
[257] Bowman Rogers, M. (2014) GSAP Revisited: Does It Really Play a Role in Processing A β ?, Alzforum.
[258] Chu, J., Lauretti, E., Craige, C. P., and Pratico, D. (2014) Pharmacological modulation of GSAP reduces amyloid-beta levels and tau phosphorylation in a mouse model of Alzheimer's disease with plaques and tangles, *Journal of Alzheimer's disease : JAD 41*, 729-737.
[259] Chu, J., Li, J. G., Hoffman, N. E., Madesh, M., and Pratico, D. (2015) Degradation of gamma secretase activating protein by the ubiquitin-proteasome pathway, *Journal of neurochemistry 133*, 432-439.
[260] Chu, J., Li, J. G., Joshi, Y. B., Giannopoulos, P. F., Hoffman, N. E., Madesh, M., and Pratico, D. (2015) Gamma secretase-activating protein is a substrate for caspase-3: implications for Alzheimer's disease, *Biological psychiatry 77*, 720-728.
[261] Oda, T., Elkahloun, A. G., Pike, B. L., Okajima, K., Krantz, I. D., Genin, A., Piccoli, D. A., Meltzer, P. S., Spinner, N. B., Collins, F. S., and Chandrasekharappa, S. C. (1997) Mutations in the human Jagged1 gene are responsible for Alagille syndrome, *Nature genetics 16*, 235-242.
[262] McDaniell, R., Warthen, D. M., Sanchez-Lara, P. A., Pai, A., Krantz, I. D., Piccoli, D. A., and Spinner, N. B. (2006) NOTCH2 mutations cause Alagille syndrome, a heterogeneous disorder of the notch signaling pathway, *American journal of human genetics 79*, 169-173.
[263] Garg, V., Muth, A. N., Ransom, J. F., Schluterman, M. K., Barnes, R., King, I. N., Grossfeld, P. D., and Srivastava, D. (2005) Mutations in NOTCH1 cause aortic valve disease, *Nature 437*, 270-274.
[264] Eldadah, Z. A., Hamosh, A., Biery, N. J., Montgomery, R. A., Duke, M., Elkins, R., and Dietz, H. C. (2001) Familial Tetralogy of Fallot caused by mutation in the jagged1 gene, *Human molecular genetics 10*, 163-169.
[265] Eagar, T. N., Tang, Q., Wolfe, M., He, Y., Pear, W. S., and Bluestone, J. A. (2004) Notch 1 signaling regulates peripheral T cell activation, *Immunity 20*, 407-415.
[266] Miele, L., Golde, T., and Osborne, B. (2006) Notch signaling in cancer, *Current molecular medicine 6*, 905-918.
[267] Roy, M., Pear, W. S., and Aster, J. C. (2007) The multifaceted role of Notch in cancer, *Current opinion in genetics & development 17*, 52-59.
[268] Miele, L., Miao, H., and Nickoloff, B. J. (2006) NOTCH signaling as a novel cancer therapeutic target, *Current cancer drug targets 6*, 313-323.
[269] Ridgway, J., Zhang, G., Wu, Y., Stawicki, S., Liang, W. C., Chanthery, Y., Kowalski, J., Watts, R. J., Callahan, C., Kasman, I., Singh, M., Chien, M., Tan,

C., Hongo, J. A., de Sauvage, F., Plowman, G., and Yan, M. (2006) Inhibition of Dll4 signalling inhibits tumour growth by deregulating angiogenesis, *Nature 444*, 1083-1087.

[270] Paganin, M., and Ferrando, A. (2011) Molecular pathogenesis and targeted therapies for NOTCH1-induced T-cell acute lymphoblastic leukemia, *Blood reviews 25*, 83-90.

[271] Weng, A. P., Ferrando, A. A., Lee, W., Morris, J. P. t., Silverman, L. B., Sanchez-Irizarry, C., Blacklow, S. C., Look, A. T., and Aster, J. C. (2004) Activating mutations of NOTCH1 in human T cell acute lymphoblastic leukemia, *Science 306*, 269-271.

[272] Nagarsheth, M. H., Viehman, A., Lippa, S. M., and Lippa, C. F. (2006) Notch-1 immunoexpression is increased in Alzheimer's and Pick's disease, *Journal of the neurological sciences 244*, 111-116.

[273] Larkin, M. A., Blackshields, G., Brown, N. P., Chenna, R., McGettigan, P. A., McWilliam, H., Valentin, F., Wallace, I. M., Wilm, A., Lopez, R., Thompson, J. D., Gibson, T. J., and Higgins, D. G. (2007) Clustal W and Clustal X version 2.0, *Bioinformatics 23*, 2947-2948.

[274] Tagami, S., Okochi, M., Yanagida, K., Ikuta, A., Fukumori, A., Matsumoto, N., Ishizuka-Katsura, Y., Nakayama, T., Itoh, N., Jiang, J., Nishitomi, K., Kamino, K., Morihara, T., Hashimoto, R., Tanaka, T., Kudo, T., Chiba, S., and Takeda, M. (2008) Regulation of Notch signaling by dynamic changes in the precision of S3 cleavage of Notch-1, *Molecular and cellular biology 28*, 165-176.

[275] Canevelli, M., Piscopo, P., Talarico, G., Vanacore, N., Blasimme, A., Crestini, A., Tosto, G., Troili, F., Lenzi, G. L., Confaloni, A., and Bruno, G. (2014) Familial Alzheimer's disease sustained by presenilin 2 mutations: Systematic review of literature and genotype–phenotype correlation, *Neuroscience & Biobehavioral Reviews 42*, 170-179.

[276] Shea, Y.-F., Chu, L.-W., Chan, A. O.-K., Ha, J., Li, Y., and Song, Y.-Q. (2016) A systematic review of familial Alzheimer's disease: Differences in presentation of clinical features among three mutated genes and potential ethnic differences, *Journal of the Formosan Medical Association 115*, 67-75.